Multiple Rieske iron-sulfur proteins of photosynthesis in the cyanobacterium *Synechocystis* sp. PCC 6803

The cytochrome *bf* complex is essential for both photosynthetic and respiratory electron transport in cyanobacteria. A Rieske iron-sulfur protein (ISP) is an essential subunit of this complex. The cyanobacterium, *Synechocystis* sp. PCC 6803 carries three genes, *petC1*, *petC2*, *petC3*, for different forms of Rieske ISPs. PetC1 is the major ISP. The functions of the PetC2 and PetC3 ISPs are not well understood. My goal was to investigate the roles of these Rieske proteins in electron transfer and redox signaling mediated by the cytochrome *bf* complex. Wild type *Synechocystis* and a mutant strain (ΔPetC1) that lacks the PetC1 ISP and thus uses the PetC2 ISP in its cytochrome *bf* complex were used for these studies. These strains were grown photosynthetically followed by shifts to dark aerobic and anaerobic conditions to test the postulated role of the PetC2 Rieske ISP in dark metabolism. Expression of the three Rieske ISP genes and control genes (*psaC*, for a photosystem I subunit; *zwf*, for glucose-6-phosphate dehydrogenase; and *rpnB*, for an RNAse P subunit) was investigated by reverse-transcriptase quantitative polymerase chain reactions (RT-qPCR). The relative abundance of photosystem and cytochrome *bf* proteins in the wild type and ΔPetC1 mutant strain was investigated by liquid chromatography, tandem mass spectrometry (LC-MS/MS). Electron transfer reactions were investigated by light-induced, kinetics spectroscopy to gain information about relative quantities of electron transfer protein complexes and components in the wild type and ΔPetC1 strains and to compare the catalytic efficiencies of the PetC1 and PetC2 Rieske ISPs. RT-qPCR data from the wild type showed elevated expression of *petC2* relative to *petC1* during dark anaerobiosis and greatly increased *petC2* expression, as might be expected, in the ΔPetC1 mutant. Gene expression and other data suggests that PetC3 has a function independent of the cytochrome *bf* complex. Kinetics spectroscopy data suggest that the ΔPetC1 mutant has a highly unusual cytochrome *bf* complex consisting primarily of the PetC2 Rieske ISP and cytochrome b_6 proteins. Surprisingly, the latter is kinetically coupled despite a very low content of the normally essential cytochrome *f* protein. The kinetics data further indicate that the PetC1 and PetC2 Rieske iron-sulfur proteins have similar catalytic efficiencies. Questions remain as to the specific roles of the PetC2 and PetC3 Rieske proteins. Overall, the research contributes to understanding electron transfer pathways and mechanisms by which cyanobacteria adapt to changing environments. This knowledge will be important for engineering cyanobacterial electron transfer pathways for biofuels applications.

MULTIPLE RIESKE IRON SULFUR PROTEINS OF PHOTOSYNTHESIS IN THE CYANOBACTERIUM *SYNECHOCYSTIS* SP PCC 6803

by

Saurabh J Ranade

A Thesis Submitted
In Partial Fulfillment of the Requirements
For the Degree of

Master of Science-Biology

at

The University of Wisconsin Oshkosh
Oshkosh WI 54901-8621

May 2012

COMMITTEE APPROVAL

Advisor

5/22/2012 Date Approved

Member

5/22/12 Date Approved

Member

5/22/12 Date Approved

PROVOST
AND VICE CHANCELLOR

5/30/12
Date Approved

FORMAT APPROVAL

4/25/12
Date Approved

To my beloved parents for all of their hard work and sacrifices which allowed me to pursue my higher education. I sincerely thank my big family which includes my maternal grandmother, uncles-aunts-cousins, younger brother and friends for their endless love. Special gratitude goes to my late grandparents who always remain as immense sources of inspiration and love.

ACKNOWLEDGEMENTS

The thesis would remain incomplete without the page of acknowledgement. My graduate study at the University of Wisconsin, Oshkosh was indeed a great learning and fun experience with a number of respectable people I met.

First and foremost of all, I would like to thank my advisor Dr. Toivo Kallas for giving me opportunity to work in his lab, for his enormous knowledge, guidance, encouragement and helping hand. I will always remain grateful to him for creating interest in me about intriguing field of research on cyanobacteria and helping me to develop as a researcher. It has been an honor for me to be his student. Furthermore, my sincere gratitude goes to Dr. Lisa Dorn and Dr. James Paulson for being on my thesis committee, advises on improvement of the thesis and being very cooperative even at very short notices. I would like to extend my gratitude to Matthew Nelson, senior lab technician for his valuable help at numerous occasions and great patience who taught me right from how to grow cyanobacteria to the complex analytical techniques. Last but not least, I would like to thank all of my labmates working with whom was a really enjoyable experience.

TABLE OF CONTENTS

TABLE OF CONTENTS (Continued)

TABLE OF CONTENTS (Continued)

LIST OF TABLES

LIST OF FIGURES

LIST OF FIGURES (Continued)

INTRODUCTION

Basic characteristics of life include growth, development and metabolism. Energy plays a key and fundamental role to make these things happen. Sun acts as the major source of energy. Energy emitted by the Sun is in the form of electromagnetic radiation which has to be converted into chemical energy to make it available to different forms of life through the energy pyramid or the energy web which consist of meshwork of trophic levels of producer, consumer and decomposer organisms. The major process of conversion of solar light energy into chemical energy is oxygenic photosynthesis. In the evolutionary history, first photosynthetic organisms evolved, used hydrogen and hydrogen sulfide as source of electrons (Olson, 2006). Cyanobacteria, first to use water as source of electrons appeared around 3,500 million years ago and gradually brought about oxygenation of the atmosphere (Carr, Friedrichs, Aita, Antoine, Arrigo, Asunama, ... Yamanaka, 2006). Atmosphere rich in oxygen saw further evolution of life and approximately 1,000-1,500 million years ago, one of the organisms formed endosymbiotic relationship with a cyanobacterium to form ancestor of all plant and algal cells (Douzery, Snell, Bapteste, Delsuc, & Philippe, 2004; McFadden, 2001). Chloroplasts of modern algal and plant cells are the descendants of the engulfed cyanobacterium (McFadden, 2001; Palmer, 2003). Cyanobacteria get their name from phycocyanin, a bluish green pigment from the family of light harvesting phycobiliproteins. Today, cyanobacteria are responsible for performing approximately 25% of global photosynthesis and 50% in the oceans. In addition to photosynthesis, many

though not all species of cyanobacteria fix atmospheric nitrogen and stand as one of the important contributors of global nitrogen fixation. Cyanobacteria are prokaryotic photoautotrophs which reside in almost every type of habitat and occur in oceans, fresh waters, tropical, arctic soils, as endosymbionts in lichens (Rikkinen, Oksanen & Lohtander, 2002), even in fur of sloths (De Muizon, McDonald, Salas & Urbina, 2004). Cyanobacteria include unicellular as well as colony forming species. Colonies are often in the form of filaments. Nitrogen fixing filamentous species fix nitrogen in thick walled differentiated cells, heterocysts. In addition to outer cytoplasmic membrane, all of the cyanobacteria possess a highly organized system of internal thylakoid membrane.

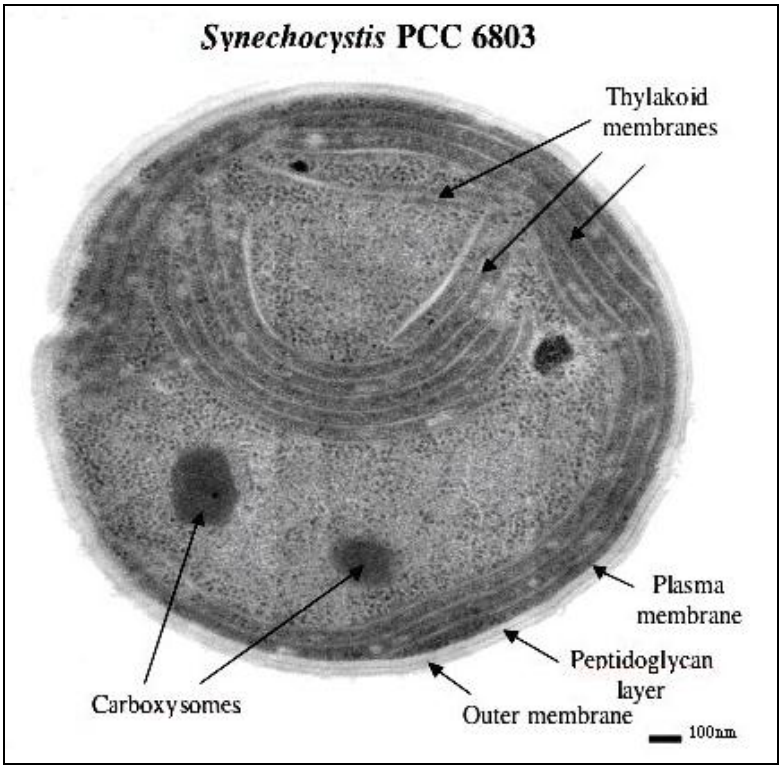

Figure 1: Transmission electron micrograph of *Synechocystis* 6803 cell (Retrieved from Donald Danforth Plant Science Center's website, Pakrasi (n.d.); with permission of Dr. Himadri Pakrasi).

Among cyanobacteria, species such as *Synechocystis* sp. PCC 6803 (hereafter *Synechocystis* 6803) are used as a model organism for better understanding of photosynthesis as well as a mean for genetic engineering. The cyanobacterium was isolated from a fresh water lake in 1968 and is the first cyanobacterial species or any photosynthetic organism to have its complete genome sequenced. *Synechocystis* 6803's genome project was completed in 1996 by Nakamura, Kaneko, Hirosawa, Miyajima & Tabata (1998). A relatively shorter generation time (~16 hours), ability to grow in absence of light under provision of carbon containing energy sources, growth in a variety of different conditions, ability to integrate foreign DNA by homologous recombination make the organism a suitable candidate of research. In addition to projects intended to study photosynthesis, several research groups are working on hydrogen as well as biodiesel production in *Synechocystis* 6803 (Antal & Lindblad, 2004; Burrows, Chaplen & Elly, 2008; Cournac, Guedney, Peltier & Vignais, 2004; Dickons, Page & Elly, 2009; Lindberg, Park & Melis, 2009; Tran, Hong & Lee, 2009).

Electron transport chain has been studied in details in a number of cyanobacteria including *Synechocystis* 6803. The thylakoid membranes are the sites of localization of photosynthetic as well as respiratory electron transport chain in cyanobacteria. As represented in Figure 2, the photosynthetic apparatus consists of membrane spanning photosystem II (hereafter PS II), photosystem I (hereafter PS I) and cytochrome *bf* complex. PS II and PS I capture sunlight with the help of light harvesting complexes, phycobilisomes causing flow of electrons between the photosystems through the plastoquinone-plastoquinol pool (hereafter PQ pool) and cytochrome *bf* complex

(Blankenship, 2002). Transport of electrons through cytochrome *bf* complex generates proton gradient across the thylakoid membrane. The proton µgradient leads to ATP synthesis by ATP synthase enzyme units present in the thylakoid membrane (Cramer, Yan, Zhang, Kurisu & Smith, 2005; Kallas, 1994, pp. 259-317).

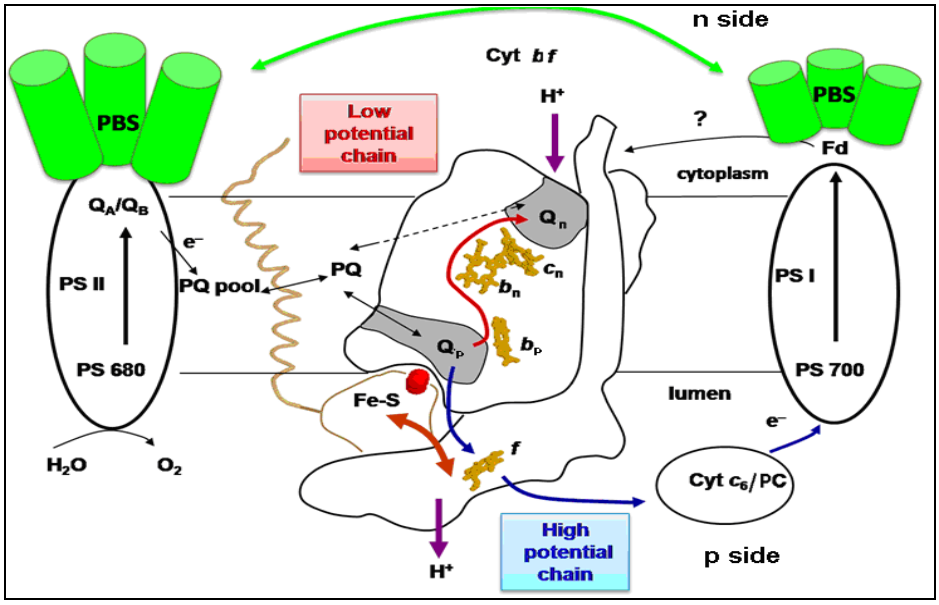

Figure 2: The electron transport chain of cyanobacteria present in thylakoid membrane (Adapted from original figure by Kallas, 1990-2007, unpublished data)

PBS: phycobilisomes; PS II and PS I: photosystem II and photosystem I; P680: reaction center of photosystem II; Q_A and Q_B: plastoquinone A and plastoquinone B; PQ pool: plastoquinone / plastoquinol pool; Cyt *bf*: cytochrome *bf* complex; Q_p: Q_O or plastoquinol oxidation site; Q_n: Q_i or plastoquinone reduction site; Fe-S: Rieske iron-sulfur protein; *f*: cytochrome *f*; b_n, b_p and C_n: hemes b_n, b_p and C_n; Cyt *c*6: cytochrome *c*6; PC: plastocyanin; P700: reaction center of photosystem I; Fd: ferredoxin; p side: positive side of thylakoid membrane where protons are translocated; n side: negative side of thylakoid membrane from where protons are translocated.
Solid single and double headed black, red and blue arrows point the direction of passage of electrons; Incomplete two headed black arrow indicates release of plastoquinol from Q_n site and its replacement by a plastoquinone from PQ pool; Double headed green arrow indicates redistribution of phycobilisomes under different light conditions; Purple arrows indicate translocation of protons across thylakoid membrane from negative side (hereafter n side) to the positive (hereafter p side) of thylakoid membrane; Double headed orange arrow shows movement of Rieske iron-sulfur protein head around a central pivot. Question mark (?) indicates possible transport of electrons to Q_p site during cyclic electron flow.

The cytochrome *bf* complex has been shown to play a key role in sensing redox state of PQ pool causing regulation of redistribution of phycobilisomes between the photosystems by mechanism of state transition (Keren & Ohad, 1998; Wollman, 2001) and alteration of gene expression (Allen, 2004; Pfannschmidt, Nilsson, Tullberg, Link & Allen, 1999). The regulatory mechanisms are important to balance between efficiency of photosynthesis and survival of the organism by minimizing formation of reactive oxygen species (Demming-Adams & Adams, 2002; Ivanov & Khorobrykh, 2003; Muller, 2000).

Apart from the redox regulation as mentioned above, cytochrome *bf* complex is essential for both respiratory as well as photosynthetic electron transport (Kallas, 1994, pp. 259-317). Structures of cytochrome *bf* complexes have been understood in alga *Chlamydomonas* (Stroebel, Choquet, Popot & Picot, 2003) and cyanobacterium *Mastigocladus* (Kurisu, Zhang & Cramer, 2003; Yamashita, Zhang & Cramer, 2003). Figure 3 represents dimer structure of cytochrome *bf* complex. Cytochrome *bf* complex consists of four major subunits namely cytochrome b_6 (PetB), Subunit IV (PetD), Rieske iron sulfur protein (PetC1) and cytochrome *f* (PetA) along with minor subunits PetG, PetL, PetM, PetN etc (Cramer, Zhang, Yan, Kurisu & Smith, 2006; DeRuyter & Fromme, 2008, pp. 217-269). Out of the cytochrome b_6f complex subunits mentioned above, cytochrome b_6 (PetB), Rieske iron sulfur protein (PetC1) and cytochrome *f* (PetA) act as the electron carriers while other subunits such as subunit IV are not directly involved in electron transport but play supportive roles (DeRuyter & Fromme, 2008, pp. 217-269). As shown in Figure 3, Rieske protein crosses over with its trans-membrane helix in one

monomer and its lumenal domain and iron sulfur cluster (Fe-S) in the other monomer of the *bf* complex.

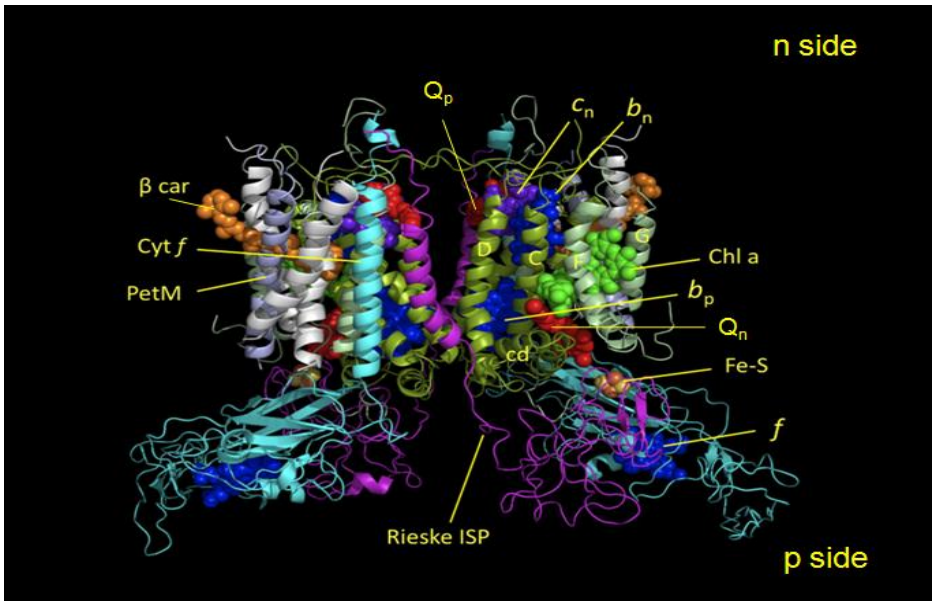

Figure 3: Membrane parallel view of the *Mastigocladus laminosus* cytochrome *bf* dimer (Adapted from original Protein Data Bank (pdb) X-ray crystal structure image 1VF5 deposited by Kurisu et al. (2003); created using Pymol software by Dr. Toivo Kallas).

Rieske ISP: Rieske iron-sulfur protein; Fe-S: iron-sulfur cluster of Rieske protein; Cyt *f*: cytochrome *f*; b_n, b_p ,C_n and *f*: hemes b_n, b_p, C_n and *f*; β car: β carotene; Chl a: chlorophyll A; Q_p: plastoquinol oxidation site; Q_n: plastoquinone reduction site (in red); C and D: amphipathic membrane spanning helices of cytochrome b_6; c and d: thylakoid membrane parallel helices of cytochrome b_6; F and G: helices of subunit IV; p side: positive side of thylakoid membrane where protons are translocated; n side: negative side of thylakoid membrane from where protons are translocated. Components of cytochrome *bf* complex from one of the dimers have been shown.

The Photosynthetic electron transport mechanism can be explained as follows. In cyanobacteria, phycobilisomes are major antenna proteins present on the outer surface of thylakoid membrane. These were thought to be associated with the PS II, but now it is clear that in some cyanobacteria, depending on environmental condition and the redox state of PQ pool, at least 50% of the phycobilisomes may be associated with PSI (Dong,

Tang, Zhao, Mullineaux, Shen, & Bryant, 2009). Phycobilisomes absorb light in the range 500-650 nm, spectrum outside of the chlorophyll absorbance. The energy absorbed by the phycobilisomes is transferred to the reaction center of PS II, P680. Excitation energy leads to charge separation and electron is excited from P680. The electron excited from PS680 is transferred via pheophytin, tightly bound plastoquinone molecule, Q_A and finally to terminal acceptor within PS II, mobile plastoquinone molecule Q_B. The loss of electron by P680 is made up by stripping of electrons from a water molecule using oxygen evolving complex (OEC) releasing oxygen and hydrogen ions in the process. Q_B after receiving two electrons (and two protons from outside of thylakoid membrane) becomes plastoquinol and moves to PQ pool. Its position is taken up by a new plastoquinone from PQ pool. The plastoquinol then reaches the multi protein cytochrome *bf* complex and is re-oxidized at the quinol oxidation or Q_p site. After oxidation of plastoquinol, plastoquinone is released into the PQ pool and hydrogen ions are released into the intra-thylakoidal space. Coordinated motion of the Rieske iron-sulfur protein (hereafter Rieske ISP) head causes one of the electrons to travel through high potential chain while another through low potential chain (Roberts, Bowman & Kramer, 2002). Cyanobacteria are known to possess different isoforms of Rieske ISPs coded by different genes and regulated under different conditions. Rieske ISPs contain a glycine-rich flexible hinge region which connects the trans-membrane domain with the soluble iron-sulfur cluster domain and is responsible for the coordinated motion of Rieske ISPs and thus efficiency of electron transfer (DeRuyter & Fromme, 2008, pp. 217-269; Schneider, Berry, Volkmer, Seidler & Rögner, 2004a). The low potential chain electron passes

through heme b_p, b_n and c_n centers of the cytochrome *bf* complex and finally ends up at quinol reduction site, Qn or Q_i where they reduce plastoquinone to plastoquinol and pick up hydrogen ions from the 'n' side of the thylakoid membrane. The high potential chain electron thus travels from Q_p or Q_O site to Rieske ISP and cytochrome *f* subunits of cytochrome *bf* complex. Plastoquinol is released into PQ pool and is replaced by another plastoquinone at Qn site. From cytochrome *f*, the electron is transferred to plastocyanin and/or cytochrome c_6. In *Synechocystis* 6803, plastocyanin appears as the electron carrier when a source of copper is added to the growth medium in adequate amounts (DeRuyter & Fromme, 2008, pp. 217-269; Zhang, McSpadden, Pakrasi & Whitmarsh, 1992). Plastocyanin and/or cytochrome c_6 donate the electron to the reaction center of PS I.

PS I, just like PS II has phycobilisomes associated with it which transfer energy to the P700 reaction center causing excitation of P700 molecules leading to a charge separation event. The electron is passed through chlorphyll A_0, phylloquinone A_1, iron-sulfur centers F_X-F_A/F_B to ferredoxin. Reduced ferredoxin is released from PS I and re-oxidized by ferredoxin-$NADP^+$ oxidoreductase (FNR) enzyme to generate NADPH, an important reducing agent. The protons translocated across the thylakoid membrane by the cytochrome *bf* complex from the 'n' side to the 'p' side as predicted by Mitchell's Q cycle, generate a gradient that is used to produce ATP by ATP synthase present in the thylakoid membrane.

Figure 4 represents linear and cyclic photosynthetic electron transport as well as respiratory electron transport in cyanobacteria emphasizing the central role of the PQ pool and cytochrome *bf* complex.

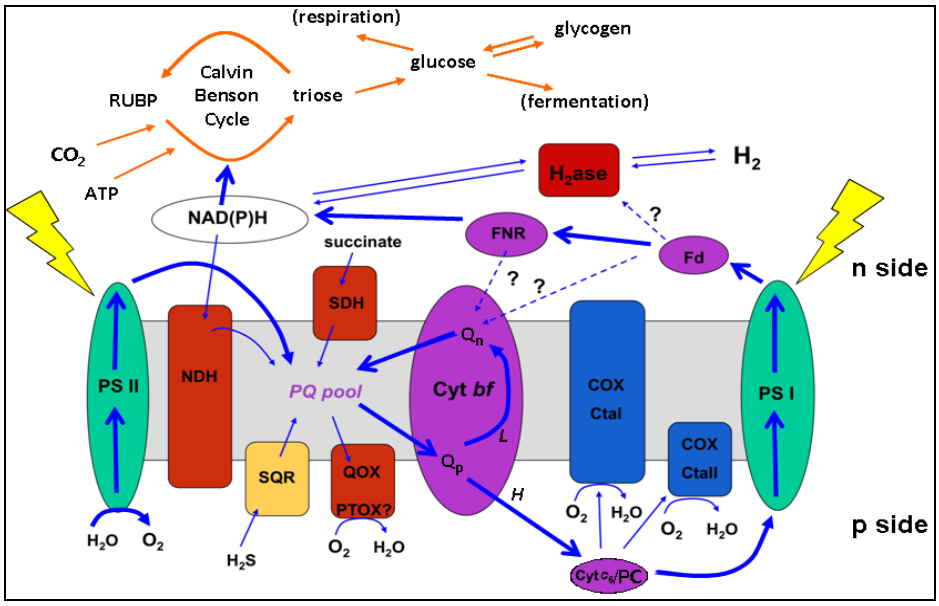

Figure 4: Routes of electron transport with PQ pool and cytochrome *bf* complex at the crossroads (Adapted from original figure by Kallas, 1990-2007, unpublished data)

PS II and PS I: photosystem II and hotosystem I; PQ pool: plastoquinone / plastoquinol pool; Cyt *bf*: cytochrome *bf* complex; Q_P: Q_O or plastoquinol oxidation site; *f*: cytochrome *f*; Cyt *c*6: cytochrome *c*6; PC: plastocyanin; Fd: ferredoxin; FNR: ferredoxin NAD(P)H oxidoreductase; SDH: succinate dehydrogenase; SQR: sulfide quinone oxidoreductase; QOX: quinol oxidase; PTOX: plastoquinone terminal oxidase; COX: cytochrome oxidase; H_2ase: Ni-Fe bidirectional hydrogenase; H and L: high and low potential chains; p side: positive side of thylakoid membrane where protons are translocated; n side: negative side of thylakoid membrane from where protons are translocated.
Solid thick single headed blue arrows point the direction of major ways of passage of electrons ; Solid thin single headed blue arrows point the direction of minor ways of passage of electrons; Incomplete single headed blue arrows along with the question marks indicate possible ways of passage of electrons; Solid single headed orange arrows indicates direction of major ways of progression of reactions during respiration and fermentation; Two ways single headed arrows indicate reversible reactions or passage of electrons.

Under optimal or tolerable light conditions, both PS II and I are involved in electron transport as explained above. This linear and non-cyclic electron flow generates NADPH as well as ATP. In the case of high light conditions, cyclic electron transport is triggered, which acts to alleviate the photoinhibition by generation of proton gradient across the thylakoid membrane (Takahashi, Milward, Fan, Chow & Badger, 2009). In the cyclic pathway, only PS I and the cytochrome *bf* complex are involved and electrons expelled

from P700 of PS I travel through ferredoxin to either heme c_n of the cytochrome *bf* complex to reduce plastoquinone molecules present at plastoquinone reduction site Q_n (Breyton, Nandha, Johnson, Joliot & Finazzi, 2006; Kurisu et al., 2003; Zhang, Whitelegge & Cramer, 2001). Alternatively, electrons flow to NADPH, which may be oxidized by NADH dehydrogenase which donates the electrons to plastoquinone molecules of the PQ pool (Mi, Endo, Schreiber, Ogawa & Asada, 1994; Yu, Zhao, Muhlenhoff, Bryant & Golbeck, 1993). The plastoquinol molecules thus formed may again bind to the plastoquinol oxidation site of the cytochrome *bf* complex. Here they are oxidized to release one electron though high potential chain while another flows through low potential chain and the cycles repeat. Cyclic electron flow can generate only ATP molecules (DeRuyter & Fromme, 2008, pp. 217-269). The thylakoid membrane contains all of the components of the respiratory electron transfer chain including NADPH dehydrogenase (NDH-1), NADH dehydrogenase type II (NDH-2) and succinate dehydrogenase (SDH) of which NDH-1 acts as proton pump to translocate protons across thylakoid membrane. NADH, NADPH generated by NDH-1 or NDH-2 and $FADH_2$ generated by succinate dehydrogenase step pass electrons into the PQ pool. From here, electrons travel further through the cytochrome *bf* complex, cytochrome *c* and finally to one of the cytochrome *c* oxidases, Cox (Cta I) or cytochrome *bd* oxidase where electrons reduce O_2 to produce water molecules. Cytochrome *c* oxidases also act as proton pumps (Hart, Schlarb-Ridley, Bendall & Howe, 2005). Hydrogen ions pumped by NDH-1 and cytochrome *c* oxidase are involved in oxidative phosphorylation by the ATP synthase.

These respiratory pathways fulfill cellular energy requirement in the absence of light (Ward, 2006).

The photosynthetic apparatus and especially PS II often faces the risk of photooxidative damage. Light causes singlet state excitation of the P680 reaction center chlorophyll which can return to the ground state via one of the several pathways. Excess energy is ideally either emitted as chlorophyll fluorescence or lost as heat. When excess P680 molecules are in excited state, some of the energy absorbed by phycobilisomes is lost as heat via the orange carotenoid binding proteins (OCP) by one of the mechanisms classified as non photochemical quenching (hereafter NPQ). Alternatively, excited P680 molecules can form a triplet (^{3}Chl*). Under high light, PS II is more prone to photodamage. The P680 ($P680^+$) cation is able to directly oxidize core PS II proteins. Alternatively, triplet P680 chlorophyll molecules formed can react with oxygen molecules forming singlet oxygen that can inhibit any protein and lipid in the vicinity (Karapetyan, 2007; Müller, Lee & Niyogi, 2001). Unlike P680, the P700 cation ($P700^+$) of PS I is not a powerful oxidizing agent. Under high light conditions, by the combined interaction of P700, P700 cation ($P700^+$), the P700 excited triplet, with antenna chlorophyll and carotenoids, excess energy is more readily dissipated by PS I. Thus PS I is less prone to photodamage than PS II (DeRuyter & Fromme, 2008, pp. 217-269; Karapetyan, 2007).

Under unbalanced light conditions, PS II receives more energy than PS I leading to photodamage. Also, as shown in Figure 4, cyclic electron flow leads to synthesis of only ATP while linear electron flow leads to synthesis of both NAD(P)H and ATP. According

to the cellular requirements, light energy is distributed between the two photosystems to obtain optimal rates of ATP and or NAD(P)H synthesis and avoid photodamage by translocation of phycobilisomes between PS II and PS I. These are the so-called state transitions (DeRuyter & Fromme, 2008, pp. 217-269; Dong et al., 2009; Karapetyan, 2007). In cyanobacteria, the redox state of the PQ pool is sensed by the cytochrome *bf* complex by an unknown mechanism resulting into state transition. The mechanism of this redox sensing and signaling is not well understood. A reduced PQ pool resulting from higher light energy absorption as well as dark incubation leads to a transition from state I to state II (i.e. the net translocation of phycobilisomes from PS II to PS I). Whereas, more oxidized PQ pool leads to transition from state II to state I, i.e. the net translocation of phycobilisomes from PS I to PS II (DeRuyter & Fromme, 2008, pp. 217-269, Mullineaux & Allen, 1990).

Rieske ISP subunits of the cytochrome *bf* complex are responsible for differential transport of electrons released during oxidation of plastoquinol through high or low potential chain. The Rieske ISPs are products of the *petC* gene family and have approximate mass of 14-19.3 kDa. These proteins possess a 2Fe-2S cluster which is bound to the 'signature' sequence 'Cys-X-His-$(X)_{15–17}$-Cys-X-X-His'. One iron atom is bound by two cysteines while another by two histidines. This coordination is thought to be a cause of the high mid-point potential of 270-360 mV of Rieske ISPs found in cytochrome *bf* complex. In addition, two cysteine residues form a disulfide bridge close to iron-sulfur cluster. The 2Fe-2S cluster coordinating amino acids as well as two additional cysteine residues are organized in two boxes that have highly conserved

sequences in all Rieske ISPs and replacement of any of the mentioned amino acids affects the mid-point potential of the 2Fe-2S cluster (DeRuyter & Fromme, 2008, pp. 217-269; Schneider, Skrzypczak, Anemüller, Schmidt, Seidler, & Rögner, 2002).

Genome of *Synechocystis* 6803 contains three open reading frames namely sll1316 (*petC1*), slr1185 (*petC2*) and sll1182 (*petC3*) that code for three Rieske ISPs PetC1, PetC2 and PetC3 respectively. Figure 5 presents amino acid sequence of the three Rieske ISPs along with the sequence motifs for binding of 2Fe-2S cluster namely Box I and Box II. As mentioned above, one iron atom is bound by first cysteine residues while other iron atom is bound by the unique histidine residues of Box I and II. Remaining cysteine residues of the boxes form a disulfide bond. Of the three Rieske ISPs, PetC1 and PetC2 are similar while PetC3 possesses different structural and functional properties. As shown in Figure 5, PetC1 shows 44% identity with PetC2 and 34% identity with PetC3. Box I and Box II are exactly same in PetC1 and PetC2 while differ by a single amino acid each in case of PetC3. PetC1 and PetC2 are similar in size with approximate molecular mass of 19kDa while PetC3 is comparatively smaller protein with molecular mass of 14kDa. Comparison of sequences shows three major deletion regions in PetC3 as shown in Figure 5, in first three lines of amino acid sequence alignment (Iwata, Saynovits, Link, Michel, 1996; Schneider et al., 2002).

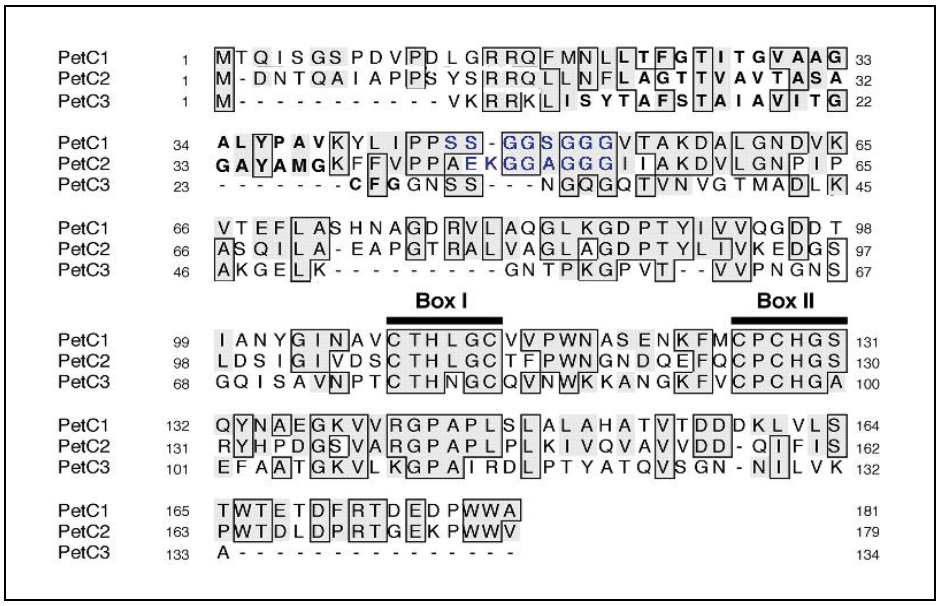

Figure 5: Amino acid sequence similarities between Rieske iron-sulfur proteins of *Synechocystis* 6803 (Adapted from Schneider et al., 2002)

Box I and Box II are iron-sulfur binding boxes; Numbers to left and right indicate amino acids. Blue characters represent glycine rich flexible hinge region.

Mid-point potentials of PetC1, PetC2 and PetC3 are 320 mV, ~300 mV and 135 mV respectively. Proteins with a mid-point potential as low as that of PetC3 are not found in cytochrome *bc* complexes (Schneider et al., 2002). Immunoblot analyses have localized PetC1 and PetC2 proteins to the thylakoid membrane while PetC3 has been found to be present in plasma membrane. Growth and deletion experiments revealed that, among PetC2 and PetC3 proteins, only PetC2 can replace the function of PetC1 suggesting a different physiological function of PetC3. A role of PetC3 in oxidation of a menaquinol such as phylloquinone has been suggested. However, with the exception of the phylloquinone, which acts as an electron transfer cofactor in PS I, there are no known menaquinones in cyanobacteria (Schultze, Forberich, Rexroth, Dyczmons, Rögner, & Appel, 2009).

Rieske ISPs which are part of both cytochrome *bf* complex as well as cytochrome *bc* complex contain a glycine rich flexible hinge region which connects the trans-membrane domain with soluble domain. In PetC2, the glycine rich region has one lysine and one glutamic acid residue which may decrease flexibility of the hinge region thus suggesting better functioning of PetC1 over PetC2 in electron transfer as this flexibility is required for faster movement of electron carrying soluble domain (Schneider et al., 2004a). Absence of the glycine rich hinge region in PetC3 suggests its role independent of cytochrome *bf* complex.

Attempts to create a double deletion mutant of *petC1*/*petC2* have not succeeded. ΔPetC1 mutant was created by insertion of chloramphenicol resistance cassette into the reading frame of *petC1* gene and part of the upstream region as shown in Figure 6. This ΔPetC1 mutant grows slowest of all of the single and double deletion mutants of the *petC* genes and cannot tolerate light intensities above 100 μmol photons $m^{-2}s^{-1}$ (Schneider et al., 2004a; Tsunoyama, Bernàt, Dyczmons, Schneider & Rögner, 2009).

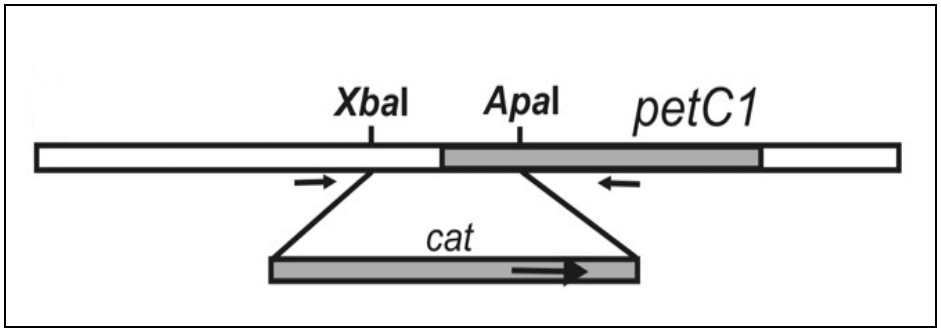

Figure 6: *petC1* gene deletion construct in *Synechocystis* 6803 ΔPetC1 mutant
(Adapted from Schneider et al., 2004a)

The *petC1* open reading frame and *cat* and chloramphenicol resistance cassette are shown in grey. Large arrow shows the direction of transcription of *cat* cassette. Small arrows represent the positions of primer binding for mutagenesis. *Xba*I and *Apa*I are restriction endonucleases' sites.

Synechocystis 6803 wild type strain has been shown to grow at least two times faster than the ΔPetC1 mutant under optimal photosynthetic grown conditions (Kallas, 1990-2007, unpublished data). Acoording to Tsunoyama et al. (2009), PetC1 deletion leads to highly reduced PQ pool due to slow transfer of electrons through cytochrome *bf* complex causing incomplete oxidation of PQ pool by PS I which compels ΔPetC1 cells reduce PSII and phycobilisome contents and to remain in state II under all growth conditions. Conversely, Nelson & Kallas (2000-2007, unpublished data) observed a higher PS II content as well as a considerable (~30%) state transition (from state II to state I) in the ΔPetC1mutantindicating the possible role of higher PS II content in exhibition of state transition by the Δ*petC1* strain from Dr. Kallas's laboratory.

petC1 gene is part of an operon *psbN-psbH-petC1-petA* (Mayes & Barber, 1991), insertion of chloramphenicol resistance cassette has disrupted the promoter region for co-transcribed *petC1* and *petA* genes forcing *petA* to use promoter region of the resistance cassette (Schneider et al., 2004a; Figure 6). Immunoblot studies have shown a higher PetC2 content, similar cytochrome b_6 content but reduced cytochrome *f* and subunit IV content in the ΔPetC1 mutant compared to the wild type strain (Tsunoyama et al., 2009). Reduced expression of *petA* gene coding cytochrome *f* along with the higher expression of *petC2* has been observed in ΔPetC1 mutant by during a microarray study (Nelson & Kallas, 2000-2007, unpublished data). Reduced cytochrome *f* and subunit IV contents of ΔPetC1 might also play a role in reduced electron transport (Schneider et al., 2004a). Spectroscopic experiments have shown ~ 50 times slower turnover of cytochrome *bf* complex in ΔPetC1 mutant (Finazzi and Kallas, 2000-2005, unpublished data) which is

thought to be related to reduced cytochrome *f* content and/or lower catalytic efficiency of PetC2.

For any cyanobacterial strain, quantum efficiency of PS II which is percentage of impinging light energy to excite a pair of electrons depends upon the quantity of PS II, activity of PQ oxidases as they prevent over reduction of PQ pool (Berry, Schneider, Vermaas & Rögner, 2002) and finally activity of cytochrome *bf* complex which may be limited by activity of PetC1 and PetC2 Rieske ISPs. The more reduced PQ pool is, the more time it takes to replace a plastoquinol at Q_B site. It has also been suggested that, redox state of PQ pool regulates state transition via cytochrome *bf* complex (Mao, Li, Ruan, Wu, Gong, Zhang, & Zhao, 2002).

A number of different studies have been revealed differential expression of Rieske ISP isoforms under different physiological conditions. A microarray gene expression study found up to 8, 15.2 and 2.1 fold up regulation of *petC2* in presence of cadmium, zinc and hydrogen peroxide respectively while up to 2.65 fold up regulation of *petC3* in presence of cadmium (Houot, Floutier, Marteyn, Michaut, Picciocchi, Legrain, …Chauvat, 2007). Another microarray study discovered up to 4 fold up-regulation of *petC2* gene under low oxygen conditions (Summerfield, Toepel & Sherman, 2008). ~32 fold up-regulation of *petC2* was observed in contrast to ~2.75 fold in case of *petC1* by reverse transcriptase, quantitative polymerase chain reaction experiments (hereafter RT-qPCR) in wild type cells in presence of high light (above 100 μmol $m^{-2}s^{-1}$). ΔPetC1 mutant was found to exhibit higher levels of cytochrome *bd* oxidase. Exposure of high light was seen to stall the growth of wild type cells; ΔPetC1 cells could not sustain high

light and died while Δ*petC2* and Δ*petC3* cells continued to grow with no decrease in growth rate while presence of all three Rieske ISPs was found essential for maximal electron transport suggesting regulatory roles played by PetC2 and PetC3 proteins specially in presence to high light (Tsunoyama et al., 2009). Recently, role of PetC2 in respiration has been suggested based on increased oxygen uptake of the ΔPetC1 mutant in the dark. In the same study, ΔPetC1 mutant was observed to exhibit lower photochemical quenching but higher NPQ. Based on previous investigations related to presence of different components necessary for photosynthetic as well as respiratory electron transport, a model for distribution of electron transfer complexes in thylakoid and plasma membrane *of Synechocystis* 6803 (Figure 7) has been proposed by Schultze et al. (2009).

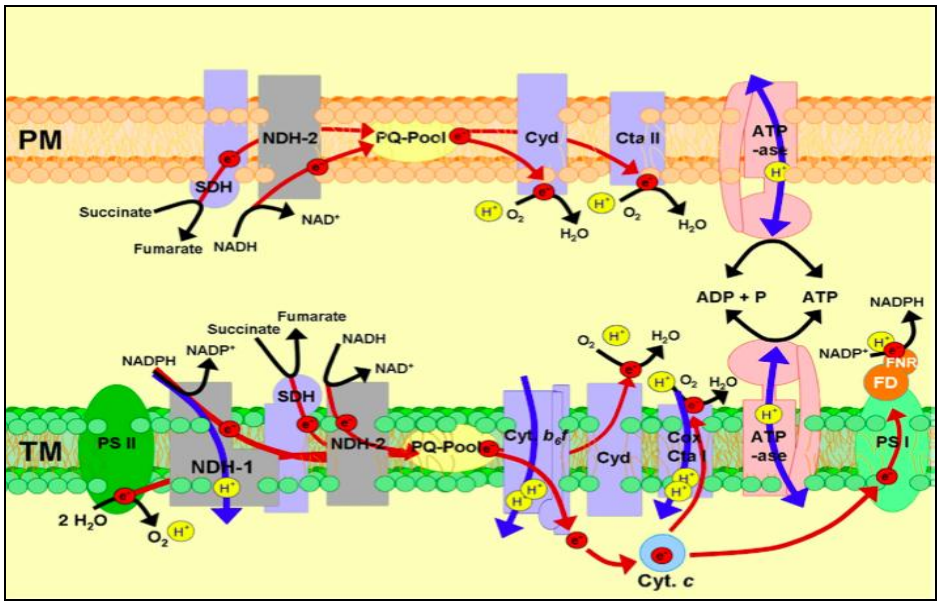

Figure 7: Distribution of electron transfer chains in membranes of *Synechocystis* 6803 (Retrieved from Schultze et al., 2009)

PM: Plasma Membrane, SDH: Succinate Dehydrogenase, NDH-2: NADH Dehydrogenase Type II, PQ pool: Plastoquinone/Plastoquinol Pool, Cyd: Cytochrome *bd* Oxidase, Cta II: Cytochrome *c* Oxidase Homologue, TM: Thylakoid Membrane, NDH-I: NADPH Dehydrogenase, COX: Cytochrome *c* Oxidase, FD: Ferredoxin, FNR: Ferredoxin-NADP+ Reductase.
Black, blue and red arrows indicate proton forming- consuming reactions, transport of protons and transport of electrons respectively. Arrowheads indicate direction of reaction.

According to the model as shown in Figure 7, the plasma membrane carries respiratory electron transfer chain components not acting as proton pumps. Proton gradient can form only when PQ pool is oxidized by cytochrome *bd* oxidase and cytochrome *c* oxidase homologue or when ATPase works in reverse direction to release excess protons out of cell. The PetC1 and PetC2 Rieske ISPs exist as components of different cytochrome *bf* complexes in thylakoid membrane. The role of the PetC3 Rieske ISP in electron transport in the plasma membrane still remains unclear (Schultze et al., 2009).

My thesis had a couple of different objectives. First objective was to study expression of three Rieske ISPs at timely intervals under dark and strict anaerobic conditions using recent and highly specific technique of RTqPCR. In addition to Rieske ISPs, I wished to study behavior of *petA* which codes for apocytochrome *f*, *psaC* which codes for PSI component VII or PsaC which bind F_A and F_B iron sulfur clusters in PS I, *zwf* which codes for glucose 6 phosphate dehydrogenase gene as an indicator of anabolic activity and or respiration along with a control gene *rpnB* which is also known as *rnpB* coding for RNA component of RNaseP which is known to express constitutively under anaerobic conditions (Pratte, Eplin & Thiel, 2006). Along with the transcriptomic approach, I attempted to find evidence at the protein level for change in expression of Rieske ISPs using metabolic labeling and isotope assisted mass spectrometry since studies like one by Matsui, Yoshimura, Wakabayashi, Imamura, Tanaka, Takahashi, … Shirai, (2007) have shown that, transcript levels are not necessarily reflected in actual protein level. As kinetic experiments are important tools to study highly dynamic electron transfer reactions; I have supplemented my transcriptomic and proteomic experiments with the kinetic data. I studied electron transport kinetics using Joliot type spectrophotometry (BioLogic's JTS-10) to estimate amounts of cytochrome *bf* components, plastocyanin and PS I calculated using the maximum absorption values of completely oxidized or reduced electron transfer chain components along with their individual extinction coefficients. Also, I have tried to answer question whether PetC1 and PetC2 Rieske ISPs differ in their activities. Finally, I made an effort to track quantum efficiency of PS II in wild type as well as ΔPetC1 mutant of *Synechocystis* 6803

from optimal to dark anaerobic conditions with a range of actinic light intensities using the same type of spectrophotometer as mentioned above. I intended to study impact of the ΔPetC1 mutation and dark-anaerobic conditions on electron transfer which depends upon the activity of cytochrome *bf* complex.

The overall goal of this thesis was to gain insight into the functions and study responses of different forms of Rieske ISPs.

MATERIALS AND METHODS

A] Cyanobacterial Strains

I] *Synechocystis* sp. PCC 6803. It is a unicellular cyanobacterium isolated from fresh water lake in 1968. It is the first photosynthetic organism to be sequenced by Nakamura et al. (1998). The organism is able to perform oxygenic photosynthesis as well as respiration if suitable carbon source is provided. The wild type strain under study was originally obtained from Pasteur Culture Collection (PCC).

II] *Synechocystis* sp. PCC 6803 ΔPetC1. The mutant strain of *Synechocystis* sp. PCC 6803 was constructed by Schneider et al. by replacement of 260 bp region involving *petC1* gene and region upstream by chloramphenicol resistance cassette (Schneider et al., 2004a). The strain is able to perform both oxygenic photosynthesis as well as respiration but exhibits slow growth and cannot tolerate high light intensities (Kallas, 1990-2007, unpublished data; Tsunoyama et al., 2009). The strain was a gift from Dr. Dirk Schneider; Ruhr University Bochum, Germany (currently, University of Freiburg, Germany).

B] Culture Conditions and Tracking of Growth

First of all, the stock cultures of both *Synechocystis* sp. PCC 6803's wild type and ΔPetC1 mutant were checked for any possible contamination by streaking on Luria Bertani (hereafter L.B.) agar medium (Appendix A) followed by incubation at 24^0C and

37^0C for time up to a week since as per our lab experience, some fungal contaminants take a week to show visible colonies on L.B. agar plates.

The cultures, once found free of contamination were grown in liquid BG-11 medium prepared using recipe of Dr. Robert Burnap; Oklahoma State University, Stillwater (Appendix A). Simultaneously, stock cultures were also streaked on BG-11 agar plates for maintaining the strains on agar medium as well isolated colonies. Inocula used had optical densities of 3-5 at 750 nm (hereafter $O.D._{750}$) and volumes of the inocula were adjusted so that cells undergo at least 6 generations (~ 6 days) before reaching $O.D._{750}$ 0.5. Cultures were grown in 600 mL BG-11 medium in Roux flask assemblies. The medium for growing mutant was supplemented with 25 µg/mL of chloramphenicol to ensure its positive selection. The cultures were supplied air containing 3% CO_2. The Roux flask assemblies were maintained in aquariums with temperatures set at 31^0C and supplied with 50 µmol photons $m^{-2}s^{-1}$ with rotating stirrer bars to provide uniform environment to the cyanobacterial cells. Before beginning the experiments, the two strains under study were grown under the conditions mentioned above using inocula of same O.D. and their growths were measured at regular intervals.

For RT-qPCR and fluorescence kinetic experiments, the cells were grown under optimal conditions until they reach $O.D._{750}$ of 0.5. After desired O.D. were achieved, and optimal condition samples were collected and dark-anaerobic conditions were imposed by clamping of all the inlets as well as outlets, wrapping of Roux flasks by aluminum foil and turning the stirring off. Under dark-anaerobic conditions samples were collected after 1^{st}, 2^{nd}, 4^{th}, 6^{th}, 8^{th} and 12^{th} hours almost in absence of light. After 1^{st} hour dark-

anaerobic harvest and onwards, Roux flasks were bubbled with argon for 15 seconds to eliminate any air from the media which might have entered during operating valves during the harvests. For protein studies, culture growing in ^{14}N medium (test culture) was mixed with equal volume of wild type culture growing in ^{15}N medium (control culture), (Appendix A) under optimal conditions. Test culture was subjected to dark-anaerobic conditions and bubbled with argon. Control culture was maintained at $O.D._{750}$ of 0.5 by intermittent dilutions. At 12^{th} hour under dark-anaerobic conditions, similar volumes of cultures were harvested. For absorption type spectrophotometry experiments, wild type and ΔPetC1 mutant were grown under optimal conditions until they reach $O.D._{750}$ of 1.0. In case of all spectrophotometry related studies, chlorophyll contents of the strains were measured.

Volumes of cultures harvested were 80 mL for RT-qPCR studies, 150 mL for test and control cultures each for protein studies, 1 mL for fluorescence type spectrophotometry experiments (for every time point and every single wavelength of actinic light) and 8 mL for the study of absorption type spectrophotometry experiments.

C] Study of Gene Expression Using RT-qPCR

I] Isolation of crude RNA. We have been employing a method of RNA isolation using hot phenol in our lab which is a modification of method described by Köhrer and Domdey (1991). To minimize the risk of RNase contamination, all of the aqueous based reagents were treated with diethylpyrocarbonate (hereafter DEPC) for 12 hours. Cultures of wild type and ΔPetC1 mutant were grown under optimal photosynthetic conditions till

$O.D._{750}$ of 0.5 after which dark anaerobic conditions were imposed as described above. 1st hour dark anaerobic condition sample onwards, culture flasks were bubbled with argon for 15 seconds. 80 mL culture volumes harvested under optimal photosynthetic as well as under 1st, 2nd, 4th, 6th, 8th and 12th hour under dark anaerobic conditions were added to Nalgene 250 mL centrifuge bottles containing pre cooled 10X metabolic stop solution (50% equilibrated phenol, 48% 0.5 M disodium EDTA, pH 8.0 and 2% ß-mercaptoethanol by volume, Appendix B) which is 1/10th the volume of culture harvested. After vigorous shaking, samples were centrifuged at 4^0C for 15 minutes at 7,000 rotations per minute (hereafter rpm) using GSA rotor in Sorvall's RC5C centrifuge. After decanting of the supernatant, pellets were drained at -20^0C for 10 minutes. The pellets were re-suspended in 1 mL suspension buffer (300 mM sucrose and 10 mM sodium acetate, pH 4.5, Appendix B) and centrifuged at 10,000 rpm for a minute. The treatment was repeated and the pellets obtained were stored at -80^0C. These stored pellets were thawed and added with 38 µL of 0.5 M disodium EDTA, pH 8.0, 320 µL suspension buffer (300 mM sucrose and 10 mM sodium acetate, pH 4.5), 340 µL 111 mM sodium acetate and 38 µL sodium dodecyl sulfate (hereafter SDS) in the given order with gentle vortexing. After SDS addition, cells were incubated at 65^0C for 10 minutes. The step of SDS addition was followed by addition of 700 mL hot acidic phenol and incubation at 65^0C for 5 minutes. After brief cooling for 45 seconds, aqueous phases were separated from phenol by centrifugation at 10,000 rpm for 10 minutes. The aqueous phases were retained and the phenol treatment was repeated. In the next step, the aqueous phases were treated twice with equal volume of 25:24:1 phenol/chlorophorm/isoamyl

alcohol followed by centrifugation at 10,000 rpm for 10 minutes. The aqueous phases obtained in previous step were further treated twice by equal volume of 24:1 chloroform/isoamyl alcohol followed by centrifugation at 10,000 rpm for 10 minutes. To the retrieved aqueous phases, $1/4^{th}$ volume of 10 M lithium chloride and 3 times volume of absolute ethanol were added and the samples were incubated at -20^0C for an hour to allow precipitation of RNA by lithium chloride. The pellets containing crude RNA (RNA containing contaminating DNA) were obtained by centrifugation at 10,000 rpm for 10 minutes at 4^0C which were washed with 70% ethanol twice. In the end, to the pellets, 50 µL of 10 mM Tris, 0.1 mM disodium EDTA, pH 8.2 (hereafter 10T/0.1E, pH 8.2; Appendix B) was added. After re-suspension, O.D. values were measured at 260 nm by taking 1 µL crude RNA in 60 µL of distilled water. Using the formula $O.D._{260}$ 1= 44 µg/µL, concentrations of crude RNA were calculated and the tubes were stored at -80^0C. All centrifugations were carried out using Eppendorf's centrifuge 5415C unless specified. For details of the procedure, see Appendix C.

II] Removal of DNA contamination from crude RNA.

a) *First DNase treatment*. The crude RNA contains contaminating DNA molecules, amounts of which vary depending on the technique and most importantly optimum treatment with the 10.0 M lithium chloride solution. The procedure of DNA removal was scaled to treat 10 µg crude RNA and is based on Turbo DNA-*free*™ Kit manual (Applied Biosystems, 2009, part number AM1907). From the thawed crude RNA containing tube, 10 µg crude RNA was taken to which were added 5 µL 10X Turbo™ DNase buffer, 1 µL Turbo™ DNase enzyme (2 units/µL) and nuclease free water to have

total reaction volume of 50 µL. After gentle mixing, the DNase reaction tubes were incubated at 37^0C for 45 minutes followed by the addition of 5 µL Turbo^{TM} DNase inactivation reagent. After 2 minutes incubation of the reaction tubes at room temperature, the samples were centrifuged at 10,000 rpm for 2 minutes using Eppendorf's centrifuge 5415C. Supernatants were transferred to new tubes without disturbing the pellets which contain digested DNA. DNase treated RNA containing tubes were stored at -80^0C. For details of the procedure, see Appendix C.

b) *Second DNase treatment*. To ensure complete removal of the contaminating DNA from the RNA samples, DNase treatment was repeated as follow. To the sample tubes undergone first DNase treatment, second DNase digest buffer (80 mM Tris, pH 7.5, 10 mM magnesium chloride, 0.025 mM calcium chloride) (Appendix B) was added as $1/10^{th}$ of the volume of contents of the DNase treated RNA tubes along with 1 µL Turbo DNase enzyme (2 units/µL). The reaction tubes were incubated at 37^0C for 45 minutes after which $1/10^{th}$ of the volume of Turbo^{TM} DNase inactivation reagent was added. After 2 minute incubation at room temperature, samples were centrifuged at 10,000 rpm for 2 minutes using Eppendorf's centrifuge 5415C and supernatants were transferred to new tube without disturbing the pellets which might contain digested DNA. O.D. values were measured at 260 nm by taking 1 µL crude RNA in 60 µL of distilled water. Using the formula $O.D._{260}$ 1= 44 µg/µL, concentrations of crude RNA were calculated and the tubes were stored at -80^0C. For details of the procedure, see Appendix C.

III] RNA purity check.

a) *PCR and RT-PCR*. PCR and RT-PCR were set up to check the quality of DNase treated RNA. The reactions were scaled to total reaction volume of 50 µL. In tubes meant for PCR were added 4 µL RNA sample, 10 µL 5X avian myeloblastosis virus (hereafter AMV) reverse transcriptase/ *Thermus flavus* (hereafter *Tfl*) DNA polymerase 5X buffer, 5 µL of 10 mM each dinucleotides, 2.5 µL each of forward primer *rpnB*-F (5'-CCTAGCACCAATTTCCCAAG-3') and reverse primer *rpnB*-R (5'-ATTCCTCAAGCGGTTCCAC-3') present as 20 pM/µL which anneal region that is part of *rpnB* gene coding for catalytic RNA subunit of RNaseP, constitutively expressed under anaerobic conditions (Pratte et al., 2006) spanning a 456 bp region, 2 µL magnesium sulfate (25 mM), 1 µL *Tfl* polymerase (5 units/µL) and nuclease free water to adjust the reaction volumes to 50 µL. For PCR; in negative controls RNA sample was replaced by 4 µL nuclease free water while positive controls were maintained with 4 µL of 1 µg/µL of crude RNA isolated by Nelson & Kallas (2000-2007, unpublished data). In tubes meant for RT-PCR, were added all the ingredients required for PCR plus 1 µL AMV reverse transcriptase (5 units/µL). For RT-PCR, negative controls were maintained with no RNA sample while for positive control, 4 µL of 1 µg/µL of crude RNA isolated by Nelson & Kallas (2000-2007, unpublished data) were used. All the enzymes and reagents used in the procedure were purchased from Promega. The thermal cycler employed in the study was Eppendorf mastercycler gradient^{TM}. The cycling program included bringing lid temperature to 95^0C, reverse transcription cycle of 45^0C for 45 minutes, 94^0C for 2 minutes for AMV reverse transcriptase inactivation and RNA-cDNA

denaturation, 40 cycles each of 94^0C for 30 seconds, 60^0C for 1 minute and 68^0C for 2 minutes for denaturation of double stranded DNA, annealing of primers to single strands of DNA and extension of DNA respectively. Once 40 thermal cycles were completed, the cycler was programmed to maintain the sample tubes at 10^0C. The PCR and RT-PCR product tubes were stored at -20^0C. For details of the procedure, see Appendix C.

b) ***Agarose gel electrophoresis*****.** To visualize the products obtained from PCR and RT-PCR checked for quality of DNase treated RNA, agarose gel electrophoreses were performed. Gels were prepared by dissolving 1.5% agarose in 1X Tris/Borate/disodium EDTA (hereafter TBE) buffer (Appendix B). Once set, the gels were placed in BioRad's electrophoresis kits to which sufficient 1X TBE buffer was added to overlay the agarose gels. To the 5 µL PCR or RT-PCR products, 1 µL gel loading buffer (purchased from New England Biolabs) was added and the reaction tubes were incubated at 65^0C for 10 minutes followed by cooling them on ice for 5 minutes. 3 µL standard DNA ladder (100bp) purchased from Bayou was used. To the tubes containing PCR or RT-PCR products and the standard DNA ladder, 2 µL 1/1000 SYBR green I (purchased from New England Biolabs) was added and after 20 minutes incubation at room temperature under dark, the samples were loaded on gels. Voltage of 75 Volts was applied for 90 minutes. The agarose gels were scanned using BioRad Molecular Imager Fx^{TM}. For details of the procedure, see Appendix C.

IV] Complementary DNA synthesis. Once, the quality of DNase treated RNA samples was confirmed by the agarose gel electrophoreses; complementary DNA (hereafter cDNA) were synthesized. For cDNA synthesis, reactions were scaled to work

with 500 ng RNA with the total volume of 50 µL per reaction. From the thawed crude RNA tube, 500 ng RNA was taken to which were added 10 µL magnesium chloride (25 mM), 10 µL 5X AMV reverse transcriptase buffer, 5 µL of 10 mM each dinucleotides, 1 µL RNAsin Plus (40 units/µL), 1.5 µL AMV reverse trancriptase (5 units/µL), 1 µL random hexamers (0.3 µg/µL) and nuclease free water to adjust the total reaction volume to 50 µL. All of the enzymes and reagents used in the procedure were purchased from Promega. The thermal cycler employed in the study was Eppendorf mastercycler gradient™. The cycling program included bringing lid temperature to 95^0C, reverse transcription cycle of 42^0C for 45 minutes, 94^0C for 2 minutes for final extension of cDNA and inactivation of RNA and reverse transcriptase. Once thermal cycling was completed, the cycler was programmed to maintain the sample tubes at 10^0C. O.D. values were measured at 260 nm by taking 1 µL cDNA sample in 60 µL of distilled water. Using the formula $O.D._{260}$ 1= 50 µg/µL, concentrations of cDNA were calculated and the tubes were stored at -20^0C. For details of the procedure, see Appendix C.

V] Designing of primers and probes for TaqMan™ of RT-qPCR assays. For RT-qPCR studies, primers and probes were designed using PrimerExpress™, Version 3.0 and Primer3, Version 0.4.0 (Rozen & Skaletsky, 2000) with the help of Dr. Toivo Kallas and Matt Nelson. Complete genomic sequence of *Synechocystis* 6803 is available on National Center of Biotechnology Information (hereafter NCBI) website with reference number NC_000911.1. Primers and probes were designed for genes sll1316 (*petC1*), slr1185 (*petC2*), sll1182 (*petC3*), ssl0563 (*psaC*), slr1843 (*zwf*), sll1317 (*petA*) and 6803s01 (*rpnB* or alternatively *rnpB*) which code for PetC1, PetC2, PetC3 Rieske ISPs,

PS I subunit VII, glucose 6 phosphate dehydrogenase, apo-cytochrome *f* and catalytic subunit of RNase P involved in processing of tRNA respectively. The primers were designed by employing parameters as suggested by 'TaqMan^{TM} universal PCR master mix protocol' (Applied Biosystems, 2002, part number 4304449 Rev. C) such as annealing temperatures (hereafter T_m) in the range of 57-61^{0}C, 2^{0}C as maximum difference between T_m of two primers, guanine and cytosine (hereafter GC) content in the range of 45-60%, presence of G or C residue at 3' end of the primers, primer length in the range of 8-22 while for probe; the parameters used were T_m in the range of 67-70^{0}C, 5-6^{0}C as difference between T_m of primers and probe, guanine and cytosine (hereafter GC) content in the range of 45-60%, probe length in the range of 23-27 and avoiding a 'G' base at the 5' end. Statistical scores for self annealing and cross annealing between primers and probes were kept zero. When this set of criterion did not produce any results, the parameters were relaxed. For example; probe for *petC1* had to be designed with a 'G' base at its 5' end. Finally, the primers and probes were checked for similarities against *Synechocystis* 6803 genome using BLASTn search tool (Altschul, Madden, Schaffer, Zhang, Zhang, Miller, & Lipman, 1997). The designed primers and probes were synthesized and supplied by University of Wisconsin Biotechnology Center, Madison WI. The probes were synthesized with fluorescent dye 5-carboxyfluorescein, (5-FAM) at 5' end while black hole quencher dye, BHQ-1 at 3'end. Table 1 lists and shows properties of all the primers and probe designed.

Table1. Probes and primers designed for RT-qPCR

Gene	Type	Sequence	Length (bases)	%G-C content	Annealing Temp T_m (^{0}C)
petC1	Probe	GGCTCCCAGTACAACGCTGAAGGT	24	58.3	68.7
(sll1316)	F Primer	TGTGTAGTGCCCTGGAATGC	20	55.0	60.5
	R Primer	CTAATTTGTCGTCGTCGGTAAC	22	45.5	60.3
petC2	Probe	AGTGGCTGGTTTGGCTGGTGATCC	24	58.3	68.7
(slr1185)	F Primer	TGCCAAGGATGTTTTGGGTAAC	22	45.5	60.3
	R Primer	GCTACCGTCCTCTTTAACAATC	22	45.5	60.3
petC3	Probe	AACGGTAAATGTTGGTACCATGGCG	25	48.0	65.8
(sll1182)	F Primer	ATCGCTGTCATCACTGGTTG	20	50.0	58.4
	R primer	AACTCTCCCTTGGCCTTGAG	20	55.0	60.5
psaC	Probe	CTGCAAACGTTGTGAGACCGCCTG	24	58.3	68.7
(ssl0563)	F Primer	CCCTAGAACCGAGGATTGTG	20	55.0	60.5
	R primer	GTTTCGGCACCCAAATAAACTC	22	45.5	60.3
zwf	Probe	AGCCCTTTGGTCGGGATTTGAGTTCA	26	50.0	67.9
(slr1843)	F Primer	CCGGTTAAAAGTCGCATTGTG	21	47.6	59.4
	R primer	TCTGCACTACCCGGTTCAAG	20	55.0	60.5
petA	Probe	ATTGTCAGTGCCGGTCAAACTGTG	24	50.0	65.2
(sll1317)	F Primer	TACCAACTGATCCTCACCAC	20	50.0	58.4
	R primer	GGTCAAAAATTCCCCAGCTTC	21	47.6	59.4
rpnB	Probe	AAGCAAGGTCGGAGGGGCAAAG	22	59.1	65.9
(6803s01)	F Primer	GAGCGCACCAGCAGTATC	18	61.1	58.4
	R primer	AATTCCTCAAGCGGTTCCAC	20	50.0	58.4

Note: The table represents names of genes along with their locus tags, sequences of probes and primers in 5' to 3' direction with their length in bases, G-C content in percentage and annealing temperatures in Celsius in presence of 50 mM Na^+ ions.
Annealing temperatures were calculated from the formula:
$Tm = 100.5 + (41 \times (yG+zC)/ (wA+xT+yG+zC)) - (820/ (wA+xT+yG+zC)) + 16.6 \times \log_{10} ([Na^+])$.
w, x, y and z are mole fractions of adenine, thymine, guanine and cytosine nucleotides in an oligonucleotide respectively while $[Na^+]$ was considered 50 mM.

VI] Primer-probe validation and efficiency studies. Before performing gene expression studies by RT-qPCR, it is important to validate the primers and probe designed which is essential for the normalization of results obtained from each primers-probe set as will be explained further. The protocol used for primer-probe validation and efficiency studies, was based on one suggested by 'TaqMan^{TM} universal PCR master mix protocol' (Applied Biosystems, 2002, part number 4304449 Rev. C). The reactions were scaled to total volume of 20 µL. In place of DNA, crude RNA which contains crude

RNA-DNA mixture was serially diluted over five $\log_{10}$ dilution points (100 ng/µL to 10 pg/µL). Thus, for every primer-probe set, 6 tubes were maintained including a negative control. Every tube contained 1 µL of crude RNA-DNA mixture as template, 10 µL Applied Biosystem's 2X universal master mix, 1 µL of forward and reverse primer (20 pM/µL), 0.25 µL probe (20 pM/µL) and nuclease free water to adjust the total reaction volume to 20 µL. Negative control tube did not have RNA template. Thermal cycling was carried out using Applied Biosystem's StepOnePlus™ real time PCR system. It involved first cycle of 95^0C for 10 minutes for activation of DNA polymerase followed by 40 cycles each of 95^0C for 15 seconds for denaturation of double stranded DNA and 60^0C for 1 minute for annealing and extension of primers. The validation reactions were carried out in triplicates using 'Quantitation relative standard curve' program. Thresholds for threshold cycle (hereafter C_T) values obtained were adjusted to 0.05 for all primer-probe sets after verifying that, threshold lies on the exponential phase of the amplification curve. Using the means of C_T values obtained for every dilution point for every primer-probe set, standard graphs were plotted as log of concentration of template in pg on X axis versus mean C_T values on Y axis. The y= mx+c equations obtained from the plots were further used for estimation of amounts of target genes in relation to each other in terms of $\log_{10}$ of concentration (pg/µL) i.e. results from gene expression assays were normalized. Note that; *Synechocystis* 6803 possesses only single copy of the genes under study making the process of normalization easier. For details of the procedure, see Appendix C.

VII] RT-qPCR; TaqMan™ gene expression assays (Standard Curve method). The protocol used for gene expression assays was based on one suggested by Applied Biosystem's 'Relative standard curve and comparative C_T experiments' protocol (Applied Biosystems, 2007, part number 4376785 Rev. D). The reactions were scaled to a total volume of 20 µL. Each reaction tube contained 2 µL cDNA sample, 10 µL Applied Biosystem's 2X universal master mix, 1 µL of forward and reverse primer (20 pM/µL), 0.25 µL probe (20 pM/µL) and nuclease free water to adjust reaction volume to 20 µL. Negative control tube did not have cDNA template. Thermal cycling was carried out using Applied Biosystem's StepOnePlus™ real time PCR system. It involved first cycle of 95^0C for 10 minutes for activation of DNA polymerase followed by 40 cycles each of 95^0C for 15 seconds for denaturation of double stranded DNA and 60^0C for 1 minute for annealing and extension of primers. Every sample per biological replicate was tested in triplicate using 'Comparative C_T; $\Delta\Delta C_T$' method. C_T values obtained were adjusted to 0.05 for all samples after verifying that, threshold lies on the exponential phase of the amplification curve. Means of C_T values obtained for three biological replicates were taken for every time point studied during the course of experiment. The gene expression levels were normalized based on equations obtained from standard curves during primer-probe validation step, plotted as $\log_{10}$ values of genomic DNA concentration ($\log_{10}$ 1 to 5 for 10 pg/µL to 100 ng/µL) vs. C_T values for every gene. This way; C_T values could be converted to $\log_{10}$ of concentration (pg/µL). Since all of the genes under study occur as a single copy on chromosomes, normalization becomes relatively easier. Graphs representing gene expression pattern were plotted as relative

gene expression on $\log_2$ scale against the hours of harvest of cultures from optimal photosynthetic condition at $O.D._{750}$ 0.5 as '0 hour' to 12^{th} hour under dark-anaerobic conditions as '12^{th} hour'. For details of the procedure, see Appendix C.

D] Metabolic Labeling and Isotope Assisted Quantitative Mass Spectrometry

I] Metabolic labeling and isolation of membrane proteins. Transcript levels are not always reflected in the protein levels. Hence, to answer the questions whether levels of electron transfer chain components are following the change in transcript levels after shift from optimal photosynthetic conditions to dark anaerobic conditions and whether the wild type strain and ΔPetC1 mutant vary in their electron transfer chain contents, proteomic approach of metabolic labeling and quantitative mass spectrometry was followed. The protocol used for the protein work was contributed by Dr. Frauke Baymann, Dr. Toivo Kallas, Matt Nelson and Dr. Edward Huttlin based on original protocol by Nelson, Huttlin, Hegeman, Harms & Sussman (2007). Cell cultures, both wild type and ΔPetC1 were grown (test cultures) in regular BG-11 medium containing ^{14}N sodium nitrate (Appendix A) until $O.D._{750}$ reached 0.5 after which dark anaerobic conditions were imposed. Simultaneously, a wild type culture was maintained at $O.D._{750}$ 0.5 in BG-11 medium containing ^{15}N sodium nitrate (Appendix A) with cells grown in presence of ^{15}N for at least 25 generations as the control. 150 mL volumes of test cultures under optimal photosynthetic conditions as well as under 12^{th} hour dark anaerobic conditions were mixed with equal volume of control culture growing under optimum photosynthetic conditions. The purpose behind taking a sample of ^{14}N grown wild type

strain under optimal photosynthetic conditions with ^{15}N grown wild type strain as control was to see whether the same strain grown in ^{14}N and ^{15}N medium shows any difference in protein levels. Cells were pelleted by centrifugation at 8,500 rpm for 10 minutes using SLA3000 rotor in Sorvall's RC5C plus centrifuge. The pellets were re-suspended in 15 mL of 5 mM HEPES-NaOH, pH 7.5 buffer and re-centrifuged in PPCO Oakridge tubes using SS34 rotor in Sorvall's RC5C centrifuge. To the pellets obtained, were added 10 mL of 5 mM HEPES-NaOH, pH 7.5 buffer along with the DNase to final concentrations of 30 μg/mL, protein inhibitors such as 2 mM dithiothreitol (hereafter DTT), 0.5 mM 4-(2-Aminoethyl) benzenesulfonyl fluoride hydrochloride (hereafter AEBSF), 1 mM amino caproic acid, 1 mM benzamidine, 1 μM pepstatin A, 10 μM leupeptin, 1 μM L-trans-epoxysuccinyl-leucylamido(4-guanidino)butane (hereafter E-64) and 1 μM bestatin. The cell suspensions were passed slowly with the rate of 1 drop/second through American Instrument Company's French pressure cell press at 20,000 psi. The step of cell press was repeated twice. The pressed cells were then centrifuged at 6,000 rpm for 10 minutes to separate cell debris and cell wall fragments from supernatant containing membrane vesicles and soluble proteins using SS34 rotor in Sorvall's RC5C plus centrifuge. Supernatants containing proteins were added to polycarbonate tubes (16-20 mL per tube) and centrifuged at 50,000 rpm for 1 hour at 4^0C using 70Ti rotor in Beckman's L8-M ultracentrifuge to separate soluble proteins from membrane proteins. Pellets containing membrane proteins were re-suspended using 16 mL of 50 mM ammonium bicarbonate and centrifugation was repeated. The pellets were finally re-suspended in 500 μL of 50

mM ammonium bicarbonate and protein contents were estimated as discussed separately. For details of the procedure, see Appendix C.

II] Estimation of membrane protein concentration. The procedure used for estimation of membrane proteins was adapted by Dr. Toivo Kallas based on instructions of Pierce's BCA™ protein assay kit (Pierce, 2008, kit number 23227). Membrane protein fractions re-suspended in 500 µL of 50 mM ammonium bicarbonate were diluted to 1:50 using 5% sodeium dodecyl sulfate (hereafter SDS). From the bovine serum albumin (hereafter BSA) stock of 2 mg/mL, a series of standards were prepared using distilled water ranging from 0.2 -2 mg/mL along with a negative control. BCA working solution was prepared by mixing 'Reagents A and B' in ratio of 50:2. Reagent A contains sodium carbonate, sodium bicarbonate, bicinchoninic acid and sodium tartrate in 100 mM sodium hydroxide while Reagent B contains 4% cupric sulfate. Using 0.5 mL of BCA working solution to 25 µL of standards, blank and samples with only 5% SDS as control and the tubes were heated at 37°C for 30 minutes. After setting up the blank, absorbance of standards followed by the samples and 5% SDS control were measured at 562 nm. For membrane protein fractions, absorbance shown by 5% SDS control was subtracted from those shown by protein fractions. A standard curve was plotted as concentration of standards against the absorbance. For details of the procedure, see Appendix C.

III] Trypsin digestion of bulk membrane proteins and C18 column purification. As suggested by Pischke, Huttlin, Hegeman & Sussman (2006); to the 100 µL bulk membrane protein fractions (9-11 µg/µL protein concentrations), equal volume of methanol was added along with the Promega's porcine trypsin in the ratio 1:40 w/w

with proteins. The reaction tubes were incubated at 37^0C for 24 hours with gentle shaking. After trypsin digestion step, formic acid was added to 5% (v/v) final concentration. Varian Spec C18 columns (200-250 µg peptide binding range) were equilibrated twice with 1 mL of 90% acetonitrile, 0.1% formic acid followed by equilibration with 0.1% formic acid. Peptide samples were bound to the column by passing them through the column 10 times, which was further washed with 0.3% formic acid. Finally, peptides were eluted with 50 µL of 90% acetonitrile, 0.1% formic acid twice, elutes were dried using a Labconco's centrivap concentrator and were re-suspended in 0.3% formic acid to 1 µg/µL final protein concentration.

IV] Liquid chromatography- tandem mass spectrometry. Liquid chromatography- tandem mass spectrometry (hereafter LC-MS/MS) was carried out on an Agilent 1100 series system coupled with Bruker Daltonics' esquire3000plus™ ion trap mass spectrometer. 20 µL of the sample proteins were loaded onto Zorbax 300 SB-C18 column (3.5 µm, 50 × 0.3 mm). The solvents used as mobile phases were 0.1% formic acid/distilled water (solvent A) and 80% acetonitrile, 0.1% formic acid (solvent B). The following gradient program was selected: 0−20 min 98% solvent A (15 µL/min), 20.01−135 min 50% solvent A (100 µL/min), 135.01−145 min 2% solvent A (200 µL/min), 145.01-170 min 2% solvent A (10 µL/min). Pressure through the column was maintained at 50+/-5 bars. Flow of elutes from the LC column into mass spectrometer was set at ~4 µL/min. Electrospray ionization voltage was set at 2.0 kV in positive mode. Temperature of the ion transfer capillary was set at 325^0C. The ion trap mass spectrometer was operated in data dependant operation mode with esquireControl

software. MS scans were acquired in the range of 50-3000 *m*/*z* followed by 2 data dependant MS/MS scans in the ion trap from the 4 most abundant ions.

The acquired files from mass spectrometer were converted into mgf format. The mgf files were searched against 6803 Genbank database through Mascot Daemon (version 2.2.00) allowing one missed cleavage site. Oxidation of methionine, deamidation of aspargine and glutamine were selected as variable modifications. The mass tolerance for MS was set at 1.2 Da and the mass tolerance for MS/MS was set at 0.8 Da. Using the data obtained from Mascot daemon, for every protein identity, extracted ion chromatograms were plotted using a function of esquireControl software for light and heavy peptides showing maximum MOWSE scores which are derived from. Probability of matching MS peaks by random chance (Pappin, Hojrup & Bleasby, 1993). Peak heights of the chromatograms were used to compare the relative levels of the respective proteins. For details of the procedure, see Appendix C.

E] Kinetics Measurement and Quantification of Electron Transfer Chain Components

To compare the relative amounts of PS I and cyochrome *bf* components such as cytochrome b_6, plastocyanin and cytochrome *f* in wild type strain and ΔPetC1 mutant, kinetics, absorbance spectrophotometry experiments were performed. Cultures of the wild type strain and ΔPetC1 mutant were grown until O.D. $_{750}$ reached 1.0. 8 mL of the cultures were taken in 15 mL conical tubes and centrifuged at 3,900 rpm for 10 minutes using Beckman's GP centrifuge. The pellets obtained were re-suspended in re-suspension

buffer (10% Ficoll, 10 mM sodium chloride, 5 mM HEPES, pH 7.5) (Appendix B) to concentrate cells 4 times. The concentrated cells were loaded into cuvette with 1 cm light path and redox kinetics were studied using BioLogic Joliot type spectrophotometer JTS-10. In the method, cells in the cuvette were continuously illuminated by actinic light emitting diode (hereafter LED) with 590 μE $m^{-2}s^{-1}$ intensity for 10 seconds in order to achieve complete reduction of cytochrome b_6 while complete oxidation of cytochrome *f*, plastocyanin and PS I followed by a dark phase. Previous trial experiments had shown very minimal positive differences (less than 5%) in maximum extents of oxidations and reductions obtained with actinic light intensity of 590 μE $m^{-2}s^{-1}$ over that of 300 μE $m^{-2}s^{-1}$. Absorption changes were recorded using 546 nm, 554 nm, 563 nm and 573 nm interference filters for *b* heme (cytochrome b_6), cytochrome *f*, plastocyanin studies with 'BG39' (3 mm) cut off filters before the detectors. For PS I, absorption changes were detected using 705 nm interference filter with 'P700' cut off filters before the detectors. Detections were made in reference to probing light that has not passed through the sample and absorption values were recorded in presence of voltage close to 4.0. The spectra were recorded in triplicates per interference filter to obtain a 'mean spectrum'. To avoid inclusion of absorption changes taken place in presence of probing light into the final spectra; after every spectrophotometric experiment, actinic light source was turned off and spectra were recorded in triplicates in presence of probing light passed through every interference filter. The mean spectra obtained in absence of actinic light were then subtracted from the mean spectra obtained in presence of actinic LED. After these subtractions, the kinetic data obtained using 546, 554, 563 and 573 nm interference filters

were deconvoluted using a function of the operating software for the spectrophotometer to obtain individual kinetics spectra for cytochrome b_6, cytochrome *f* and plastocyanin. Finally, the results were assessed and maximum extents of reduction in case of cytochrome b_6 while maximum extents of oxidation for cytochrome *f*, plastocyanin and PS I were recorded. The kinetics data are represented as time in seconds on X axis and dI/I on Y axis where dI = I_{ref} (light intensity recorded by reference detector) – $I_{measurement}$ (light intensity after passing through the sample detected by sample detector) / $I_{reference}$ (light intensity recorded by reference detector). Also, using a function of the operating software, the data was converted into Microsoft Excel format. Using formula | [-0.43 (maximum value of dI/I) / 10^6] cm^{-1} ÷ [extinction coefficient] $mM^{-1}cm^{-1}$| for cytochrome b_6 and plastocyanin while a slightly different formula | [-0.43 (minimum value of dI/I) / 10^6] cm^{-1} ÷ [extinction coefficient] $mM^{-1}cm^{-1}$| for cytochrome *f* and PS I, the amounts of electron transfer chain components in pM were calculated (Personal communication between Dr. Toivo Kallas and Zohra Mana (2007), Application specialist of Biologic). Considering both strains, value of wild type strain's cytochrome *f* was taken as 1.0 and the values of contents of remaining electron transfer chain components were normalized to 1.0. For details of the procedure, see Appendix C.

F] Catalytic Efficiencies of the PetC1 and PetC2 Rieske Iron-Sulfur Proteins.

To compare the catalytic efficiencies of PetC1 and PetC2 Rieske ISPs, another absorption type spectrophotometry experiment was performed. Cultures of wild type strain were grown until $O.D._{750}$ reached 1.0. 8 mL of the cultures were taken in 15 mL

conical tubes and centrifuged at 3,900 rpm for 10 minutes using Beckman's GP centrifuge. The pellets obtained were re-suspended in re-suspension buffer (10% Ficoll, 10 mM sodium chloride, 5 mM HEPES, pH 7.5) (Appendix B) to concentrate cells 4 times. The concentrated cells were loaded into cuvette with 1 cm light path and redox kinetics were studied using BioLogic's Joliot type spectrophotometer JTS-10. In the method, cells in the cuvette were continuously illuminated by actinic LED with 14, 37, 80, 150 and 300 μE $m^{-2}s^{-2}$ intensity for 9 milliseconds followed by a dark phase. Absorption changes were detected using 546 nm, 554 nm, 563 nm and 573 nm interference filters for *b* heme (cytochrome b_6), cytochrome *f* and plastocyanin studies with 'BG39' cut off filters before detectors. Detections were made in reference to probing light that has not passed through the sample and absorption values were recorded in presence of voltage close to 4.0. The spectra were recorded 30 times per interference filter per actinic light intensity to obtain a 'mean spectrum'. To avoid inclusion of absorption changes taken place in presence of probing light into the final spectra; after every spectrophotometric experiment, actinic LED was turned off and spectra were recorded in presence of only probing light for every interference filter 30 times. The mean spectra obtained in absence of actinic light were then subtracted from the mean spectra obtained in presence of actinic LED. After these subtractions, the kinetic data obtained using 546, 554, 563 and 573 nm interference filters was deconvoluted using a function of the operating software for the spectrophotometer to obtain individual kinetics spectra for cytochrome *f* along with those of cytochrome b_6 and plastocyanin. Finally, the results were assessed and the actinic light intensities which enabled to obtain spectra with

minimum noise were chosen. The kinetics data is represented as time in seconds on X axis and dI/I on Y axis where dI = I_{ref} (light intensity recorded by reference detector) – $I_{measurement}$ (light intensity after passing through the sample detected by sample detector) / $I_{reference}$ (light intensity recorded by reference detector). Half times of re-reduction were calculated using a function of the operating software for the spectrophotometer. Also, using a function of the operating software, the data was converted into Microsoft Excel format. For details of the procedure, see Appendix C.

G] Impact of the PetC1 Mutation and Dark Anaerobiosis on PQ pool Redox State.

I] Estimation of chlorophyll content. Chlorophyll contents of the cultures were estimated using a procedure and equation based on that of Porra, Thompson & Kriedmann (1989) as modified by Dr. Toivo Kallas. 1 mL culture samples were concentrated 20 times by centrifugation at 14,000 rpm for 15 minutes using an Eppendorf centrifuge 5415C. 50 µL of the concentrated culture samples were mixed with 950 µL methanol. After 5 minutes of gentle mixing by tilting in the dark, samples were centrifuged at 14,000 rpm for 5 minutes. Supernatants were collected and absorption values were recorded at 665.2 nm and 750 nm. The equation used for determining chlorophyll content was: Chlorophyll (µM) = [(Absorption 665.2 nm – Absorption 750 nm) / 71.43] × [1000/50] × 1000. For details of the procedure, see Appendix C.

II] Impact of the PetC1 mutation and dark anaerobiosis on PQ pool redox status. To study the impacts of ΔPetC1 mutation and dark anaerobic conditions on the redox state of PQ pool, which reflects electron transfer activity of cytochrome *bf*

complex, fluorescence spectrophotometry experiment was performed. Cultures of wild type and ΔPetC1 mutant were grown under optimal photosynthetic conditions till $O.D._{750}$ of 0.5 after which dark anaerobic conditions were imposed as described. Chlorophyll contents were measured using procedure derived from Porra et al. (1989). 12 mL culture volumes were harvested (2 mL × 6, 15 mL conical tubes) at every time point (1 mL for every actinic light intensity) and fluorescence experiments were performed from optimal photosynthetic conditions to 1^{st}, 2^{nd}, 4^{th}, 6^{th}, 8^{th} and 12^{th} hour under dark anaerobic conditions. Samples collected for dark anaerobic conditions were bubbled with argon for 5 seconds. Also, 1^{st} hour dark anaerobic condition onwards, culture flasks were bubbled with argon for 15 seconds. The cells were loaded into cuvette with 1 cm light path and chlorophyll fluorescence was studied using BioLogic's Joliot type spectrophotometer JTS-10 with 'BG39' (6 mm) cut off filter before reference detector and fluorescence specific 'Fluo' cut off filter before sample detector. In the method, cells in the cuvette were dark adapted for 115 seconds to ensure cells stay in state II. The first phase was followed by exposure of the cultures to continuous actinic light intensities of 14, 37, 80, 150, 300 and 590 μE $m^{-2}s^{-1}$ for 70 seconds. Second phase is followed again by the dark phase of 230 seconds. For every time point, different culture samples were used for different light intensities mentioned above. Throughout the experiment, cultures were illuminated with short (200 ms) intense pulses of 7900 μE $m^{-2}s^{-1}$ followed by short pulses (10 μs) of weak probing light to detect the maximum fluorescence at those points. The fluorescence detected is given by PS II since PS I fluoresces only above 725 nm. Fluorescence is recorded as time in seconds on X axis and fluorescence units on Y axis

which is a relative measurement of I_{fluo} (light intensity after passing through the sample and recorded as fluorescence by measurement detector). / I_{ref} (light intensity recorded by reference detector). Using a function of the operating software, the data was converted into Microsoft Excel format. From the fluorescence spectra obtained, *F*m' (maximum fluorescence value elicited by saturating light pulse during continuous illumination by actinic light) and *F*s (steady state fluorescence value exhibited by chlorophyll) values were recorded. *F*s values at the beginning of continuous illumination, after first saturating flash i.e. *F*s1 and at the end of illumination, after last saturating flash i.e. *F*s2 were recorded. Two values of quantum efficiency were calculated per spectrum using formula ΦPSII = (*F*m' –*F*s)/ *F*m' (Evans, 1986) where *F*s value was taken either *F*s1 or *F*s2. Hence, two separate graphs (at the beginning of continuous actinic illumination and at the end of continuous actinic illumination) were plotted for every time of harvest, for both strains as continuous actinic light intensity on X axis and quantum efficiency on Y axis. For details of the procedure, see Appendix C.

RESULTS

A] Growth Kinetics of *Synechocystis* sp. PCC 6803 Wild type and ΔPetC1 Strains

To compare the growth rates of the two strains used in this study, cultures were grown in Roux flasks as described in Materials and Methods and culture turbidity ($O.D._{.750nm}$) was recorded at regular intervals as shown in Figure 8.

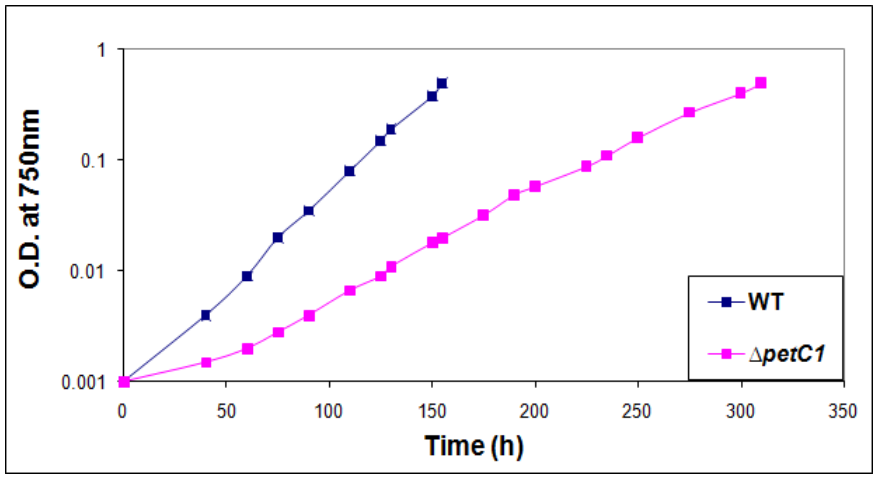

Figure 8: Growth of wild type and ΔPetC1 strains of *Synechocystis* 6803

The plot shows growth curves for the wild type and ΔPetC1strain (measured as OD_{750nm}) grown under optimal photosynthetic conditions (50 µE m^{-2} s^{-1}light intensity, 31^0C, 3% CO_2)

As shown in Figure 8, the wild type strain grew faster than the ΔPetC1 mutant reaching an $O.D._{.750}$ of 0.5 in 155 hours relative to 310 hours for the mutant. The generation time of the wild type strain was calculated to be ~16 hours while that of the ΔPetC1 mutant was calculated ~48 hours.

B] Gene Expression Studies with Reverse-Transciptase Quantitative PCR (RT-qPCR)

I] cDNA synthesis from DNA-free RNA. As described in the Materials and Methods, crude RNA was initially isolated from the harvested cells. The yield of crude RNA isolated from 80 mL of the cultures varied from 0.96 to 3.27 μg/μL while the average concentration was approximately 1.8 μg/μL in total volume of 50 μL. Although the lithium chloride used in the last step of RNA isolation precipitates a small amount of DNA, the crude RNA still contains contaminating DNA and each sample underwent DNA removal treatment twice to obtain DNA-free RNA. Yields of DNA-free RNA were 68-90% of the crude RNA with an average yield of ~78%. To ensure the quality of the DNA-free RNA, PCR and RT-PCR were carried out on every sample. Products of these reactions were run on agarose gels along with positive and negative controls comprised of crude RNA-DNA from wild type *Synechocystis* 6803 and nuclease free water, respectively. RNA samples that underwent PCR reactions did not produce any bands indicating successful removal of contaminating DNA, while RNA samples used in RT-PCR produced visible bands indicating the presence of high quality RNA in these samples. Representative agarose gels of PCR and RT-PCR products from RNA obtained from both the wild type and ΔPetC1 mutant along with positive and negative reaction controls are shown in Figure 9.

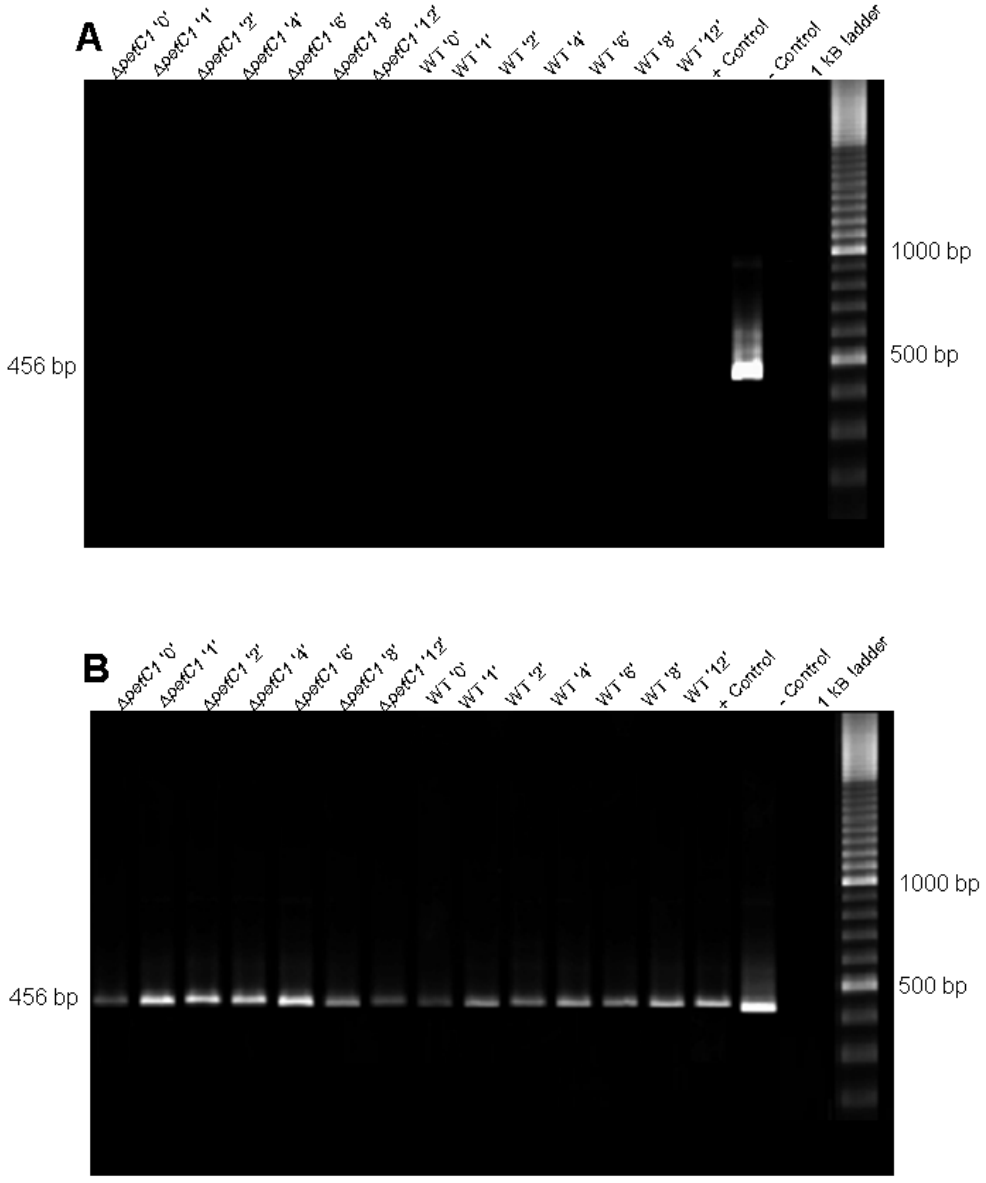

Figure 9: RNA quality tests. Panel A: PCR products**; Panel B:** RT-PCR products

Electrophoreses were performed in 1.5% agarose gels, 1X TBE buffer as described in Materials and Methods. Labels indicate the strain and time of RNA harvest from 0 hours (optimal photosynthetic conditions) to 1 – 12 hours after shifts to dark-anaerobic conditions. Shown also are positive and negative controls, and size standards (1 kb ladder, Bayou Biolabs).

As shown in Figures 9A and 9B, PCR amplification of purified RNAs did not show any bands while RT-PCR reactions showed 456 bp amplification bands as defined by the

rpnB forward and reverse primers. These data indicate the absence of any contaminating DNA and good quality of the RNA samples. DNA-free RNAs were used to synthesize cDNA.

II] Primer-probe design and efficiency tests. Primers and probes were designed for the genes under study as listed in Table 1 following parameters as suggested by 'TaqMan^{TM} universal PCR master mix protocol' (Applied Biosystems, 2002, part number 4304449 Rev. C) which include avoiding of a 'G' strand at 5' end of a probe which can quench the fluorescence. By mistake, *petC1* probe designed had a 'G' base at its 5' end. Primer-probe efficiency checks were performed thrice using 'crude RNA' wild type *Synechocystis* 6803 (isolated by Matt Nelson) as the template which was diluted over five $\log_{10}$ dilution values. Means of C_T (cycles to threshold) values obtained for each point were taken to draw standard curves for each primer set. Table 2 lists efficiency values obtained for all primer-probe sets together with the equations of the standard curves. These equations were used to derive relative values of transcripts expression levels obtained during assays.

Table 2. Mean efficiencies and standard curve equations for primer-probe sets

Primer-probe set	Efficiency (%)	Equation
petC1	94.212	y = -3.5346x + 38.801
petC2	86.941	y = -3.8302x + 37.850
petC3	95.541	y = -3.4854x + 35.883
psaC	92.142	y = -3.6140x + 36.456
zwf	95.684	y = -3.4802x + 36.480
petA	90.669	y = -3.6727x + 37.713
rpnB	88.921	y = -3.7449x + 39.342

Table shows primer-probe sets tested for each gene along with the mean target amplification efficiencies derived from the equation $C_n = Ci \times (1+E)^n$ where n is number of cycles, C_i is initial copy number, C_n is copy number at cycle n and E is efficiency of target amplification. Hence if E = 1 or 100%, $C_n = C_i \times 2^n$ i.e. product will be doubled each amplification cycle (Applied Biosystems, 2008, publication number 136AP01-01). Equations obtained from standard curves are in the format y = mx+c.

Quantitative PCR thresholds were set at 0.05 and target amplification efficiencies were within 10% of each other. Each individual efficiency curve as well as ones obtained from means for primer-probe tests had R^2 values between 0.99 to 1.0. C_T values for particular concentrations of template for a primer-probe set were found very close with standard deviations less than 1.67 as suggested by the Applied Biosystem's application note (Applied Biosystems, 2008, publication number 136AP01-01). These data demonstrated high confidence in the derived equations for estimation of relative concentrations of template genes in the efficiency tests.

III] RT-qPCR; TaqMan^{TM} gene expression assays (Standard Curve method). RT-qPCR assays were used to study the responses of Rieske iron-sulfur protein isoform genes, and related electron transport and catabolism genes to dark anaerobic conditions. As explained in Materials and Methods, the assays each involved three biological replicates. Mean C_T values obtained from the biological replicates were compared to standard curve equations obtained for each primer-probe set to obtain relative expression levels of target genes. These data were plotted to show the time course of gene expression in response to transitions to dark conditions. Figures 10A and 10B summarize the results of mean gene expression levels (shown for clarity without standard deviation, error bars) for the wild type and ΔPetC1 strains of *Synechocystis* 6803, respectively. In addition, figures 11A to 11G show the same gene expression results in wild type and ΔPetC1 strain plotted individually along with error bars. Note that gene expression results obtained from the three biological replicates are fairly consistent with respect to each other (standard deviations of the means varied from 0 to +/- 2.2). These values reflect variances

in the qPCR C_T values, which are the numbers of amplification cycles required to reach a pre-determined signal threshold value of 0.05. A difference of 1.0 between two C_T values indicates a two-fold great transcript level in one of the samples.

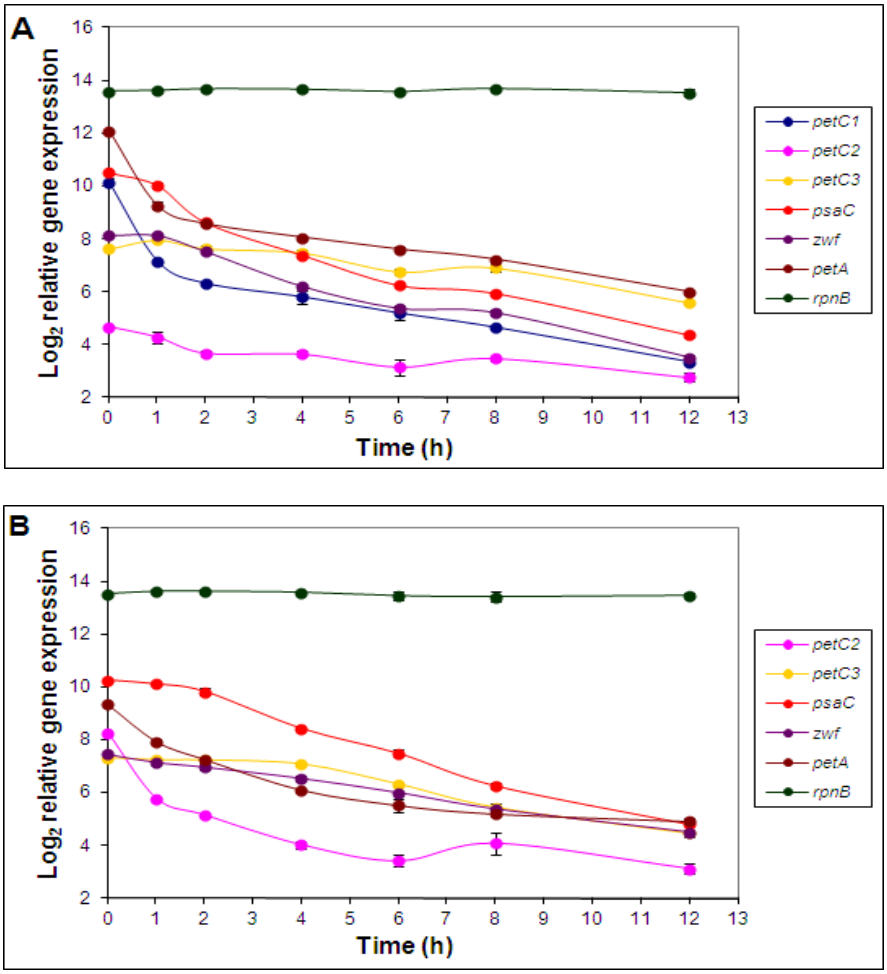

Figure 10: Relative gene expression levels under optimal photosynthesis and after shifts to dark anaerobiosis (Standard Curve method). Panel A: Wild type strain**; Panel B:** ΔPetC1 mutant

Mean $\log_2$ gene expression data from 3 biological replicates shifted from optimal photosynthesis (at 0 hours) to dark anaerobic conditions are represented. Gene expression levels were normalized based on equations (Table 2) of the standard curves plotted as $\log_{10}$ values of genomic DNA concentration ($\log_{10}$ 1 to 5 for 10pg/µl to 100ng/µl) vs. C_T values for each primer-probe set. Textboxes detail the genes under study.

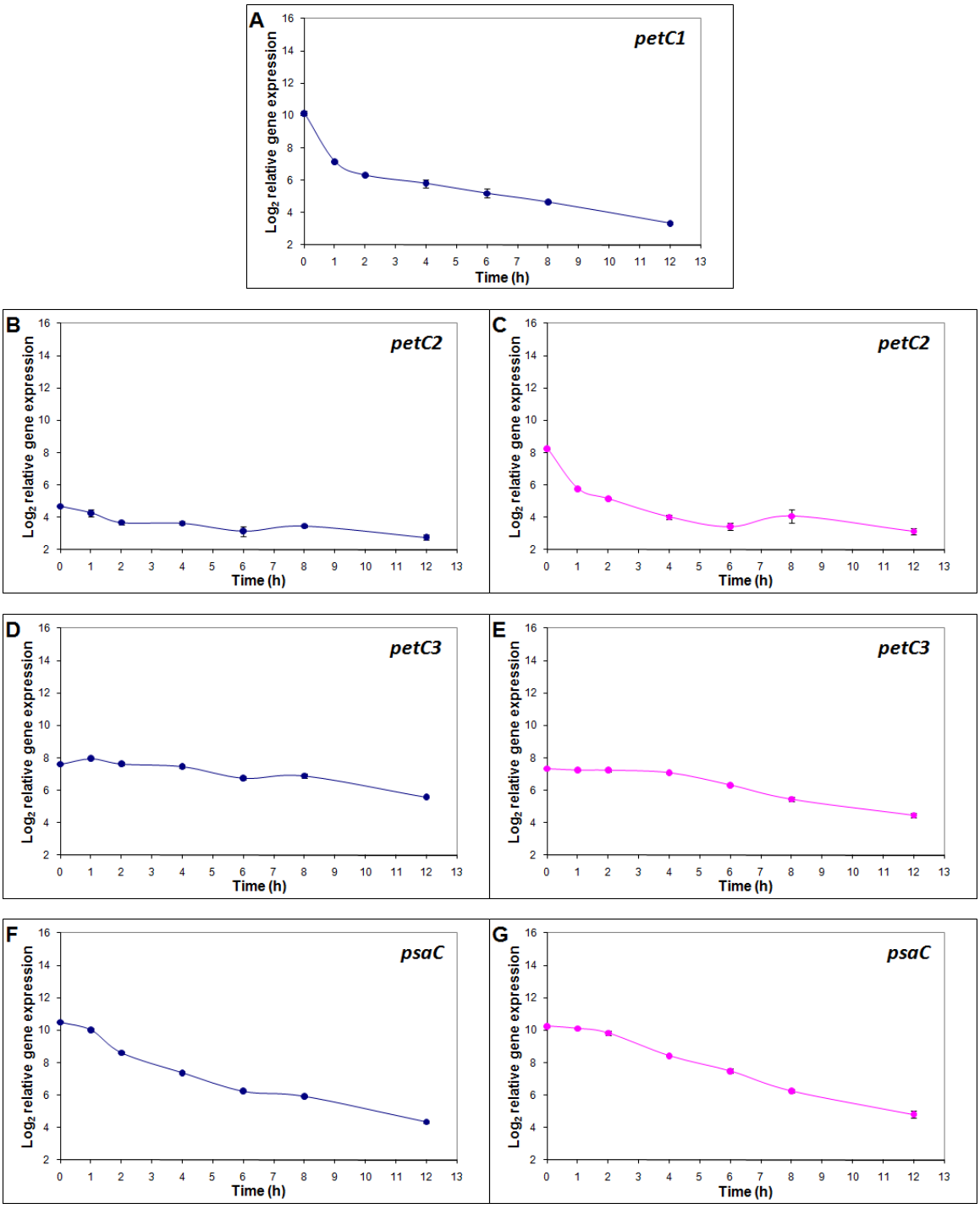
A
petC1
B
petC2
C
petC2
D
petC3
E
petC3
F
psaC
G
psaC
Log2 relative gene expression
Time (h)

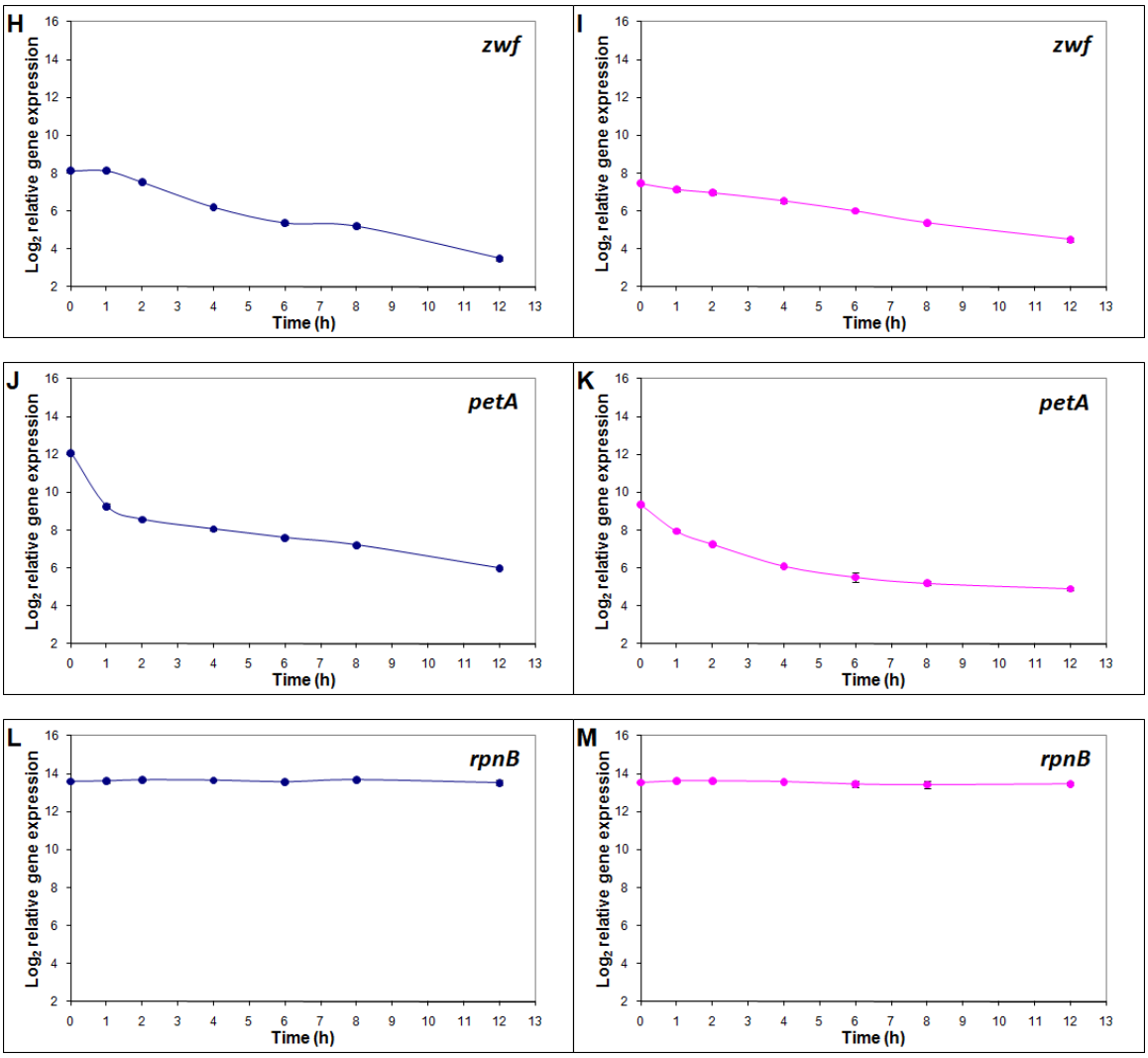

Figure 11: Individual plots of gene expression under optimal photosynthesis and after shifts to dark anaerobiosis (Standard Curve method). Panel A: *petC1*; Panels B and C: petC2; Panels D and E: *petC3*; Panels F and G: *psaC*; Panels H and I: *zwf*; Panels J and K: *petA*; Panels L and M: *rpnB*

Mean $\log_2$ gene expression values from 3 biological replicates shifted from optimal photosynthesis (at 0 hours) to dark anaerobic conditions are represented (without error bars). Panels A, B, D, F, H, J and L represent gene expression data for the wild type strain (shown as blue lines) while panels C, E, G, I, K and M represent gene expression data for the ΔPetC1 mutant (shown as pink lines). Gene expression levels were normalized based on equations (Table 2) of the standard curves plotted as $\log_{10}$ values of genomic DNA concentration ($\log_{10}$ 1 to 5 for 10 pg/µl to 100 ng/µl) vs. C_T values for each primer-probe set.

As evident from Figures 10A and 10B, under dark anaerobic conditions, genes under study were down regulated in both the wild type and ΔPetC1 mutant strains of *Synechocystis* 6803. In the wild type strain, under optimal photosynthetic conditions, transcript level of *petC1* was ~44 times higher (log_2 difference of 5.47) than that of *petC2* (Figure 10A). Also; down regulation of *petC2* was not as prominent as that of *petC1* and after 12 hours in darkness, transcript level of *petC1* remained only ~1.50 times higher (log_2 difference of 0.58) than that of *petC2* (Figure 10A and 11A, 11B). But, in the ΔPetC1 mutant; under dark anaerobic conditions, down regulation of *petC2* was prominent. After 12 hours in darkness, the level of *petC2* transcript was ~35 times (log_2 difference of 5.13) down regulated compared to that observed under optimal photosynthetic conditions. After 2 hours under dark anaerobic conditions, the level of *petC2* transcript in the ΔPetC1 mutant exceeds that in the wild type strain and finally, after 12 hours, the level of *petC2* transcript in ΔPetC1 mutant was ~1.29 times higher (log_2 difference of 0.37) compared to that in the wild type strain (Figures 10A, 10B and 11A-11C). Based on previous observations of up regulation of *petC2* and *petC3* transcript levels under stress (Houot et al., 2007; Summerfield et al., 2008; Tsunoyama et al., 2009), I expected similar results in this study. But, in the wild type strain; the *petC2* transcript level under dark-anaerobic conditions neither exceeded that under optimal-photosynthetic conditions, nor it did exceed *petC1* transcript level at a given time point (Figures 10A, 10B and 11A-11C).

ΔPetC1 mutant has seemed to compensate for the loss of the PetC1 Rieske ISP by up-regulating the *petC2* gene. The *petC2* transcript level in the ΔPetC1 mutant was ~12

times (log_2 difference of 3.58) higher than that of *petC2* gene in the wild type strain (Figures 10A, 10B and 11B, 11C) at optimal photosynthetic conditions. These data are consistent with the microarray results of Nelson & Kallas (2000-2007, unpublished data) and immunoblot results of Tsunoyama et al. (2009) and Schultze et al. (2009). At any time point under study, the combined transcript levels of *petC1* and *petC2* genes were always greater in the wild type strain than those of *petC2* gene in the ΔPetC1 mutant (Figures 10A, 10B and 11A-11C). Levels of the *petC3* transcript were similar until 4th hour under dark anaerobic conditions for both strains after which the difference in the transcript levels increases gradually until the 12th hour under dark anaerobic conditions. Also, *petC3* transcript levels under these conditions exceedeed individual levels of *petC1* and *petC2* transcripts in both strains (Figures 10A, 10B and 11A-11E) suggesting that PetC3 has an essential, perhaps regulatory role for cell survival, regardless of the ΔPetC1 mutation.

Under optimal photosynthetic conditions, the *petA* transcript level (which codes for apocytochrome *f*, the precursor of cytochrome *f*) was ~6.64 times (log_2 difference of 2.73) higher in wild type strain than the ΔPetC1 mutant. The higher transcript level of *petA* in the wild type relative to ΔPetC1 was maintained throughout the experiment (Figures 10A, 10B and 11J, 11K). Down-regulation of *petA* in the mutant appears to arise from disruption of the mRNA transcript for co-transcribed *petC1* and *petA* genes resulting from construction of the ΔPetC1 mutant (Schneider et al., 2004a). Lower *petA* transcription in the ΔPetC1 mutant has been previously shown by microarray results of Nelson & Kallas (2000-2007, unpublished data) and is in accord with the immunoblot

results of Schultze et al. (2009) and my spectrophotometric data (shown below). In the wild type, *petA* transcript levels were observed higher than those of *petC1* at all time points. Similarly, in the ΔPetC1 mutant, *petA* transcript levels were observed higher than individual levels of *petC1*and *petC2* at all time points (Figures 10A, 10B and 11A, 11B, 11J, 11K). The observation of higher combined transcript levels of *petC1*, *petC2* (Figures 10A, 10B and 11A-11C) and *petA* genes in the wild type strain relative to the mutant (Figures 10A, 10B and 11J, 11K) may indicate a higher cytochrome *bf* content of the wild type strain. Levels of *psaC* transcripts coding for subunit VII (PsaC) of PS I, which is directly involved in electron transport were similar in both strains under all time points suggesting similar quantities of PS I (Figures 10A, 10B and 11F, 11G). Transcript levels of the *zwf* gene, which is an indicator of anabolic activity and respiration, were found slightly higher (~1.5 times) in the wild type strain over those in ΔPetC1 mutant until 2nd hour under dark anaerobic conditions after which the trend got reversed and after 12 hours in darkness (Figures 10A, 10B and 11H, 11I) which correlates closing gap in the transcript levels of *petC2* in the wild type and ΔPetC1 mutant (Figures 10A, 10B and 11 B, 11C).

The control gene employed in the study (*rpnB* or *rnpB* which codes for the catalytic RNA subunit of RNaseP) maintained the highest transcript level of all genes tested and also constant levels in both strains up to 12 hours of dark anaerobic incubation (Figures 10A, 10B and 11L, 11M) indicating that this gene serves well as a control.

C] Metabolic Labeling and Isotope-assisted Quantitative Mass Spectrometry

To study changes in the protein levels of electron transfer chain components following shifts from optimal photosynthesis to dark anaerobic conditions and to compare levels of electron transfer proteins in the wild type and ΔPetC1 mutant, metabolic labeling and quantitative mass spectrometry was performed. As explained in Materials and Methods, protein contents of bulk membrane protein fractions were estimated with BCA assays, which showed protein contents in the range of 9-11 μg/μL. Peptide samples obtained after overnight trypsin digestion and C18 column purification were suspended in 0.3% formic acid and analyzed by mass spectrometry. Figure 12 shows an example of a total ion chromatogram (i.e. the total ion signal over the course of a full ~150 min LC-MS/MS run), in this case a ^{14}N-grown, ΔPetC1 12 hour dark anaerobic sample mixed with control, ^{15}N-grown wild type from optimal photosynthetic conditions.

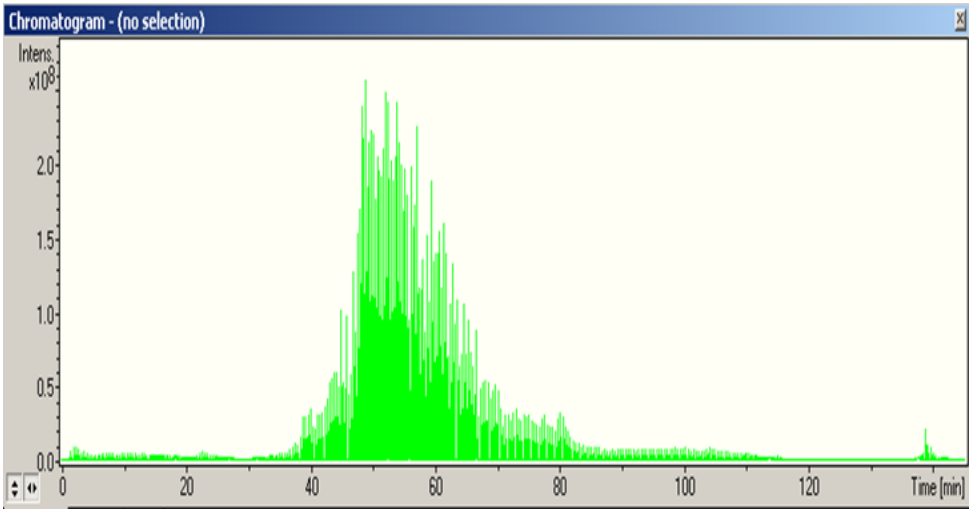

Figure 12: Total ion chromatogram of peptides from metabolically labeled, mixed wild type and ΔPetC1 samples

Total ion chromatogram of membrane peptide sample eluted from a Zorbax 300 SB-C18 column (3.5µm, 50 × 0.3mm), mobile phase solvent A (0.1% formic acid), solvent B (80% acetonitrile, 0.1% formic acid). The sample was from a ^{14}N-grown ΔPetC1 12 hour dark anaerobic culture mixed with ^{15}N-grown wild type maintained under optimal photosynthetic conditions. Axes show signal intensity as a function of LC-MS/MS run times.

As shown in Figure 12, most of the peptides were eluted from the LC column between 35 and 85 minutes of the LC-MS/MS runs which corresponds to the passage of 45-55% Solvent B (containing 80% acetonitrile, 0.1% formic acid) through the LC column. Similar chromatograms were obtained from all of the four samples under study.

Peptide fragment (MS/MS) mass data obtained from the mass spectrometer were converted into Mascot mgf data files and searched via Mascot Daemon software against a *Synechocystis* PCC 6803 Genbank database stored on the UW Oshkosh Mascot server (version 2.2.00). These searches resulted into identification of 25, 21, 10 and 18 proteins (excluding trypsin) from a) ^{14}N-wild type grown under optimal photosynthetic conditions vs. ^{15}N-wild type control, b) ^{14}N-wild type 12 hour dark anaerobic sample vs.

^{15}N-wild type control, c) ^{14}N-ΔPetC1 grown under optimal photosynthetic conditions vs. ^{15}N-wild type control, and d) ^{14}N-ΔPetC1 12th hour dark anaerobic sample vs. ^{15}N-wild type control, respectively. Note that, test cultures were grown in BG-11 medium containing ^{14}N. In each case, the control culture was wild type grown under optimal photosynthetic conditions in BG-11 medium containing ^{15}N. All cultures were harvested at cell densities near $O.D._{750}$ 0.5. Tables 3-6 list all of the proteins identified by LC-MS/MS and Mascot database searches from these experiments. Higher MOWSE scores indicate a higher probability of correct protein identification (Pappin et al., 1993).

Table 3: Proteins identified in ^{14}N-wild type vs. ^{15}N-wild type from optimal photosynthetic conditions

Proteins	MOWSE score
P700 apoprotein subunit Ia	262
P700 apoprotein subunit Ib	179
photosystem I subunit II	151
phycocyanin associated linker protein	148
photosystem I subunit III	128
negative aliphatic amidase regulator	104
protein synthesis elongation factor Tu	90
photosystem II CP47 protein	87
photosystem I subunit XI	78
nitrate transport 45 kDa protein	69
Slr0483	53
cytochrome *b*$_6$	53
phycobilisome LCM core-membrane linker polypeptide	50
Sll1106	49
phycocyanin associated linker protein	47
phycobilisome LC linker polypeptide	46
Ycf4	46
phycobilisome rod-core linker polypeptide CpcG	41
ribulose biphosphate carboxylase large subunit	41
photosystem I subunit VII	40
30S ribosomal protein ss	39
photosystem II CP43 protein	37
Sll1638	35
phycocyanin b subunit	35
CheA like protein	34

Wild type 'experimental' and 'control' cultures grown in ^{14}N and ^{15}N media under optimal photosynthetic conditions (3% CO_2, 50 µmol photons m^{-2} s^{-1}) were mixed, processed as descried in Materials and Methods, and analyzed by LC-MS/MS for peptide and protein identification. The proteins were identified using Mascot (version 2.2.00) software and searches against a *Synechocystis* PCC 6803 database. MOWSE scores represent the probability of significant matches (Pappin et al., 1993).

Table 4. Proteins identified in ^{14}N-wild type 12 hour dark anaerobic culture vs. ^{15}N-wild type from optimal photosynthetic conditions

Proteins	MOWSE score
photosystem I subunit III	129
P700 apoprotein subunit Ia	110
photosystem I subunit II	100
phycocyanin associated linker protein	99
photosystem I subunit XI	95
photosystem I subunit IV	81
phycobilisome rod-core linker polypeptide CpcG	77
carbon dioxide concentrating mechanism protein CcmM	69
protein synthesis elongation factor Tu	69
Sll0359	68
photosystem I subunit VII	64
P700 apoprotein subunit Ib	60
negative aliphatic amidase regulator	59
phycocyanin b subunit	56
photosystem II CP47 protein	53
phycocyanin a subunit	44
photosystem II 11kD protein	42
nitrate transport 45kD protein	41
ATP synthase d subunit	41
photosystem II CP43 protein	39
Sll1106	37

Wild type 'experimental' culture grown in ^{14}N medium under 12 hours dark anaerobic conditions was mixed with wild type 'control' culture grown in ^{15}N medium under optimal photosynthetic conditions (3% CO_2, 50 µmol photons m^{-2} s^{-1}), processed as as descried in Materials and Methods, and analyzed by LC-MS/MS for peptide and protein identification. The proteins were identified using Mascot (version 2.2.00) software and searches against a *Synechocystis* PCC 6803 database. MOWSE scores represent the probability of significant matches (Pappin et al., 1993).

Table 5. Proteins identified in ^{14}N-ΔPetC1 from optimal photosynthetic conditions vs. ^{15}N-wild type from optimal photosynthetic conditions

Proteins	MOWSE score
photosystem II CP47 protein	92
phycocyanin b subunit	84
P700 apoprotein subunit Ia	70
photosystem I subunit III	60
P700 apoprotein subunit Ib	55
photosystem I subunit II	47
phycocyanin associated linker protein	37
Sll0483	36
photosystem I subunit XI	36
photosystem I subunit VII	35

ΔPetC1 'experimental' culture grown in ^{14}N medium and wild type 'control' culture grown in ^{15}N medium under optimal photosynthetic conditions (3% CO_2, 50 μmol photons m^{-2} s^{-1}) were mixed, processed as as descried in Materials and Methods, and analyzed by LC-MS/MS for peptide and protein identification. The proteins were identified using Mascot (version 2.2.00) software and searches against a *Synechocystis* PCC 6803 database. MOWSE scores represent the probability of significant matches (Pappin et al., 1993).

Table 6. Proteins identified in ^{14}N-ΔPetC1 12 hour dark anaerobic culture vs. ^{15}N-wild type from optimal photosynthetic conditions

Proteins	MOWSE score
photosystem I subunit II	119
P700 apoprotein subunit Ib	88
photosystem I subunit III	70
50S ribosomal protein L12	70
P700 apoprotein subunit Ia	69
negative aliphatic amidase regulator	64
phycocyanin associated linker protein	59
allophycocyanin b chain	58
photosystem II CP47 protein	57
photosystem I subunit VII	57
allophycocyanin a chain	50
phycocyanin associated linker protein	49
Sll1873	46
protein synthesis elongation factor Tu	46
phycocyanin b subunit	44
photosystem I subunit XI	42
Ferredoxin NADP oxidoreductase	37
carbon dioxide concentrating mechanism protein CcmM	34

ΔPetC1 'experimental' culture grown in ^{14}N medium under 12 hours dark anaerobic conditions was mixed with wild type 'control' culture grown in ^{15}N medium under optimal photosynthetic conditions (3% CO_2, 50 μmol photons m^{-2} s^{-1}), processed as as descried in Materials and Methods, and analyzed by LC-MS/MS for peptide and protein identification. The proteins were identified using Mascot (version 2.2.00) software and searches against a *Synechocystis* PCC 6803 database. MOWSE scores represent the probability of significant matches (Pappin et al., 1993).

As shown in Tables 3-6, the proteins identified were mostly PS II, PS I or phycobillisome related proteins. Of these, phycobilisomes are photosystem associated but soluble proteins (DeRuyter & Fromme, 2008, pp. 217-269). Unfortunately, none of the Rieske ISPs or cytochrome *f* could be detected in any of the samples. Among non-photosystem, electron transport proteins, only proteins such as cytochrome b_6 and ferredoxin NADP oxidoreductase (FNR) could be detected. These were in the wild type optimal photosynthetic control (Table 3) and ΔPetC1 12 hour dark anaerobic samples (Table 6). Although FNR is a PS I docking protein, it is a soluble protein (DeRuyter & Fromme, 2008, pp. 217-269). Detection of PS II and PS I peptides may be used to determine the relative abundance at these protein complexes in thylakoid membranes.

Tables 3-6 show proteins identified on the basis of individual ^{14}N and ^{15}N-labeled peptides or from both kinds of peptides in a sample. To compare relative protein abundance, I had to consider only such proteins in which the same ^{14}N and ^{15}N-labeled peptides were detected. For proteins with more than one similar ^{14}N and ^{15}N-labeled peptide, ones with higher combined MOWSE score (the sum of individual, peptide MOWSE scores) were selected. For every peptide set, an extracted ion chromatogram (EIC) was obtained and relative expression levels were determined by comparing the areas under the EIC curves. Figure 13A shows an MS spectrum obtained for tryptic fragment 'K.VSVDNNPVPTSFEK.W' of P700 subunit Ia apoprotein from the ΔPetC1 12 hour dark anaerobic sample. For any peptide, MS spectra are obtained over a short time frame during the MS run from a number of peptide ions of the same kind, which are then subjected to MS/MS treatment. Figure 13B presents the MS/MS spectrum of this

^{14}N-labeled peptide while Figure 13C shows the MS/MS spectrum of the ^{15}N labeled peptide from the MS spectrum shown in Figure 13A. MS and MS/MS spectra are shown as signal intensity as a function of *m*/*z* ratio. Figures 13A, 13B and 13C present the MS spectrum, and MS/MS spectra of the light and heavy peptide ions, respectively, obtained in a single time frame. Finally, Figure 13D shows the extracted ion chromatogram of the same peptide set plotted as intensity against retention time. In extracted ion chromatograms, the heights and areas of the peaks belonging to the light and heavy peptides were directly compared to determine the relative expression levels of a particular protein. Based on Figure 13D, the ^{14}N-labeled peptide (protein) from the ΔPetC1 12 hour anaerobic sample was ~30% more abundant than the ^{15}N-labeled peptide (protein) from the wild control under optimal photosynthetic conditions.

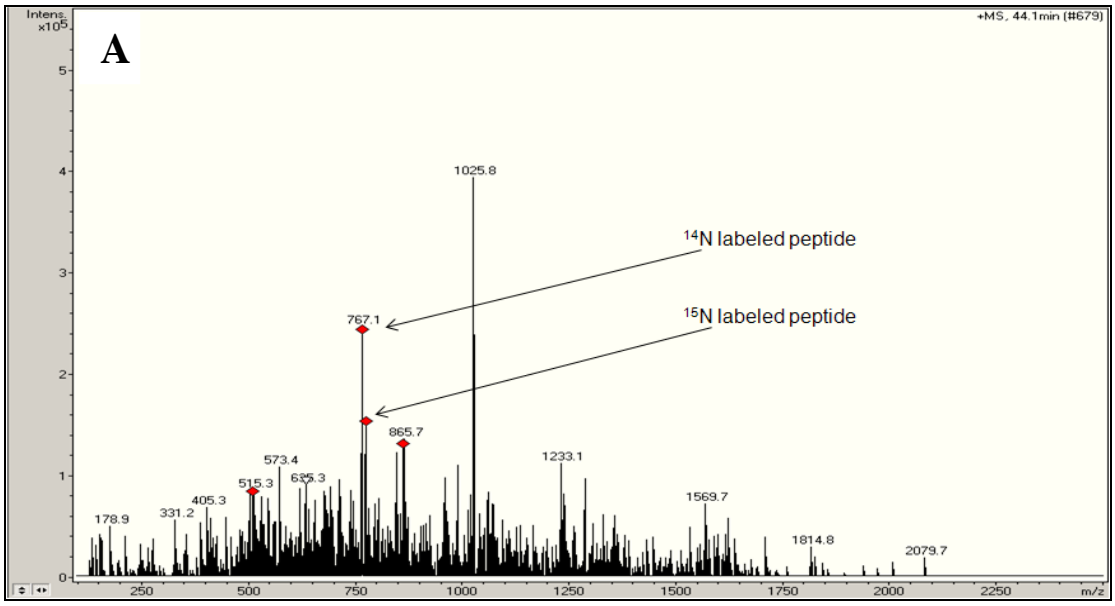
A
Intens.
x10^5
+MS, 44.1min (#679)
1025.8
14N labeled peptide
15N labeled peptide
767.1
865.7
573.4
515.3
405.3
331.2
178.9
1233.1
1569.7
1814.8
2079.7
m/z

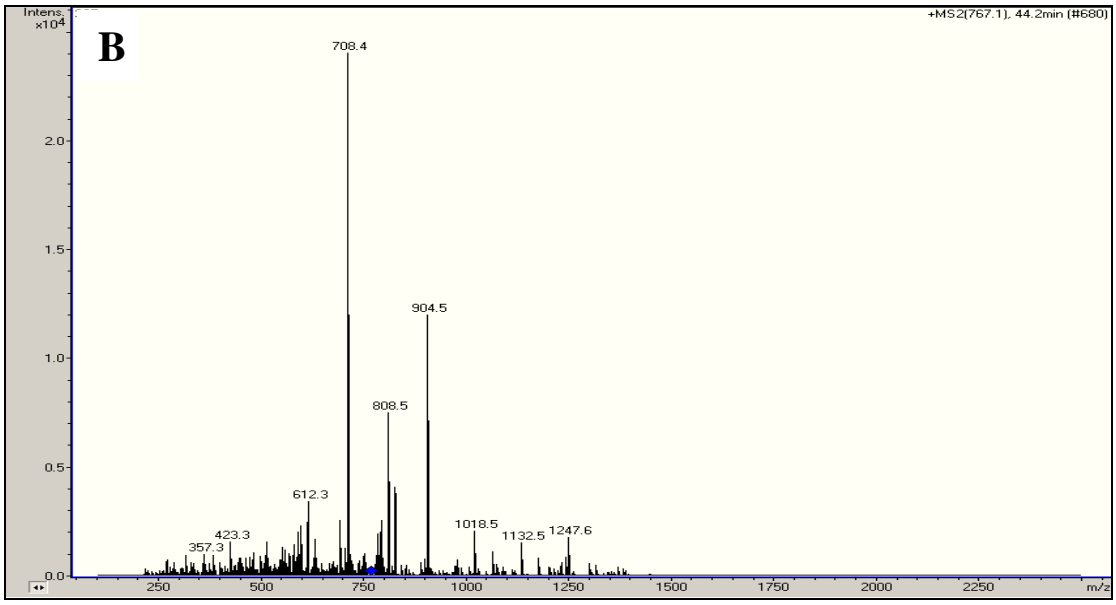
B
Intens.
x10^4
+MS2(767.1), 44.2min (#680)
708.4
904.5
808.5
612.3
423.3
357.3
1018.5
1132.5
1247.6
m/z

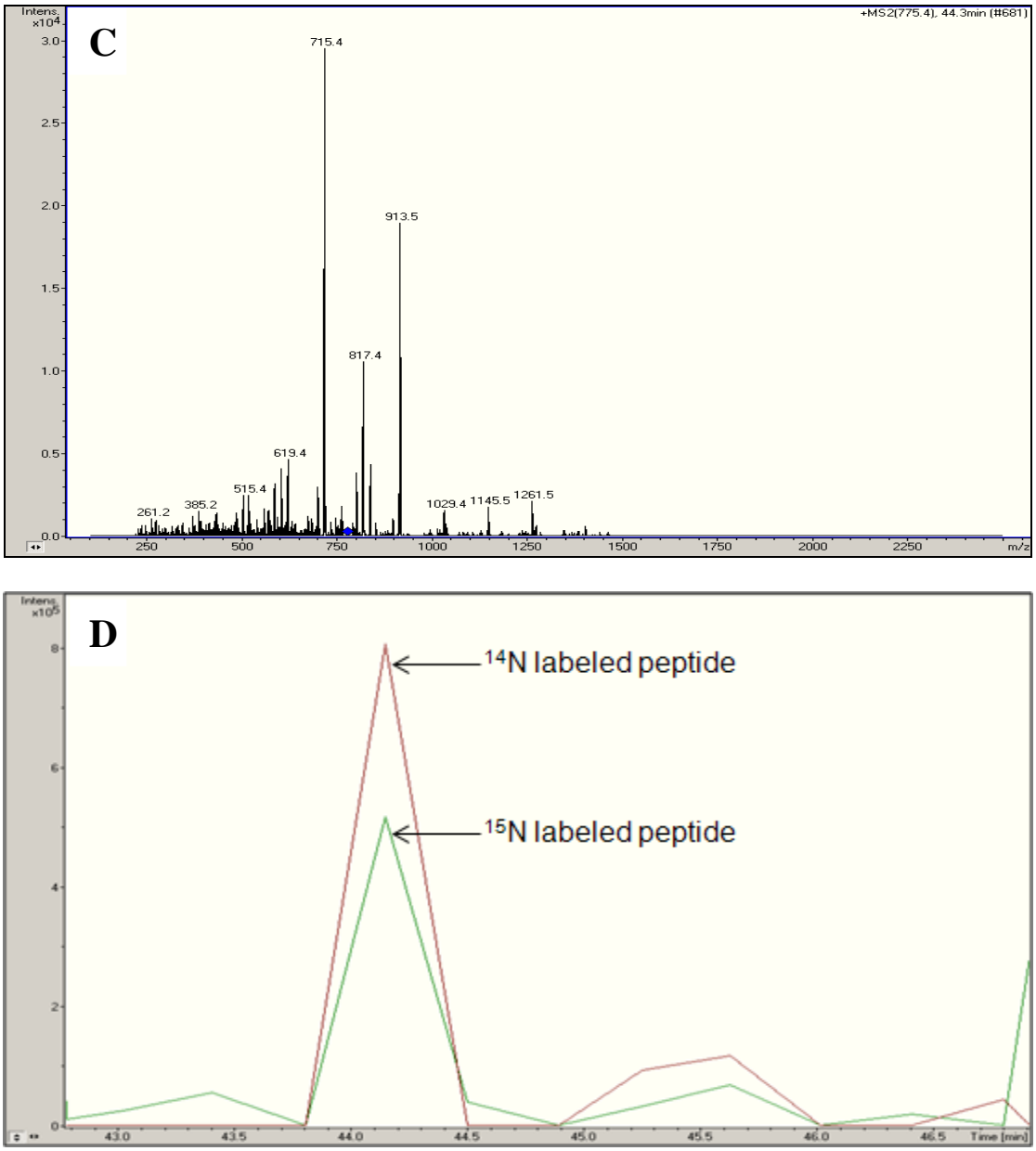

Figure 13: Representative MS spectrum, MS/MS spectra and extracted ion chromatogram. Panel A: MS spectrum of light and heavy peptides**; Panel B:** MS/MS spectrum of the light peptide**; Panel C:** MS/MS spectrum of the heavy peptide**; Panel D:** Extracted ion chromatograms of the light and heavy peptides**.**

The light (^{14}N-labeled) and heavy (^{15}N-labeled) peptides belong to the 'K.VSVDNNPVPTSFEK.W' tryptic peptide of P700 apoprotein subunit Ia. Samples are from the ^{14}N-ΔPetC1 12 hour dark anaerobic sample mixed with ^{15}N-labeled wild type 'control' sample from optimal photosynthetic conditions. The MS and MS/MS spectra shown are not on the same scale. Extracted ion chromatograms are represented as signal intensity as a function of MS run time. Peak heights obtained from the chromatogram were compared to determine relative contents of a particular protein in the test and the control samples.

Tables 7-10 present relative expression levels of proteins, for which comparative peptide data were available, in experimental cultures versus control cultures. The expression levels of ^{15}N-labeled proteins obtained from control, wild type, optimal photosynthesis cultures were set to 100%. Expression levels of ^{14}N-labeled proteins obtained from experimental cultures are shown relative to these 100% values. Because of large differences in signal intensities of different sets of identified peptides, the expression levels represented in tables 7-10 are relative only to the ^{15}N-labeled wild type control within each mixed sample and are not normalized to each other.

Table 7: Relative protein levels based on detected light and heavy peptide pairs in ^{14}N-wild type vs. ^{15}N-wild type from optimal photosynthetic conditions

^{14}N labeled proteins from 'test' samples	Expression relative to control (%)
P700 apoprotein subunit Ia	124.07
P700 apoprotein subunit Ib	100.38
photosystem I subunit II	101.66
photosystem I subunit III	150.49
photosystem II CP47 protein	125.36
photosystem I subunit XI	85.41
cytochrome *b*$_6$	116.87
photosystem I subunit VII	140.89

Wild type 'experimental' and 'control' cultures grown in ^{14}N and ^{15}N media under optimal photosynthetic conditions (3% CO_2, 50 µmol photons m^{-2} s^{-1}) were mixed, processed as descried in Materials and Methods, analyzed by LC-MS/MS, and proteins identified via Mascot (version 2.2.00) database searches. Table 7 shows relative protein expression levels in ^{14}N-labeled wild type 'experimental' culture as percentage of the expression level in ^{15}N-labeled, wild type 'control' culture. Protein levels are relative only to the same protein in the control culture and cannot be compared to each other. Both cultures were harvested at $O.D._{750}$ ~0.5.

Table 8: Relative protein levels from detected peptide pairs in ^{14}N-wild type 12 hour dark anaerobic culture vs. ^{15}N-wild type from optimal photosynthesis

^{14}N labeled proteins from 'test' samples	Expression relative to control (%)
photosystem I subunit III	86.34
P700 apoprotein subunit Ia	170.97
photosystem I subunit II	116.78
photosystem I subunit XI	49.45
photosystem I subunit IV	115.21
photosystem I subunit VII	58.30
photosystem II CP47 protein	332.52

A^{14}N-wild type 'experimental' culture incubated 12 hours under dark anaerobic conditions was mixed with ^{15}N-wild type 'control' culture grown under optimal photosynthetic conditions (3% CO_2, 50 µmol photons m^{-2} s^{-1}), processed as descried in Materials and Methods, analyzed by LC-MS/MS, and proteins identified via Mascot (version 2.2.00) database searches. Expression levels are shown as percentage relative to the ^{15}N-wild type, optimal photosynthesis control. Table 8 shows relative protein expression levels in ^{14}N-labeled wild type 'experimental' culture as percentage of the expression level in ^{15}N-labeled, wild type 'control' culture. Protein levels are relative only to the same protein in the 'control' culture and cannot be compared to each other. Both cultures were harvested at $O.D._{750}$ ~0.5.

Table 9: Relative protein levels from detected peptide pairs in ^{14}N-ΔPetC1 optimal photosynthetic culture vs. ^{15}N-wild type from optimal photosynthesis

^{14}N labeled proteins from 'test' samples	Expression relative to control (%)
photosystem II CP47 protein	72.17
P700 apoprotein subunit Ia	73.30
photosystem I subunit III	84.71
photosystem I subunit II	94.78
photosystem I subunit VII	128.35

A^{14}N-ΔPetC1 mutant 'experimental' culture and ^{15}N-wild type 'control' culture grown under optimal photosynthetic conditions (3% CO_2, 50 µmol photons m^{-2} s^{-1}) were mixed, processed as descried in Materials and Methods, analyzed by LC-MS/MS, and proteins identified via Mascot (version 2.2.00) database searches. Expression levels are shown as percentage relative to the ^{15}N-wild type, optimal photosynthesis control. Table 9 shows relative protein expression levels in ^{14}N-labeled ΔPetC1 'experimental' culture as percentage of the expression level in ^{15}N-labeled, wild type 'control' culture. Protein levels are relative only to the same protein in the 'control' culture and cannot be compared to each other. Both cultures were harvested at $O.D._{750}$ ~0.5.

Table 10: Relative protein levels from detected peptide pairs in ^{14}N-ΔPetC1 12 hour dark anaerobic culture vs. ^{15}N-wild type from optimal photosynthesis

^{14}N labeled proteins from 'test' samples	Expression relative to control (%)
photosystem I subunit II	131.00
photosystem I subunit III	62.33
P700 apoprotein subunit Ia	155.66
P700 apoprotein subunit Ib	52.82
photosystem II CP47 protein	119.34
photosystem I subunit VII	73.82
photosystem I subunit XI	97.00

A^{14}N-ΔPetC1 'experimental' culture incubated 12 hours under dark anaerobic conditions was mixed with ^{15}N-wild type 'control' culture grown under optimal photosynthetic conditions (3% CO_2, 50 μmol photons m^{-2} s^{-1}), processed as descried in Materials and Methods, analyzed by LC-MS/MS, and proteins identified via Mascot (version 2.2.00) database searches. Expression levels are shown as percentage relative to the ^{15}N-wild type, optimal photosynthesis control. Table 10 shows relative protein expression levels in ^{14}N-labeled ΔPetC1 'experimental' culture as percentage of the expression level in ^{15}N-labeled, wild type 'control' culture. Protein levels are relative only to the same protein in the 'control' culture and cannot be compared to each other. Both cultures were harvested at $O.D._{750}$ ~0.5.

Table 7 shows relative levels of proteins detected in a ^{14}N-labeled, wild type 'experimental' culture relative to a ^{15}N-labeled, wild type 'control' culture, both grown under optimal photosynthetic conditions to $O.D._{750}$ 0.5. As these were replicate cultures, I expected to see very similar expression levels for the identified proteins. However, the relative expression levels varied from about -38% to +56%. Protein levels in the wild type after 12 hours dark anaerobic incubation relative to the 'control' were 50% lower for PS I subunit XI, but 71% higher for PS I apoprotein Ia, and >300% higher for the PS II CP47 protein (Table 8). In the ΔPetC1 mutant grown under optimal photosynthetic conditions, with the exception of PS I subunit VII, which showed a 28% increase, all of the other PS I subunits and as well as the PS II CP47 protein showed 6-28% lower levels relative to the 'control' (Table 9). Finally, in the ΔPetC1 mutant after 12 hours dark anaerobic incubation, the P700 apoprotein subunit Ib showed a 50% decrease, the P700 apoprotein subunit Ia a 50% increase, and the PS II CP47 protein a 19% increase in

abundance relative the to wild type 'control' grown under optimal photosynthetic conditions (Table 10). These data are from single biological replicates and because of the relatively large variations $\pm$ 40-60% in specific protein contents in replicate wild type cultures (Table 7), few conclusions can be drawn at present. Based on these preliminary data, one has to conclude that the protein levels of PS I and PS II components were largely similar in the experimental cultures relative to the wild type optimal photosynthesis, 'control' culture. The one significant exception appears to be the ~3-fold higher expression of the PS II CP47 protein in the wild type after 12 hours of dark anaerobic incubation (Table 8).

D] Quantification of Electron Transfer Components by Kinetics Spectrophotometry

To compare the amounts of cytochrome *bf* components, plastocyanin and PS I, an absorbance kinetics experiment was performed. As described in Materials and Methods, wild type as well as ΔPetC1 strains grown under optimal photosynthetic conditions to $O.D._{750}$ 1.0 were concentrated 4-fold and kinetics spectra were obtained for the cytochrome *bf* components, plastocyanin and PS I. The culture samples were exposed to green (530 nm) actinic light intensity of 590 μE $m^{-2}s^{-1}$ for 10 seconds to ensure reduction of the cytochrome b_6 hemes in the Cyt *bf* low-potential chain (to the extent possible) and complete oxidation of cytochrome *f*, plastocyanin and PS I. Figure 14 shows kinetic spectra for all of these electron transfer chain components, for both strains under study.

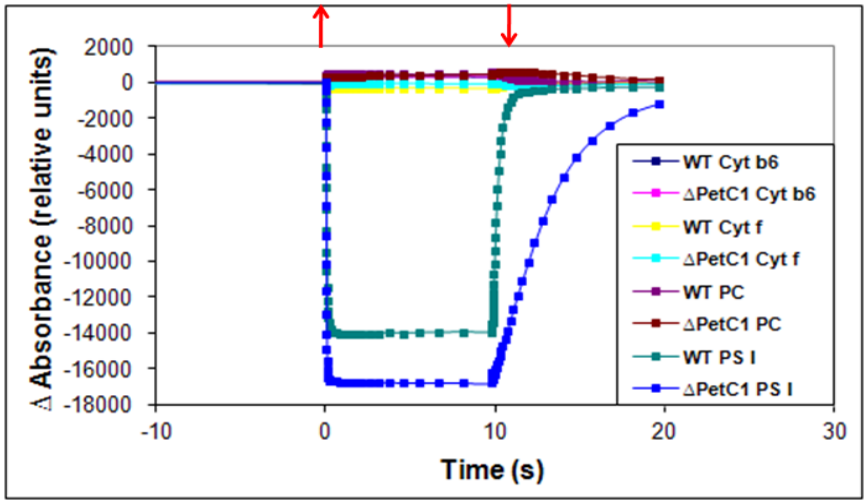

Figure 14: Redox kinetics of Cyt *bf* and PS I electron transfer chain components

Legend: cyt b_6: cytochrome b_6; cyt *f*: cytochrome *f*; PC: plastocyanin; PS I: photosystem I. Kinetics data for Cyt b_6, Cyt *f*, PC and PS I from wild type and ΔPetC1 strains grown under optimal photosynthetic conditions to $O.D._{750}$ 1.0 are shown as relative absorbance changes (i.e. dI/I at 554, 563, 573, and 705 nm relative to reference wavelengths for Cyt *f*, Cyt b_6, PC, and PS I P700, respectively) as a function of time. $dI = I_{ref}$ (light intensity recorded by the reference detector) minus I_{meas} (light intensity passing through the sample detected by sample detector) / I_{ref}. Arrows indicate the onset and termination of actinic illumination. Downward deflections represent oxidation and upward deflections reduction.

As shown in Figure 14, PS I showed a very large oxidation signal compared to other electron transfer chain components. This difference arises in part from the higher extinction coefficient of the PS I P700 reaction center chlorophylls relative to cytochromes *f*, b_6 and plastocyanin (shown below). Redox spectra for the individual electron transfer chain components are shown in Figures 15A to 15D.

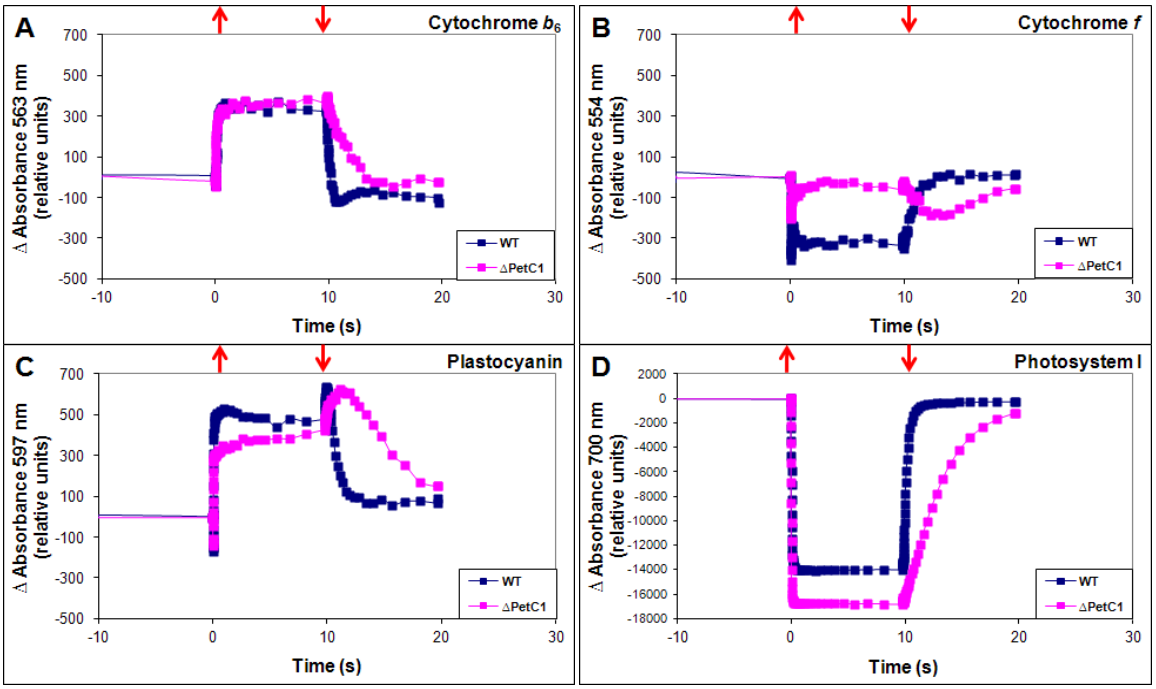

Figure 15: Individual redox traces of Cyt *bf* and PS I electron transfer chain components. Panel A: cytochrome b_6**; Panel B:** cytochrome *f*; **Panel C:** plastocyanin**; Panel D:** photosystem I**.**

Kinetics data were obtained from wild type and ΔPetC1 strains as described in Figure 14. Arrows indicate the onset and termination of actinic illumination. Downward deflections represent oxidation and upward deflections reduction of Cyt b_6, Cyt *f*, and P700. In contrast, upward deflections represent oxidation of PC and downward deflections reduction. Panels A, B and C are plotted on the same scale.

Redox kinetics of cytochrome b_6 are shown in Figure 15A. The extent of reduction was similar in the wild type and ΔPetC1 strains suggesting similar cytochrome b_6 contents, which is in agreement with the immunoblot results of Tsunoyama et al. (2009) but contrary to those of Schultze et al. (2009). However, the slower re-oxidation of cytochrome b_6 in the ΔPetC1 mutant suggests slower electron transport through cytochrome *bf* complex. Figure 15B shows redox kinetics of cytochrome *f*. The wild type showed an oxidation signal ~2 times larger than in ΔPetC1 suggesting a cytochrome *f* content ~2-fold higher in the wild type relative to ΔPetC1; athough not ~5.5 and ~8-fold

higher as suggested by RT-qPCR data (Figures 10A, 10B and 11J, 11K) and microarray results of Nelson & Kallas (2000-2007, unpublished data) respectively. The observation is supported by the immunoblot results of Tsunoyama et al. (2009). Because of the low cytochrome *f* content of the ΔPetC1 strain, the cytochrome *f* signal obtained is weak and often not easy to detect above background noise. Hence, in the case of the ΔPetC1 mutant, it is difficult to comment about the re-reduction kinetics of cytochrome *f*.

Figure 15C presents the redox kinetics of plastocyanin. It should be noted that contrary to the other electron transfer chain components under study, upward deflections reflect oxidation of plastocyanin and downward deflections reduction (Smillie & Levin, 1963). The similar extent of PC oxidation in wild type and ΔPetC1 strains suggests similar plastocyanin contents. However, the slower re-reduction of plastocyanin in ΔPetC1 indicates a slower transport of electrons through cytochrome *bf* complex, consistent with the Cyt b_6 results (Figure 15A). Finally, redox traces of PS I P700 are presented in Figure 15D. A marginally larger extent of P700 oxidation observed in the ΔPetC1 strain relative to wild type suggest a somewhat higher PS I content in the mutant than the wild type. This observation is in agreement with 77K fluorescence spectroscopy results of Nelson & Kallas (2000-2007, unpublished data) but contrary to the 77K fluorescence spectroscopy results of Schneider et al. (2004a). As observed in Figures 15A and 15C, slower P700 re-reduction in the ΔPetC1 mutant again indicates a slower electron flow through cytochrome *bf* complex.

To calculate the quantities of electron carriers from light-induced absorbance changes, a differential form of the Beer-Lambert law was used that applies to the

infinitesimally small absorbance changes detected with the BioLogic JTS-10 spectrophotometer (Personal communication between Dr. Toivo Kallas and Zohra Mana (2007), Application specialist of Biologic). In this formulation, the molar quantity of a redox center (*X*) can be determined as follows:

$$X = \frac{0.43(dI / I)cm^{-1} \quad 10^{6}}{mM^{-1}cm^{-1}}$$

where *dI*/*I* is the maximum oxidation or reduction signal, ε is the extinction coefficient of the redox center ($mM^{-1}cm^{-1}$), and cm^{-1} is the length of the light path through the sample. Thus to quantify cytochrome b_6 and plastocyanin, the formula | [-0.43(maximum value of dI/I) / 10^6] cm^{-1} ÷ [extinction coefficient] $mM^{-1}cm^{-1}$| was used, while for cytochrome *f* and PS I, | [-0.43(minimum value of dI/I) / 10^6] cm^{-1} ÷ [extinction coefficient] $mM^{-1}cm^{-1}$| was used. For cytochrome b_6, the extinction coefficient value at 563 nm was taken as 21 $mM^{-1}cm^{-1}$ as shown by Stuart and Wasserman (1973) in a study of spinach chloroplast. The extinction coefficient values of cytochrome *f* at 554 nm was taken as 18 $mM^{-1}cm^{-1}$ as shown by Hurt and Hauska (1970) in a study of spinach chloroplast. For plastocyanin, the extinction coefficient value at 597 nm was taken as 4.9 $mM^{-1}cm^{-1}$ as shown by Katoh, Suga, Shiratori & Takamiya (1961) as well as Hurt and Hauska (1970) in spinach chloroplast. Finally, the extinction coefficient value for PS I at 700 nm was taken as 57 $mM^{-1}cm^{-1}$ as shown by Witt, Bordignon, Carbonera, Dekker, Karapetyan, Teutloff, … Schlodder (2003) in *Synechocystis* 6803. To compare the quantities of the different redox centers, the value obtained for wild type cytochrome *f* was set to 1.0, and the values of the other electron transfer chain components were normalized to this. Table 11 shows the

quantitites of electron transfer chain components obtained by this analysis together with the PS I: cytochrome *f* ratio.

Table 11: Relative quantities of wild type and ΔPetC1 electron transfer chain components determined from light-induced redox changes

	WT (pM)	ΔPetC1 (pM)
Cyt b_6	7.66	8.20
Cyt *f*	9.77	4.84
PC	55.73	54.92
PS I	106.10	126.81
PS I: : Cyt *f*	~11	~26

Legend: WT, wild type; ΔPetC1, mutant strain; Cyt b_6, cytochrome b_6; Cyt *f*, cytochrome *f*; PC, plastocyanin; PS I, photosystem I. The contents of electron transfer chain components (*X)* for the wild type and ΔPetC1 grown under optimal photosynthetic conditions were calculated according to the formula: X: -0.43 (dI/I) $cm^{-1} \times 10^{-6} / \varepsilon m M^{-1} cm^{-1}$. Extinction coefficients for cytochrome b_6 at 563 nm, cytochrome *f* at 554 nm, plastocyanin at 597 nm and PS I at 700 nm were 21 $mM^{-1}cm^{-1}$ (Stuart & Wasserman, 1973), 18 $mM^{-1}cm^{-1}$ (Hurt & Hauska, 1981), 4.9 $mM^{-1}cm^{-1}$ (Hurt & Hauska, 1981; Katoh et al., 1961) and 57 $mM^{-1}cm^{-1}$ (Witt et al., 2003), respectively.

As shown in Table 11, in the wild type, the relative amounts of cytochromes b_6 and *f* are similar. Contents of cytochrome b_6 were fairly similar in the wild type and ΔPetC1 mutant, which is in agreement with the immunoblot results of Tsunoyama et al. (2009) but contrary to those of Schultze et al. (2009). Similarly, the plastocyanin contents of the strains were also similar. However, the wild type possessed cytochrome *f* content more than two times higher than that of the mutant. This observation is in agreement with RT-qPCR results (Figures 10A, 10B and 11J, 11K), microarray results of Nelson & Kallas (2000-2007, unpublished data) and immunoblot results of Tsunoyama et al. (2009). The PS I content of the ΔPetC1 mutant strain was ~20% higher than that of the wild type strain in accordance with the 77K fluorescence spectroscopy data of Nelson Nelson & Kallas (2000-2007, unpublished data) but contrary to the 77K fluorescence spectroscopy data of Schneider et al. (2004a) who observed similar PS I contents in the wild type and

ΔPetC1 strains. The ratios of PS I to cytochrome *f* (and thus to the Cyt *bf* complex) were found to be ~11:1 and ~26:1 in the wild type and ΔPetC1 strain respectively. These data reveal that the ΔPetC1 mutant possesses a low amount of Cyt *bf* complex and a very unusual *bf* complex with similar cytochrome b_6 contents (Tsunoyama et al., 2009; Table 11) but much lower subunit IV (Tsunoyama et al., 2009) and cytochrome *f* contents (Tsunoyama et al., 2009; Table 11) resulting into slower electron transport. These data further suggest that this low content of the cytochrome *bf* complex and of cytochrome *f* in particular, explain the observed, low electron transport activity of the PetC2 – Cyt *bf* complex in the ΔPetC1 mutant.

E] Study of Catalytic Efficiencies of the PetC1 and PetC2 Rieske ISPs

Flash induced oxidation-reduction kinetics of cytochrome *f* in *Synechocystis* 6803 wild type and the ΔPetC1 mutant have been studied by Finazzi and Kallas (2000-2005, unpublished data). These studies revealed a very slow cytochrome *f* re-reduction rate in the mutant. After normalization of the cytochrome *f* redox spectra from the wild type and ΔPetC1 mutant, the re-reduction rate of cytochrome *f* in the mutant was found to be ~50 times slower than in the wild type. Hence, initially, it was thought that the cytochrome *bf* complex containing the PetC2 Rieske ISP must be much less efficient than the normal PetC1 containing cytochrome *bf* complex. But as now suggested or shown by several studies (Nelson & Kallas, 2000-2007, unpublished data; Shultze et al., 2009; Figure 15C), the ΔPetC1 mutant appears to have a lower content of cytochrome *f* and perhaps of the entire cytochrome *bf* complex. Thus the slower electron flow through the cytochrome

bf complex observed by Finazzi and Kallas (2000-2005, unpublished data) may be solely related to the lower cytochrome *bf* content in the ΔPetC1 mutant.

In an attempt to answer the question of the catalytic activities of the PetC1 and PetC2 Rieske proteins, a light-induced, electron transfer kinetics experiment similar to the one performed by Finazzi and Kallas (2000-2005, unpublished data) was performed. A principal difference between those experiments and the ones reported here is that, Finazzi-Kallas used a Xenon flash lamp to trigger photosynthetic electron transport. The short half-time of this flash (~4 μsec) results in a single oxidation of the photosystems and thus in a single turnover of the cytochrome *bf* complex. In contrast, the BioLogic JTS-10 spectrophotometer employed for my thesis research uses light-emitting diodes (LEDs) to trigger photosynthesis. The minimum half-time of an LED flash to trigger a reasonable signal is on the order of milliseconds (msec). Thus it is much more difficult to approach single-turnover kinetics of the cytochrome *bf* complex, needed to investigate the intrinsic electron transfer activities of different forms of the complex. Nonetheless, the results of these studies proved to be very interesting.

Recall that the wild type and ΔPetC1 strains possess cytochrome *bf* complexes that contain PetC1 and PetC2 Rieske iron-sulfur proteins, respectively. As described in Materials and Methods, both strains were grown under optimal photosynthetic conditions to $O.D._{750}$ 1.0, and were concentrated 4-fold for cytochrome *f* kinetics studies. To assess the intrinsic electron transfer efficiencies of these cytochrome *bf* complexes, I attempted to use minimal intensities and short durations of actinic (excitation) light to approach single turnovers of the cytochrome *bf* complex. For both strains, actinic light intensities

of 14 μE $m^{-2}s^{-1}$ and 37 μE $m^{-2}s^{-1}$ produced very noisy kinetics traces that could not be used. The minimal actinic light intensities that produced useable signals were 80 μE $m^{-2}s^{-1}$ for the wild type and 150 μE $m^{-2}s^{-1}$ for the ΔPetC1 mutant. Figures 16A and 16B present cytochrome *f* oxidation-reduction traces obtained from the wild type and ΔPetC1 strain at several different actinic light intensities. Half times of re-reduction were calculated for each trace as shown in the Figure.

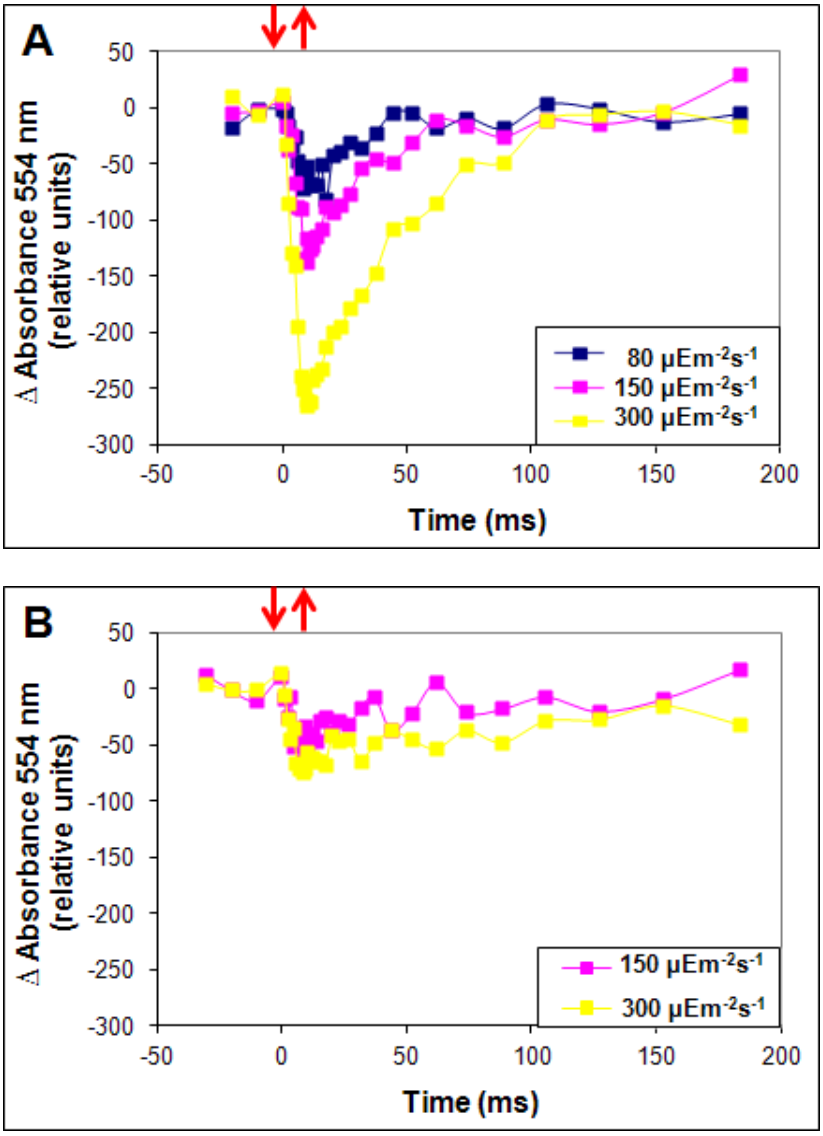

Figure 16: Cytochrome *f* oxidation-reduction kinetics at different excitation light intensities in *Synechocystis* 6803 wild type (A) and ΔPetC1 mutant (B).

Cytochrome *f* kinetic data were obtained from the wild type and ΔPetC1 mutant grown under optimal photosynthetic conditions to $O.D._{750}$ 1.0. Cells were concentrated to $O.D._{750}$ ~4.0 for kinetics measurements. Green actinic light (530 nm, $t_{1/2}$ 50 μsec) was used at the intensities shown to trigger photosynthesis. Arrows indicate the onset and termination of actinic illumination. Downward deflections represent oxidation and upward deflections reduction.

As shown in Figures 16A and 16B, actinic light intensities of 300 μE $m^{-2}s^{-1}$ and 150 μE $m^{-2}s^{-1}$ led to cytochrome *f* oxidation signals at least 3 times larger in the wild type

than the ΔPetC1 mutant, again consistent with a larger cytochrome *f* content in the wild type. Cytochrome *f* re-reduction half-times in the wild type at 80, 150 and 300 μE $m^{-2}s^{-1}$ actinic light intensities were 17, 20 and 27 ms, respectively. In the ΔPetC1 mutant at actinic light intensities of 150 and 300 μE $m^{-2}s^{-1}$, these half-times were 36 and 90 ms, respectively. At an actinic light intensity of 300 μE $m^{-2}s^{-1}$, the ratio of cytochrome *f* reduction half-times, wild type: ΔPetC1 were 27:90 or 3:10. When the actinic light intensity was decreased to 150 μE $m^{-2}s^{-1}$, the ratio of cytochrome *f* re-reduction half-times, wild type: ΔPetC1 became closer at 20:36 or ~5.6:10. Because useable oxidation-reduction signals could not be produced in the ΔPetC1 mutant at actinic intensities of 80 μE $m^{-2}s^{-1}$ or lower, further comparisons at lower actinic light intensities were not possible. Still, the available data showed clearly that as the actinic light intensity decreased, the cytochrome *f* re-reduction half-times began to converge. Thus the kinetic data suggest that the catalytic efficiencies of PetC1-Cyt *bf* complex in wild type *Synechocystis* 6803 and the PetC2-Cyt *bf* complex in the ΔPetC1 mutant, and accordingly the catalytic efficiencies of the PetC1 and PetC2 Rieske ISPs may be similar, or at least not greatly different as previously believed. In other words, the time required by the PetC1 and PetC2 Rieske ISPs to ferry electrons to cytochrome *f* may be fairly similar.

F] Impact of the ΔPetC1 Mutation and Dark Anaerobiosis on PQ Pool Redox State

To study the impact of the PetC1 Rieske ISP deletion and dark anaerobic conditions on electron transfer PQ pool redox, the quantum efficiency of PS II was investigated, which reflects the redox status of the PQ pool. First, chlorophyll contents of the wild type

and ΔPetC1 mutant were determined to obtain comparable chlorophyll contents for fluorescence measurement. For the wild type and ΔPetC1 mutant grown to O.D. $_{750}$ 0.5, chlorophyll contents were 5.5 μM and 8.7 μM, respectively. At least in the exponential phase of growth, at the same O.D.$_{750}$, the chlorophyll content of ΔPetC1 was always higher than that of the wild type. The observation of higher chlorophyll content in the ΔPetC1 strain relative to wild type strain is consistent with the findings of Tsunoyama et al. (2009). PS II quantum efficiencies were measured using the formula, ΦPSII = (*F*m'– *F*s)/ *F*m' (Evans, 1986) from the fluorescence spectra obtained as explained in Materials and Methods. Quantum efficiencies of PS II were measured in the wild type and ΔPetC1 mutant harvested from optimal photosynthetic and after dark anaerobic exposures as long as 12 hours. PS II quantum efficiencies of cells harvested from these conditions were determined over a range of actinic light intensities.

Figures 17A and 17B show examples of 'pulsed' fluorescence traces obtained from the wild type and ΔPetC1 mutant. In these experiments, chlorophyll fluorescence (>665 nm, reflecting primarily PSII fluorescence) is used to monitor state transitions (redistribution of light harvesting proteins) as well as PQ pool redox as described in the figure legend. Fluorescence is measured via weak pulses of blue light delivered during short intervals of darkness, and can thus be used to measure fluorescence from cells incubated in darkness or during continuous illumination. Maximum fluorescence (*F*m or *F*m') elicited by saturating pulses of actinic light reflects the PSII light absorbing capacity and thus its antenna size. Figures 17A and B shows fluorescence from cells

incubated in darkness, then in 590 µE $m^{-2}s^{-1}$ continuous actinic illumination, and then returned to darkness.

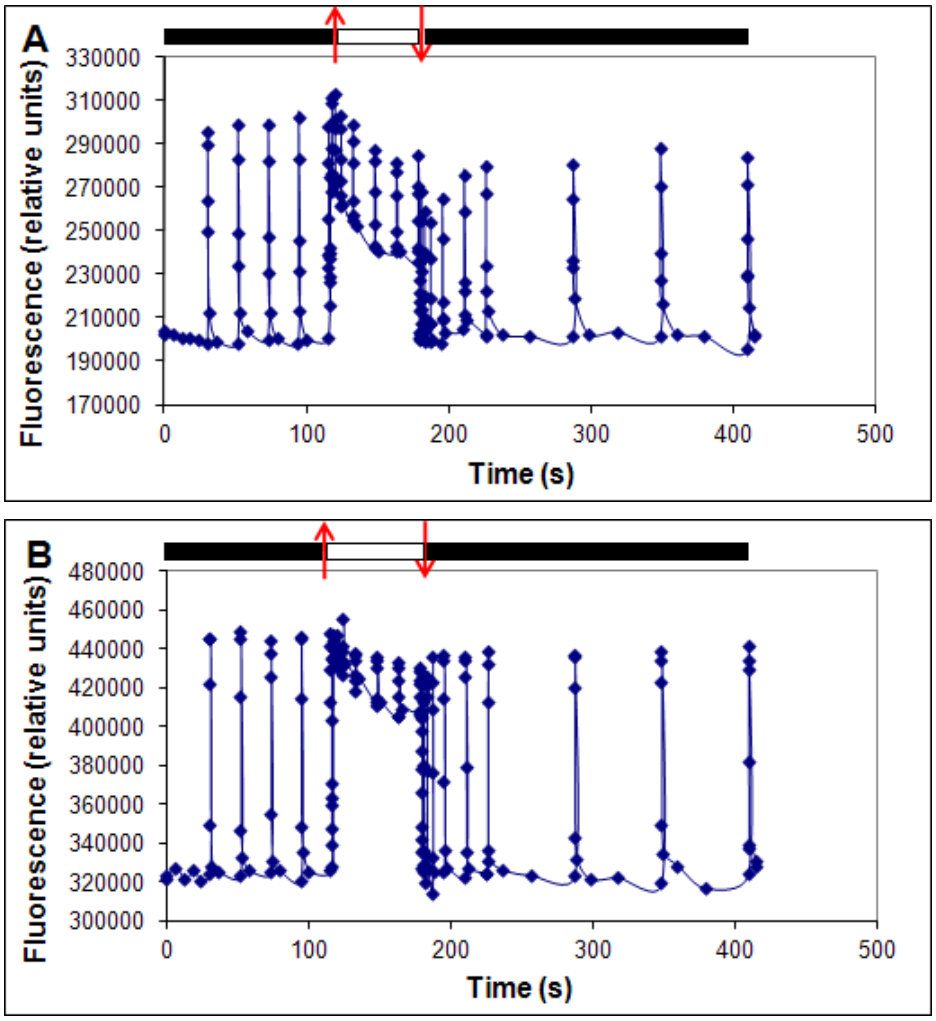

Figure 17: Fluorescence kinetics in *Synechocystis* 6803 wild type (A) and ΔPetC1 (B) during dark-light-dark transitions

Wild type and ΔPetC1 strains were grown under optimal photosynthesis to $O.D._{750}$ 0.5 (~5 µM chl). During the experiment, dark adapted cells were assayed for 120 s, then exposed to green light (520 nm, 590 µE m^{-2} s^{-1}) for 60 s, and then returned to darkness for 240 s. Arrows indicate the onset and termination of the continuous actinic illumination while black and white boxes indicate the dark period and period of continuous illumination respectively. Chlorophyll fluorescence (>665 nm) was measured during 'dark pulses' (~150 µs) with excitation delivered by 10 µs pulses of weak, blue light. Saturating 200 ms pulses of light (520 nm, 7900 µmol m^{-2} s^{-1}) were delivered at intervals. *F*m and *F*m': Maximum PS II fluorescence after saturating pulses during darkness and continuous illumination, respectively. *F*s1 and *F*s2: Basal PS II fluorescence at the beginning and end of the illumination period.

The difference between *F*m' and *F*m values indicates the extent of state transitions (light harvesting antenna redistribution). In the experiment shown in Figures 17A and 17B, the wild type showed a small state transition but the ΔPetC1 mutant failed to do so, as indicated in the literature (Tsunoyama et al., 2009) but contrary to previous 77K fluorescence spectroscopy results of Nelson & Kallas (2000-2007, unpublished data). Lower, basal *F*s1 fluorescence levels during continuous illumination in the wild type relative to ΔPetC1 indicate a less reduced PQ pool than in the ΔPetC1 mutant. Using the values of *F*m' and either *F*s1 or *F*s2, quantum yields of PS II were calculated. Also, as per my observations, basal PS II fluorescence is directly related to the PS II content of the cells. At least in the exponential phase, just like the chlorophyll content, the PS II content of the ΔPetC1 mutant was always higher than in the wild type (Figures 17A and 17B, seen as higher *F*m and *F*m' signals in the mutant). This is in agreement with the 77K fluorescence spectroscopy experiments performed by Nelson & Kallas (2000-2007, unpublished data) but contrary to those of Schneider et al. (2004a) who reported ~60% lower PS II in the *Synechocystis* 6803 ΔPetC1 mutant relative to wild type, after normalization of chlorophyll contents. For a given strain, no significant change was observed in the basal PS II fluorescence in cells harvested at different times, indicating relatively constant amounts of PS II over the tested time points, from optimal photosynthetic to 12 hour dark anaerobic conditions.

PS II quantum efficiencies were investigated over a range of continuous actinic light intensities in the wild type and ΔPetC1 mutant harvested from optimal photosynthesis and after exposures to dark, anaerobic conditions. Figures 18A-18F show

PS II quantum yields as a function of actinic light intensity in cells harvested from these conditions. PS II quantum yields were determined both before the onset (e.g. *F*s1 in Figure 17) of non-photochemical quenching (NPQ) (Figures 18A, 18C and 18E), and at the end of the actinic illumination period (*F*s2 in Figure 17) (Figures 18B, 18D and 18F).

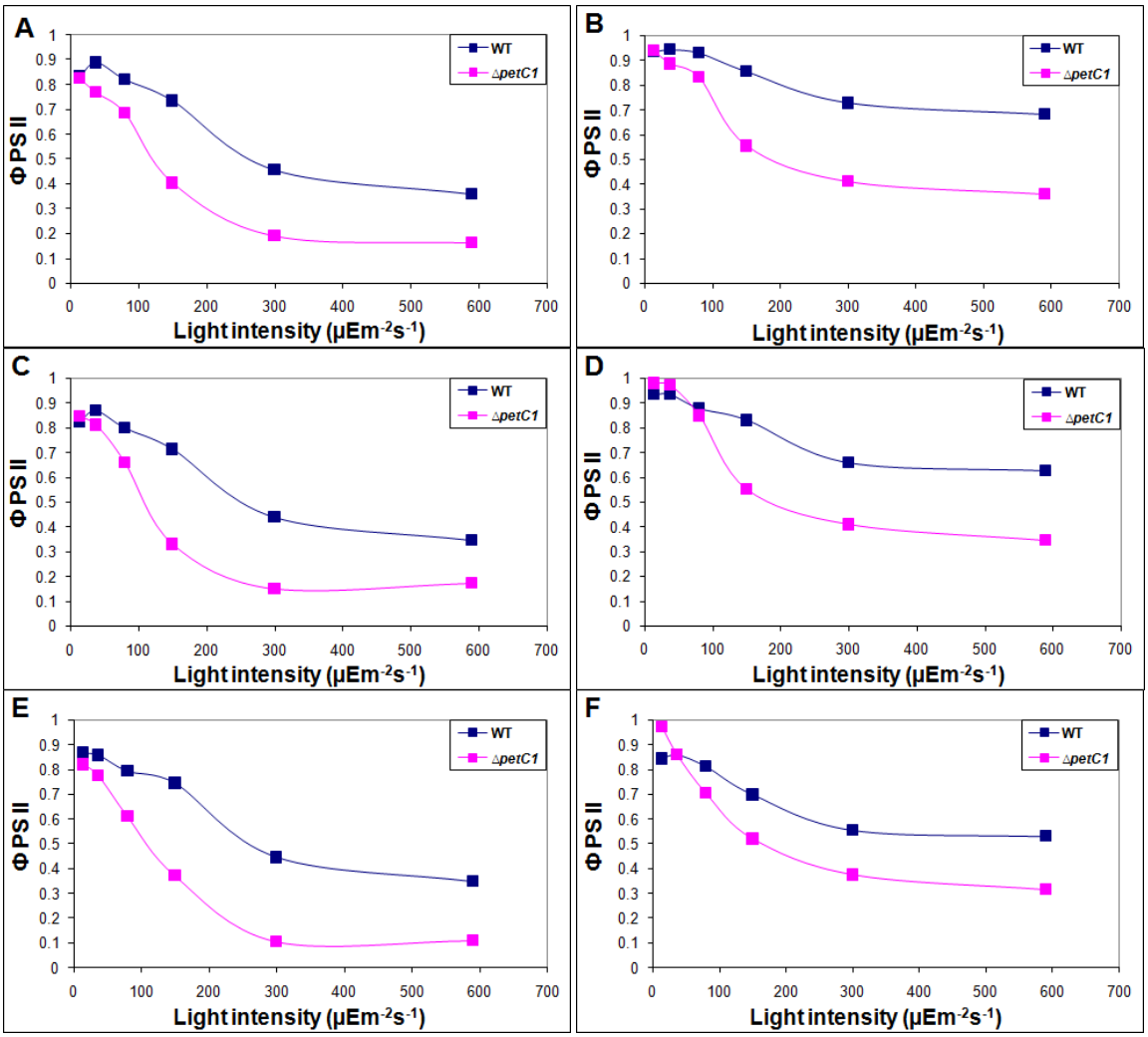

Figure 18: Quantum efficiency of PS II (ΦPSII) in *Synechocystis* 6803 wild type and ΔPetC1 harvested from optimal photosynthesis and after dark anaerobiosis. Panels A and B: Optimal photosynthetic conditions**; Panels C and D:** after 1st hour dark anaerobic conditions**; Panels E and F:** after 12th hour dark anaerobic conditions**; Panels A, C and E:** before non photochemical quenching (e.g. *F*s1 in Figure 17)**; Panels B, D and F:** after non photochemical quenching (e.g. *F*s2 in Figure 17)**.**

Legends: WT, Wild type strain; ΔPetC1, mutant strain. PS II quantum yields (obtained from fluorescence traces such as in Figure 17) from the wild type and ΔPetC1 from optimal photosynthetic conditions and after dark anaerobiosis are shown as a function of light intensity. PS II quantum yield were calculated as: ΦPSII = (*F*m'–*F*s)/ *F*m' (Evans, 1986). A quantum efficiency of 1.0 means that the PQ pool is fully oxidized and readily able to accept electrons from PS II. A quantum efficiency of 0 means that, the PQ pool is completely reduced and unable to accept any electrons from PS II, thus resulting in maximum PS II fluorescence.

Figures 18A to 18F show representatives PS II quantum yield data. Similar studies were carried out at all seven time points from optimum photosynthetic to 12 hour dark-anaerobic conditions. The higher quantum yields after NPQ (see again the points Fs2 relative to Fs1 in Figure 17) indicate a greater oxidation of the PQ pool resulting from dissipation of PS II excitation energy as heat via a non-photochemical quenching mechanism. Increased differences in PS II quantum yields before and after the onset of NPQ, with increasing light intensity, underlines the importance of NPQ in protecting PS II in the presence of high light. As shown in the Figures 18A, 18C and 18E, increases in actinic light intensity result in decreased PS II quantum yields. This is in agreement with the results of Weis and Berry (1987) as well as Harbinson, Genty & Baker (1989) who observed decrease in quantum efficiency with increase in actinic light intensity in sunflower and pea chloroplasts, respectively. At lower light intensities, before the onset of NPQ, the differences between quantum yields exhibited by the the wild type and ΔPetC1 strains appeared to be smaller. For PS II quantum yields observed after NPQ and at low light intensities, the ΔPetC1 mutant exhibited quantum yields comparable to or higher than those in the wild type. These data from low actinic light intensities suggest that the ΔPetC1 mutant can operate efficiently at low light with a flux of electrons through the PQ pool and cytochrome *bf* complex comparable to that in the wild type. However, as light intensities increased (150 μE $m^{-2}s^{-1}$ and higher), the PS II quantum yield of the wild type declined much less steeply than in ΔPetC1, indicating that the mutant had difficulty re-oxidizing the PQ pool. In both strains, the PS II quantum efficiencies declined sharply from 14 to 300 μE $m^{-2}s^{-1}$ followed by very small decreases

from 300 to 590 μE $m^{-2}s^{-1}$. Thus a light intensity of 300 μE $m^{-2}s^{-1}$ appears to be saturating for both strains under all conditions tested.

The higher quantum efficiency at high light intensities in the wild type relative to the ΔPetC1 mutant indicates that the wild type is better able to oxidize the PQ pool. Re-oxidation of the PQ pool depends on the quantity and performance of cytochrome *bf* complexes and of terminal oxidases that are able to remove electrons from the PQ pool (Tsunoyama et al., 2009). The activity of the cytochrome *bf* complex in turn depends, among other factors, on the performance of the Rieske ISP subunit. The ΔPetC1 strain has been shown to possess higher terminal oxidase activity (Schneider, Berry, Rich, Seidler & Rögner, 2001; Schneider et al., 2004a; Tsunoyama et al., 2009;) but a lower cytochrome *f* content than the wild type as now shown by several studies (Nelson & Kallas, 2000-2007; Schultze et al., 2009; unpublished data; Tsunoyama et al., 2009; Figures 10A, 10B, 11J, 11K, 15C). Lower Rieske ISP transcript levels (*petC1* and *petC2* combined) in ΔPetC1 relative to wild type also suggest lower cytochrome *f* contents (Nelson & Kallas, 2000-2007, unpublished data; Schultze et al., 2009; Tsunoyama et al., 2009; Figures 10A, 10B, 11A, 11B, 11C). Hence, the lower PS II quantum yields exhibited by the ΔPetC1 mutant cannot be specifically related to the catalytic activities of the PetC1 and PetC2 Rieske proteins.

It is well known that in absence of light, the PQ pool in cyanobacteria typically becones reduced by respiratory electron transport (Mullineaux & Allen, 1986). Thus, I expected to see decreased PS II quantum efficiencies in both the wild type and ΔPetC1 mutant after shifts from optimal photosynthetic to dark anaerobic conditions.

But, as seen in Figures 18A-18F, even after 12 hours of dark anaerobic exposure, the quantum yields within each strain remained fairly similar in cells harvested from photosynthetic versus anaerobic conditions. At a given light intensity, the redox state of the PQ pool remained fairly constant over all of the time points under study, even after 12 hours under dark anaerobic conditions. These data further indicate that *Synechocystis* 6803 has evolved finely tuned mechanisms to rapidly regulate the redox potential of the PQ pool to prevent over-reduction and thus photodamage. The presence and up-regulation of PQ-oxidizing, terminal oxidase enzymes is one such mechanism. From the similar patterns of PS II quantum yield curves obtained from cells harvested from photosynthetic growth and after dark anaerobiosis (Figures 18A-18F), it appears that the activity of terminal oxidases closely follows and is proportional to the redox state of PQ pool. At the same time, the cytochrome *bf* complex clearly plays a major and perhaps predominant role in PQ pool redox maintenance. In all cases, at increasing light intensities, the ΔPetC1 mutant, with its lower cytochrome *bf* content, showed a much lower PS II quantum efficiency than the wild type.

DISCUSSION

Several eukaryotic (higher plants and algae) but primarily prokaryotic, cyanobacterial genomes have been shown to possess multiple genes coding for Rieske ISP components of cytochrome *bf* complexes. Possible functions of Rieske ISP isoforms have been most extensively studied in cyanobacteria (Schneider & Schmidt, 2005). *Anabaena* sp. PCC 7120 (hereafter *Anabaena* 7120) contains four different genes, *petC1, C2, C3* and *C4* among which *petC3* shows only 20% sequence similarity to *petC1* (which encodes the 'typical' Rieske ISP) in contrast to 70% similarity shown by *petC2* and *petC4*. PetC1, 2 and 4 proteins show molecular weights of ~19kDa while PetC3 has a molecular weight of ~14 kDa. These observations in *Anabaena* 7120 are in agreement with those in *Synechocystis* 6803 except for the absence of PetC4 isoform in the latter (Schneider, Berry, Rich, Seidler & Rögner, 2001). Another extensively studied cyanobacterium, *Synechococcus* sp. PCC 7002 (hereafter *Synechococcus* 7002) possesses three Rieske ISP isoforms, PetC1, C2 and C3, of which PetC1, encoded by the *petC1* gene in the *petC1-petA* operon, forms the functional Rieske ISP of the cytochrome *bf* complex. The presence of a functional *petC1* gene has been observed to be essential for survival in *Synechococcus* 7002 (Yan & Cramer, 2003). In contrast, *Thermosynechococcus elongates* and *Gloeobacter violaceus* carry only a single *petC* gene which is part of an operon and is co-transcribed with *petA* gene coding for cytochrome *f* (Kallas, Spiller & Malkin, 1988a; Kallas, Spiller & Malkin, 1988b; Nakamura, Kaneko, Sato, Ikeuchi, Katoh, Sasamoto, … Tabata, 2002; Nakamura,

Kaneko, Sato, Mimuro, Miyashita, Tsuchiya, … Tabata, 2003; Schneider, Altenfeld, Thomas, Schrader, Muhlenhoff & Rögner, 2000). In phylogenic trees, only the *petC1* or *petC* genes that are co-transcribed with *petA* are closely related to Rieske ISP genes of chloroplasts (Schneider & Schmidt, 2005). Recently, a ΔPetC mutant of alga *Chlamydomonas reinhardtii* has been successfully engineered which shows only heterotrophic growth (De Vitry, Finazzi, Baymann & Kallas, 1999). These observations from a number of cyanobacteria indicate that, PetC1 is the major Rieeske protein to be a part of cytochrome *bf* complex. Based on the absence of more than one *petC* isoforms in plants as well as in primitive cyanobacteria such as *Thermosynechococcus elongates* and *Gloeobacter violaceus*, emergence of other *petC* genes appear to be the outcome of later evolutionary steps, after the endosymbiotic event which involved engulfing of a cyanobacterum by a eukaryotic cell (Schneider, Volkmer, Berry, Seidler & Rögner, 2004b).

In *Synechocystis* 6803, the role of PetC1 as the major Rieske ISP is well supported (Nelson & Kallas, 2000-2007, unpublished data; Schneider et al., 2004a; Schultze et al., 2009; Tsunoyama et al., 2009). A ΔPetC1 mutant has been constructed (Schneider et al., 2004a) and has been a great tool for understanding the functions of PetC1 as well as the PetC2 Rieske protein, which is most similar to PetC1. Over expression of PetC2 in the ΔPetC1 mutant to compensate for loss of the PetC1 protein has now been shown in several studies (Nelson & Kallas, 2000-2007, unpublished data; Schultze et al., 2009; Tsunoyama et al., 2009), and is further supported by work presented in this thesis. Recent studies also show up-regulation of the *petC2* and *petC3* genes in response to stress

conditions such as low oxygen supply, presence of zinc, cadmium, hydrogen peroxide and exposure to high light intensity (Houot et al., 2007; Summerfield et al., 2008; Tsunoyama et al, 2009) suggesting that PetC2 and PetC3 Rieske ISP isoforms may have regulatory roles. Preferential, elevated expression of the *petC1* gene under optimal photosynthetic conditions relative to *petC2* is apparently not related simply to a better catalytic activity of the PetC1 Rieske ISP relative to PetC2. Although, lower flexibility in the PetC2 glycine rich domain (which is required for electron transfer by Rieske ISPs) has been suggested as a possible reason for lower efficiency in PetC2 (Schneider et al., 2004a), data presented in this thesis suggest that the PetC2 ISP may be as efficient as PetC1 (see Results Section E.)

In 77K fluorescence spectroscopy experiments, the ΔPetC1 mutant has been reported to possess a lower amount of PS II relative to PS I compared to the wild type (Schneider et al., 2004a). Contrary to those results, similar experiment carried out in our lab showed that, after normalizing PS I fluorescence, APetC1 cultures grown under a variety of conditions showed ~25% higher PS II contents relative to similarly grown wild type strains (Nelson & Kallas, 2000-2007, unpublished data). The ΔPetC1 mutant is also more sensitive to high light intensity than the wild type, and this sensitivity has been suggested to arise from hindrance of electron transport through the cytochrome *bf* complex and thus incomplete oxidation of PQ pool (Tsunoyama et al., 2009).

My thesis research attempted to understand the functions of Rieske ISP isoforms of *Synechocystis* 6803 at transcriptomic, proteomic and kinetic levels and their impacts on PQ pool redox status and regulation of photosynthesis. The goal of this work was to gain

better understanding of the linked photosynthetic and respiratory electron transport chains of cyanobacteria under optimal photosynthetic as well as stress conditions.

A] Gene Expression Studies with Reverse-Transciptase Quantitative PCR (RT-qPCR, Standard Curve method)

For the transcriptomic studies; the method employed for RNA isolation was a modification of hot phenol method derived from the original protocol of Kohrer and Dömday (1991). The modified hot phenol method involves the immediate injection of harvested cultures into a metabolic stop solution to arrest the highly dynamic processing and turnover of cyanobacterial mRNA transcripts. In our lab, the hot phenol method is preferred over RNA isolation by commercially available Qiagen™ reagents, as used by Tsunoyama et al. (2009) for a couple of reasons. RNA isolation using the Qiagen™ reagents involves at least 10 minutes of sample processing before the addition of metabolic stop reagents. As shown by RT-qPCR experiments performed in our lab by Zangl & Kallas (2006, unpublished data), gene expression levels may change rapidly by many fold between 0 to 10 minutes after culture harvest. Also, from my experience, although RNA isolated by the Qiagen method takes less time and the purity of RNA is high (>90%); the hot phenol method gives a very high yield of RNA (up to 3.27µg/µl or ~80 µg per 40 mL culture), with a purity of 'crude RNA' that varies from 68-90%. The hot phenol reagents, once prepared, have long high shelf life compared to those from the Qiagen™ kit. Although I typically treated the crude RNA twice with DNase, I found that a single DNase treatment is sufficient to get rid of contaminating DNA. The time of

incubation at 37^0C is very important. Although, the manufacturer suggests a 20-30 minute incubation (Applied Biosystems, 2009, part number AM1907), I found that an incubation period of 45 minutes works best.

RT-qPCR with TaqMan™ probes was used to investigate the expression responses of specific genes, because of the high specificity of this method relative to others, notably the SYBR green method. In the TaqMan™ assay, the same user-selected, signal-threshold value is automatically set by the software for every sample. For *petC1*, the probe designed met all criteria suggested by the 'TaqMan™ universal PCR master mix protocol' (Applied Biosystems, 2002, part number 4304449 Rev. C) except the presence of 'G' at its 5' end. The presence of a 'G' close to the 5' fluorescent dye was indeed observed to quench fluorescence as revealed by primer-probe efficiency check and gene expression results by lower maximum fluorescence plateau levels in ΔRn (where Rn is the fluorescence of the reporter dye divided by the fluorescence of the passive reference dye while ΔRn is the difference of Rn and and the baseline fluorescence signal) vs. cycle number plots (data not shown). However, a lower fluorescence signal plateau should not affect data interpretation since this does not influence cycle to threshold (C_T) calculations.

As adviced in the manufacturer's application note (Applied Biosystems, 2008, publication number 136AP01-01), for a set of genes under a study, efficiency values between 90-110% are acceptable to which I tend to disagree. In the Standard Curve method, the equation of the graphs is important to normalize the gene expression data as long as the R^2 values are above 0.98 and the C_T values obtained from gene

expression data fall within the range of C_T values obtained using DNA or crude RNA standard diluted over several $\log_{10}$ dilution values in efficiency studies. This way, the C_T values obtained from different primer-probe sets for the same template concentration can be normalized on a scale of $\log_{10}$ concentration (pg/µl). For other methods, as well, of presenting RT-qPCR data, large differences in the efficiencies of two primer-probe sets would certainly affect the interpretation of relative gene expression results. In that case, normalization can be performed by adjusting the C_T values by normalizing primer-probe efficiencies to 100%.

RT-qPCR investigation of transcript levels from *Synechocystis* 6803 wild type and the ΔPetC1 mutant grown under optimal photosynthetic conditions and then shifted dark anaerobic conditions, with samples taken over a range of seven time points, presented a good picture of selected gene expression responses under these conditions (Figures 10A, 10B & 11A-11M). Down-regulation (Figures 10A, 10B & 11A-11M) of all of the genes involved in photosynthesis and respiration after switching from optimal photosynthetic conditions to dark anaerobic conditions clearly reveal dark anaerobic condition as 'stress' for the strains under study. Much higher *petC1* transcript levels relative to *petC2* in the wild type under optimal photosynthetic conditions, and elevated *petC2* transcripts in the ΔPetC1 mutant relative to the wild type (Figures 10A, 10B and 11A-11C), give credence to previous observations of PetC1 being the major Rieske ISP (Schneider et al., 2004a; Tsunoyama et al., 2009). These data also clearly support previous findings that the PetC2 Rieske ISP may replace PetC1 in absence of PetC1 (Schneider et al., 2004a; Tsunoyama et al., 2009). Previous studies observed up-regulation of *petC2* and *petC3* genes under

certain stresses (Houot et al., 2007; Summerfield et al., 2008; Tsunoyama et al., 2009). However, I did not see up-regulation *petC2* or *petC3* under the dark, anaerobic conditions tested here. Based on results of oxygen uptake studies, Schultze et al. (2009) suggested a possible role of PetC2 in respiration. If this is correct, then up-regulation of *petC2* under dark-anaerobic conditions would not be expected.

My RT-qPCR study of wild type and ΔPetC1 cultures grown under optimal photosynthesis and then shifted to dark aerobic conditions showed ~44 times down-regulation of the *petC1* gene. Also, interestingly, in the wild type, transcript levels of *petC2* decreased only gradually during the anaerobic incubation while those in ΔPetC1 decreased drastically, over 35-fold by the end of the 12 hour period. Recall, however, that the *petC2* transcripts started at much higher levels in the ΔPetC1 mutant under photosynthetic conditions than in the wild type (Figures 10A, 10B & 11A-11C). Combined levels of *petC1* and *petC2* transcripts in the wild type were always higher than *petC2* transcript levels of the ΔPetC1 mutant. The wild type in addition had higher *petA* transcript levels consistent with higher electron flow through the cytochrome *bf* complex in the wild type strain (Figures 10A, 10B and 11A-11C, 11J, 11K).

The ΔPetC1 mutant has been shown previously to contain an unusual cytochrome *bf* complex containing comparable cytochrome b_6 levels but lower cytochrome *f* and subunit IV levels (Tsunoyama et al., 2009). Data from this thesis support and extend these findings, as shown in Table 5, and discussed further below. Decreased transcript levels of the *petA* gene in the ΔPetC1 strain relative to wild type supports the idea that insertional mutagenesis of *petC1* (during construction of the ΔPetC1 mutant) also resulted in altered

and lower transcription of the downstream *petA* gene in the *petC1-petA* operon (Tsunoyama et al., 2009). As shown by immunoblot studies, the decreased *petA* transcript level in the ΔPetC1 mutant (Figures 10A, 10B and 11J, 11K), also observed by microarray studies (Nelson & Kallas, 2000-2007, unpublished data) is actually reflected at the protein level (Tsunoyama et al., 2009).

Similar levels of *petC3* transcripts were found in both the wild type and ΔPetC1 mutant, along with higher *petC3* trancript levels than those of *petC1* and *petC2* genes throughout the experiments under dark anaerobic (Figures 10A, 10B and 11A, 11B, 11C, 11D, 11E) as well as dark aerobic conditions (data not shown). These data appear to support the results of Schultze et al. (2009) who concluded that the PetC3 Rieske ISP has a function independent of the cytochrome *bf* complex. The observation of the ΔPetC3 strain being ~25% bigger in size and containing almost twice chlorophyll and plastocyanin contents over the wild type (Tsunoyama et al., 2009) may indicate a role of PetC3 in either regulation or as a secondary electron donor/acceptor. Comparable levels of *psaC* transcripts (which codes for subunit VII of PS I) in both the wild type and ΔPetC1 strains (Figures 10A, 10B and figures 11F, 11G) suggests that PS I contents were similar in these strains under the conditions tested. These data are in accord with 77K fluorescence spectroscopy results of Schneider et al. (2004a) and proteomic data (Table 7) that will be discussed below.

Finally, higher transcript levels of *zwf* (for the respiratory glucose 6-phosphate dehydrogenase enxyme) in the ΔPetC1 mutant relative to the wild type, after exposures of 2 hours and longer to dark anaerobic (Figures 10A, 10B and 11H, 11I) as

well as dark aerobic conditions, may further suggest that the PetC2 Rieske ISP has a role in respiration.

In addition to the genes that were studied by RT-qPCR, inclusion of *petB* (cytochrome b_6), *petD* (subunit IV), genes coding for key subunits of PS II, *petE* (plastocyanin), *cydA* (cytochrome-*bd* oxidase subunit I) in further studies would present a broader picture of gene expression of other electron transfer chain components in response to the *petC1* deletion in the ΔPetC1 mutant.

B] Metabolic Labeling and Isotope-assisted Quantitative Mass Spectrometry

As described in the Results section, I used a proteomic approach that was intended to support the transcriptomic data and provide direct information about the impact of the PetC1 deletion on membrane protein composition in the ΔPetC1 mutant. In these experiments, the control, wild type culture was inoculated from a colony and grown in ^{15}N BG-11 medium for 25 days (>8 generations). For this reason I assumed >98% ^{15}N incorporation into the proteins of the control culture and did not perform a separate assay to determine ^{15}N content. The experimental protocol for metabolic labeling and quantitative mass spectrometry was derived from the protocol of Nelson et al. (2007) which had been successfully followed previously in our lab. After the trypsin digestion step and before C18 column purification, addition of formic acid to 5% (v/v) final concentration was crucial for stopping the tryptic reaction and acidifying peptides for optimal binding to the C18 silica embedded tips. My initial attempt to use formic acid at 0.3% (v/v) final concentration did not yield any final LC-MS/MS results, suggesting that

peptides had not bound to the C18 column. In LC-MS/MS runs, the flow of elutes from the LC column into the mass spectrometer could only be set at ~4µl/min compared to a more 'ideal' flow of ~1µl/min, which had given good results in the past. Even after careful preparation of protein samples, I could not get only 10-25 protein identities for the four samples under study. Also, for many protein identities, there were no same types of light and heavy peptides available for direct comparison.

Protein identities includes predominantly PS I components followed by PS II components and phycobilisome associated proteins. Phycobilisomes being soluble light-harvesting proteins, and with the exception of possible membrane-bound linker subunits, should not be present within thylakoid membranes. However, phycobilisomes are associated with thylakoid membranes and extremely abundant in cyanobacteria (DeRuyter & Fromme, 2008, pp. 217-269) suggesting that they were present as impurities in the test samples. Because of 40 to 60% variations in protein contents in ^{14}N wild type against ^{15}N wild type, both grown under optimal photosynthetic conditions (Table 7), no firm conclusions can be drawn from these data. The only apparently significant change was 3-fold increase in the PS II, CP47 chlorophyll-binding antenna protein (PsbB) in the wild type during anaerobic incubation. This protein was detected as well in the ΔPetC1 anaerobic sample, but its content did not change significantly. However, data from light-induced, redox kinetics experiments do strongly support the down-regulation of cytochrome *bf* subunits but not photosystem I in the ΔPetC1 mutant, as will be further discussed below. Because of lack of time, I did not get chance to work on at least two additional biological replicates for protein studies. The plan was to obtain

many more protein identifications and comparisons by analyzing two additional biological replicates on a much more sensitive, LTQ-Orbitrap mass spectrometer at the University of Wisconsin, Madison Biotechnology Center.

C] Quantification of Electron Transfer Components by Kinetics Spectrophotometry

To estimate the concentration of electron transfer chain components by light-induced, maximal oxidation or reduction signals, I had initially planned to use dibromothymoquinone (hereafter DBMIB), which is known to block electron flow throught the quinol-oxidation (Q_p) site of the cytochrome *bf* complex (Trebst, 1980). Use of DBMIB had shown good results in *Synechococcus* sp. PCC 7002 (hereafter *Synechococcus* 7002) in our lab as an effective mean of blocking electron transport through the cytochrome *bf* complex (Kallas, 1990-2007, unpublished data). Unfortunately, in both the wild type and ΔPetC1 strains of *Synechocystis* 6803 under study, DBMIB was also found to donate electrons directly to plastocyanin and PS I as observed previously in pea chloroplasts (Bose, 1985; Schansker, Tóth & Strasser, 2005). In other studies, such as one by Vener, Van Kan, Rich, Ohad & Andersson (1997), no changes were observed in redox states of cytochrome *f*, plastocyanin and PS I after addition of DBMIB in spinach chloroplasts, suggesting diverse effects of DBMIB on different systems. Consequently, I used high actinic light intensities in the absence of DBMIB to try to achieve either maximum oxidation of cytochrome *f*, plastocyanin and the PS I P700 reaction center chlorophylls, or maximum reduction could of cytochrome b_6.

My experiments (Figures 15A-15D, Table 11) clearly indicate the presence of a cytochrome *bf* complex in the ΔPetC1 mutant that has an unusual protein and redox center composition with respect to similar cytochrome b_6 contents but at least a 2-fold lower cytochrome *f* content relative to wild type. In wild type, the ratio of cytochrome b_6 to cytochrome *f* is close ~1 while in ΔPetC1 mutant, it is ~0.5. Lower contents of cytochrome *f* and subunit IV of the cytochrome *bf* complex in this mutant were also observed in the immunoblot study of Tsunoyama et al. (2009). In contrast, Schultze et al. (2009) reported a lower content of cytochrome b_6 in the ΔPetC1 mutant. I also found a slightly (~20%) higher PS I content in the ΔPetC1 mutant relative to wild type, consistent with the 77K fluorescence results of Nelson & Kallas (2000-2007, unpublished data) performed in our lab, whereas similar experiment by Schneider et al. (2004a) had found comparable PS I contents. Taken together, these data indicate that the *Synechocystis* ΔPetC1 mutant has a highly unusual PetC2-Cyt *bf* complex that has a typical cytochrome b_6 content, but much lower contents of the cytochrome *f* and subunit IV proteins. This suggests that the major components of this complex are a Rieske ISP (i.e. PetC2) and cytochrome b_6, such as what might be found in a primordial Rieske-cytochrome *b* complex (Kramer, Nitschke & Cooley, 2008, pp. 451-473). The low content of cytochrome *f*, and thus an impaired high-potential chain, also explains the slow turnover of this complex in the ΔPetC1 mutant.

D] Study of Catalytic Efficiencies of the PetC1 and PetC2 Rieske ISPs

Electron transport through the PetC2-Cyt *bf* complex of the ΔPetC1 mutant was found to be ~50 times slower than the wild type by Finazzi and Kallas (2000-2005, unpublished data). Based on the presence of glutamic acid and lysine residues in the flexible hinge domain of the PetC2 Rieske ISP, a lower catalytic efficiency of PetC2 compared to PetC1 was suggested by Schneider et al. (2004a). However, it should be noted that, Yan & Cramer (2003) as well as De Vitry et al. (1999) did not observe any significant impairment of the performance of PetC1 Rieske ISPs of cytochrome *bf* complexes by amino acid substitutions in the flexible hinge, compared to more dramatic impacts of similar changes in Rieske ISPs of cytochrome *bc* complexes (Darouzzet, Moser, Dutton & Daldal, 2001). Unfortunately, the Joliot-type (BioLogic JTS-10), LED spectrophotometer employed in the short-flash experiments to compare catalytic efficiencies of PetC1- and PetC2-Rieske ISP-containing cytochrome *bf* complexes was not sensitive enough to track absorbance changes elicited by very small actinic light intensities from 14 to 80 μE $m^{-2}s^{-1}$ to allow direct comparison of the cytochrome *f* signals shown by the wild type and ΔPetC1 strains. As described in the Results section, weak actinic light flashes of short duration were necessary to approach single turnovers of the cytochrome *bf* to assess the intrinsic catalytic efficiencies of the PetC2- and PetC1-containing complexes. Nonetheless, data were obtained at decreasing actinic light intensities in both the wild type and the ΔPetC1 mutant (Figures 16A and 16B). These data show that as the actinic light intensity decreased, cytochrome *f* re-reduction rates increased. At the lowest actinic light intensities, the cytochrome *f* reduction rate in the

ΔPetC1 mutant began to approach the faster rates observed in the wild type. These data suggest that the PetC2-Cyt *bf* complex in ΔPetC1 (and thus the PetC2 Rieske ISP) may be as efficient as the normal PetC1-Cyt *bf* complex and PetC1 Rieske ISP in the wild type. These data further support the conclusion that the slow turnover of the cytochrome *bf* complex in the ΔPetC1 mutant results from a low cytochrome *f* content and not from a lower catalytic efficiency of the PetC2 Rieske ISP.

E] Impact of the ΔPetC1 Mutation and Dark Anaerobiosis on PQ Pool Redox State

In the exponential phase of growth, at the same cell density, the chlorophyll content of the ΔPetC1 strain was always higher than that in the wild type as previously observed by Tsunoyama et al. (2009). The program I used to track PS II fluorescence with the JTS-10 spectrophotometer has an actinic light illumination period of just 60 seconds (see Figures 17A, 17B). Thus, I could not observe the total extent of non-photochemical quenching (NPQ, detected as a progressive decrease in PS II fluorescence evident in Figures 17A, 17B) exhibited by the strains under study. Similarly, PS II contents in the ΔPetC1 mutant strains were found to be higher (based on higher PS II chlorophyll fluorescence) than in the wild type, supporting 77K fluorescence spectroscopy results of Nelson & Kallas (2000-2007, unpublished data)), but contrary to those of similar experiment by Schneider et al. (2004a). Higher chlorophyll content of the ΔPetC1 strain can be correlated to a higher PS II content (Figures 17A and 17B) and higher PSI content as shown by Figures 14, 15D and Table 11. I have found a correlation between

chlorophyll as well as PS II content and the basal fluorescence shown by a strain (data not shown).

In my experiments, the ΔPetC1 strain failed to a show state transition as observed by Tsunoyama et al. (2009). However, I also failed to see state transitions in the wild type (Figures 17A, 17B) suggesting that one or both of these strains was not behaving properly. Volkmer, Schneider, Bernàt, Kirchhoff, Wenk & Rögner (2007) suggested that the ΔPetC1 mutant may reside permanently in state II (PQ pool reduced) under all conditions because of its impaired ability to oxidize the PQ pool. My observation of a very minimal state transition in the wild type is contrary to ~25% state transition (increased PS II fluorescence upon a dark to light transition) observed by Nelson & Kallas (2000-2007, unpublished data) and Tsunoyama et al. (2009) who also observed ~30% state transition in the ΔPetC1 mutant. In the experiments with the JTS-10 spectrophotometer Kallas (1990-2007, unpublished data) observed state transitions of ~50% in the wild type grown to stationary phase. I had grown cultures for my experiments under optimal photosynthetic conditions (3% CO_2, 50 μmol photons m^{-2} s^{-1}, for *Synechocystis* 6803) in stirred Roux flasks, while cultures used by Tsunoyama et al., (2009) and Nelson & Kallas (2000-2007, unpublished data) were grown in glass tubes or with shaking in Erlenmyer flasks. Thus growth conditions as well as cell age appear to be important factors in state transition responses, and may account for the observed differences in these experiments.

Decreased PS II quantum yield with increase actinic light intensity has been demonstrated (Harbinson et al., 1989; Weis & Berry, 1984). Similarly lower quantum

yields of PS II in the ΔPetC1 mutant relative to wild type; because of its more reduced PQ pool (Schneider et al., 2004a) was expected. But, absolutely no reduction in PS II quantum yields even after 12 hours under dark anaerobic conditions was surprising, and indicates no change in the redox status of the PQ pool. This homeostasis of PQ pool redox potential may be explained by an increase in the activity of terminal oxidases that directly oxidize the PQ pool and thus prevent its over reduction. Increased cytochrome *bd* oxidase activity in the ΔPetC1 strain has been previously suggested (Schneider et al., 2001; Schneider et al., 2004a) and shown by immunoblot studies (Tsunoyama et al., 2009). Under dark anaerobic conditions, the terminal oxidase activity appears to increase proportionally in both the wild type and ΔPetC1 mutant strains to keep the redox status of the PQ pool intact. In this process, based on the unaltered status of the PQ pool, the cytochrome *bf* complex, although altered as in the ΔPetC1 mutant, seems to sense the redox state of PQ pool, and perhaps signal adjustments, quite efficiently. My observations from absorbance experiments performed with Joliot-type JTS-10 spectrophotometer, showed a reduction in electron transport through the cytochrome *bf* complex in both the wild type and ΔPetC1 strains after anaerobic incubations (data not shown). This observation may be related to reduction in cytochrome *bf* content under dark anaerobic conditions rather than an over-reduced PQ pool (which would impede cytochrome *bf* turnover by a lack of oxidized plastoquinone to accept electrons from the quinone-reductase, Q_n-site of the complex). Higher contents of cytochrome *bd* oxidase in the ΔPetC1 mutant may definitely play an important role in the survival of this mutant strain. The contribution of terminal oxidases in transport of electrons out of the PQ pool

may be studied by performing fluorescence experiments in presence of cyanide, as cyanide acts as an efficient inhibitor of all terminal oxidases (Berry et al., 2002).

For all of the approaches and comparisons I have done in my thesis between the wild type and ΔPetC1 strain, I decided to use an optical density ($O.D._{750nm}$) of 0.5 or 1.0 as the common parameter for normalizing cell density rather than protein or chlorophyll content. Considering the similar sizes of the wild type and ΔPetC1 mutant (Tsunoyama et al., 2009), I intended to compare the performance of these strains with the 'cell' as the basic unit for comparison. Normalization of optical density values to cell counts for the wild type and mutant might have provided an even better comparison.

Impaired performance of the *Synechocystis* 6803 ΔPetC1 mutant can be blamed on its lower cytochrome *bf* content, notably cytochrome *f* as suggested and shown (Nelson & Kallas, 2000-2007, unpublished data; Schultze et al., 2009; Tsunoyama et al., 2009; Figures 10A, 10B, 11J, 11K, 15B). Data presented here further suggest that the PetC2 Rieske ISP may be as efficient as the major PetC1 Rieske ISP as shown by data in Figures 16A and 16B. Construction of a ΔPetC1 mutant that retains an active promoter site for *petA* such that, normal amounts of PetA are incorporated into a PetC2-Cyt *bf* complex would be of great interest. This would pave a way to directly compare the wild type PetC1-cytochrome *bf* complex with a PetC2-cytochrome *bf* complex in a ΔPetC1 mutant that maintains all other cytochrome *bf* and electron transfer components at normal levels.

CONCLUSION

In *Synechocystis* PCC 6803, as in other cyanobacteria and chloroplasts, the cytochrome *bf* complex plays a central role in electron transport in which the Rieske iron-sulfur protein (ISP) is a key element. Along with the Rieske ISP, cytochrome *f* is also essential for the catalytic activity of the cytochrome *bf* complex. In absence of a viable PetC1 Rieske ISP, as well as under dark anaerobic as well as dark aerobic stress conditions, the function of PetC1 appears to be gradually replaced by an alternative PetC2 Rieske ISP. Thus PetC2 may have a role in respiration or dark, anaerobic electron flow pathways. Expression of another, alternative, PetC3 Rieske ISP seems to be least affected by dark anerobic or aerobic conditions, thus suggesting an important role, either regulatory or protective, played by the PetC3 Rieske ISP independent of the cytochrome *bf* complex. Disruption of the promoter region of the *petA* gene for cytochrome *f* during creation of the PetC1 mutation (Schneider et al., 2004a) resulted in lower expression of cytochrome *f* and may be the sole responsible factor behind slower electron transport in the ΔPetC1 mutant. The PetC1 mutation results in an unusual cytochrome *bf* complex in the mutant strain comprised primarily of a PetC2 Rieske ISP and cytochrome b_6 as predominant subunits, perhaps resembling a primordial, 'Rieske-cytochrome *b*' complex (Kramer et al., 2008, pp. 451-473). Considering the contribution of such an unusually composed cytochrome *bf* complex on slower electron transport, the catalytic activities of the PetC1 and PetC2 Rieske ISPs were found to be similar if not identical. The ΔPetC1 mutation is responsible for a more reduced PQ pool in the ΔPetC1 mutant than in its wild

type counterpart. The redox state of the PQ pool is sensed by the cytochrome *bf* complex so that under dark anaerobic stress, over reduction of the PQ pool is avoided, apparently by an elevated activity of terminal oxidases. This terminal oxidase activity is responsible for protection of cells from photodamage. Based on preferential expression of the *petC1* gene over the *petC2* gene, perhaps a chance outcome of evolution and incorporation of the encoded PetC1 Rieske ISP into cytochrome *bf* complexes under optimal photosynthetic conditions, the PetC1 ISP has become the major Rieske ISP of photosynthesis.

There are numerous scopes to broaden this research. RT-qPCR work can be extended to study expression responses of *petB* (cytochrome b_6), *petD* (subunit IV), genes coding for key subunits of PS II, *petE* (plastocyanin), *cydA* (cytochrome-*bd* oxidase subunit I), and others, or supported by global gene expression studies to further investigate the roles of PetC1 and PetC2 Riesle ISPs under optimal photosynthetic and dark anaerobic as well as other stress conditions. Unfortunately, using the available mass spectrometry equipment, electron transfer proteins, with the exception of some PS II and PS I components, could not be detected. With refinement of protein expression studies including employment of biological replicates or use of more sensitive mass spectrometers, reliable protein data to support the gene expression data could be obtained. Optical and fluorescence kinetics experiments can be performed in the presence of cyanide to investigate the role of terminal oxidases involved in prevention over-reduction of the PQ pool under dark anaerobic conditions. Finally, creation of a ΔPetC1 mutant that retains an active promoter site for *petA* allowing incorporation of normal amounts of

cytochrome *f* into a PetC2-cytochrome *bf* complex would be of great interest for assessing the catalytic efficiencies and roles of PetC1 and PetC2 Rieske iron-sulfur proteins.

APPENDIX A

Microbial Media

I] BG-11 medium

a) ***1000X Trace metal mix***

1. Add 700 mL of dH_2O to 1000 mL flask and add following ingredients while stirring.

Ingredient	g/L	Final concentration (mM)
H_3BO_3	2.86	46.3
$MnCl_2.4H_2O$	1.8	9.15
$ZnSO_4.7H_2O$	0.222	0.77
$Na_2MoO_4.H_2O$	0.39	1.61
$CuSO_4.5H_2O$	0.079	0.32
$Co(NO_3)_2.6H_2O$	0.0494	0.17

2. Once the contents are dissolved, bring the final volume to 1000 mL and store in a sterile bottle at 4^0C.

b) ***100X BG-11***

1. Add 700 mL of dH_2O to 1000 mL flask and add following ingredients while stirring.

Ingredient	Quantity	Final concentration
$NaNO_3$*	149.58 g/L	1.76 M
$MgSO_4.7H_2O$	7.49 g/L	30.39 mM
$CaCl_2.2H_2O$	3.6 g/L	24.49 mM
Citric acid	0.6 g/L	3.12 mM
0.5 M Na_2EDTA, pH 8.0	0.56 mL	0.28 mM
1000X Trace metal mix	100 mL	100X

* While preparing BG-11 medium with ^{15}N, use $NaNO_3$ with heavy isotope of nitrogen i.e. $Na^{15}NO_3$. Apart from this, all the ingredients remain same for BG-11 medium with ^{15}N.

2. Once the contents are dissolved, bring the final volume to 1000 mL and store in a sterile bottle at 4^0C.

c) ***BG-11 liquid medium (1 liter)***

1. Add following ingredients (which are stored at 4^0C) in a 2000 mL conical flask.

Ingredient	Quantity (mL)	Final concentration
100X BG-11	10.0	1X
1.0 M TES	5.0	5.0 mM
42.857 mM Ferric ammonium citrate	1.0	0.043 mM
189 mM Na_2CO_3	1.0	0.189 mM
175 mM K_2HPO_4	1.0	0.175 mM

2. Add dH_2O to bring final volume to 1000 mL. Autoclave the medium for 20 minutes and once it cools down, store at room temperature in sterile bottles.
3. When growing ΔPetC1 mutant, add chloramphenicol solution in ethanol to the medium to obtain final concentration of 25 μg/mL.

d) ***BG-11 solid medium (1 liter)***

1. Add following ingredients (which are stored at 4^0C) in a 1000 mL conical flask.

Ingredient	Quantity (mL)	Final concentration
100X BG-11	10.0	1X
1.0 M TES	5.0	5.0 mM
42.857 mM Ferric ammonium citrate	1.0	0.043 mM
189 mM Na_2CO_3	1.0	0.189 mM
175 mM K_2HPO_4	1.0	0.175 mM

2. Add dH_2O to bring final volume to 500 mL.

3. Separately, dissolve 15 g Bacto agar in dH_2O in 1000 mL conical flask to bring final volume to 500 mL.
4. Autoclave the flasks separately for 20 minutes and still hot, mix the contents in one flask. Pour 40 mL of the medium to sterile Petri plates. Let the medium in plates cool down to room temperature before placing lids and store at 4^0C.

II] Luria Bertani (L.B.) agar medium (1 liter)

1. Add following ingredients to 500 mL dH_2O in a 2000 mL conical flask.

Ingredient	Quantity (g)
Tryptone	10.0
Yeast extract	5.0
NaCl	10.0
Agar	15.0

2. Adjust the pH to 7.0 using 200 µL 5.0 M NaOH solution and add 15.0 g Bacto agar. Stir well and bring the final volume to 1000 mL.
3. Autoclave the medium for 20 minutes. Pour 25 mL of the medium into each sterile Petri plate. Let the medium in plates cool down to room temperature before placing lids and store the plates at 4^0C.

APPENDIX B

Buffers and Reagents

I] 10T/0.1E buffer

1. Add following DEPC treated ingredients to a sterile 50 mL conical tube.

Ingredient	Quantity (mL)
1.0 M Tris-HCl, pH 8.2	0.5
0.5 M Na_2EDTA, pH 8.0	0.01
Nuclease free water	49.49

* While preparing 10T/0.1 E buffer with pH 7.5, use 1.0 M Tris with pH adjusted to 7.5 using HCl.

2. pH of the buffer is approximately 8.2. Store the tube at 4^0C.

II] Cell suspension buffer (50 mL)

1. Add following DEPC treated ingredients to a 50 mL sterile conical tube.

Ingredient	Quantity (mL)
600 mM sucrose	15.0
1.0 M Na acetate	0.3
Nuclease free water	15.0

2. Mix the contents gently. Store the tube at 4^0C.

III] Chloroform: isoamyl alcohol (24:1) (50 ml)

1. To an oven baked (180^0C/12 hours) 50 mL brown bottle (or oven baked transparent Wheaton bottle covered by aluminum foil), add 48 mL chloroform and 2 mL isoamyl alcohol.
2. Mix the contents gently. Store the bottle at 4^0C.

IV] DEPC treated water/nuclease free water (1 liter)

1. To 1000 mL dH_2O in a 2000 mL oven baked flask (180^0C/12 hours), add 100 µL DEPC to final concentration of 0.1% and stir overnight with the mouth of the flask covered with ethanol sterilized Parafilm™.
2. Autoclave the DEPC treated water for 20 minutes. Once it gets cooled down, store in an oven baked bottle (180^0C/12 hours) at 4^0C.
3. The reagents involved in crude RNA isolation should be treated in the same way, with 0.1% DEPC except phenol, chloroform, ethanol and isoamyl alcohol.

V] Equilibrated phenol (~550 mL)

1. Weigh 200 g of phenol crystals to a clean 500 g brown reagent bottle containing a clean stirrer bar. Heat the phenol to 65^0C to dissolve the crystals.
2. Once phenol crystals get dissolved, add 200 mg 8-hydroxyquinolone to final concentration of 0.1%. Stir to dissolve.
3. Add 15.15 Tris to 250 mL dH_2O to get final concentration of 0.5 M. Stir to dissolve and autoclave the solution. Once the solution cools down, degas with argon for 5 minutes and add it to the phenol and stir rigorously for 30 minutes.
4. Allow the aqueous and non aqueous phases to separate overnight at 4^0C. Test the pH of phenol which should be ~8.0.
5. Add 6.06 g of Tris to 100 mL dH_2O to get final concentration of 100 mM. Stir to dissolve, adjust the pH to 8.2 using HCl. Autoclave the solution and once it cools

down, degas with argon for 5 minutes and add it to the phenol and stir for 15 minutes.

6. Allow the aqueous and non aqueous phases to separate overnight at 4^0C. Store the bottle at 4^0C.

VI] Metabolic stop solution 10X (8 ml)

1. Add following ingredients to a 200 mL Nalgene centrifuge bottle.

Ingredient	Quantity (mL)
Equilibrated phenol	4.0
0.5 M Na_2EDTA, pH 8.0*	3.84
ß mercaptoethanol	0.16

* DEPC treated

2. The contents being polar as well as non polar do not get mixed. Store the bottle at 4^0C.

VII] Phenol: chloroform: isoamyl alcohol (25: 24: 1) (50 mL)

1. To an oven baked (180^0C/12 hours) 50 mL brown bottle (or oven baked transparent Wheaton bottle covered by aluminum foil), add 25 mL of equilibrated phenol (with taking care not to add the Tris containing aqueous phase) followed by 24 mL chloroform and 1 mL isoamyl alcohol.
2. Add 5-10 mL of aqueous Tris containing aqueous phase from equilibrated phenol's bottle over the mixture to prevent oxidation of phenol. Store the bottle at 4^0C.

VIII] Second DNase digest buffer (10 mL)

1. Add following DEPC treated ingredients to a sterile 15 ml conical tube.

Ingredient	Quantity (mL)
200 mM Tris-HCl, pH 7.5	2.0
100 mM $MgCl_2$	1.0
5 mM $CaCl_2$	0.05
Nuclease free water	6.95

2. Store the tube at 4^0C.

IX] TBE buffer 5X

1. Add following ingredients to 500 mL dH_2O in a 2000 mL flask.

Ingredient	Quantity (g)
Tris base	54.0
Boric acid	27.5
Na_2EDTA	2.695

2. Adjust the pH to 8.3 using HCl and bring the final volume to 1000 mL.
3. Autoclave the buffer for 20 minutes and once it cools down, store at room temperature in a sterile bottle. Autoclaving causes better dissolving of the ingredients.
4. For agarose gel electrophoresis, add 1 part of 5X TBE to 4 parts of dH_2O to get the final concentration of 1X.

APPENDIX C

Protocols

I] Isolation of crude RNA

1. Grow wild type and ΔPetC1 cultures (500-550 mL) to 0.5 OD_{750} under optimal photosynthetic conditions after which, impose dark anaerobic conditions as described. Add 80 mL of the culture volumes collected under optimal photosynthetic conditions and 1^{st}, 2^{nd}, 4^{th}, 6^{th}, 8^{th} and 12^{th} hour under dark anaerobic conditions into 250 mL Nalgene centrifuge bottles pre-filled with freshly prepared, ice cold, 8 mL of 10X metabolic stop solution. Shake vigorously for 2 minutes. 1^{st} hour dark anaerobic condition sample onwards, bubble the cultures with argon for 15 seconds.
2. Centrifuge at 7,000 rpm using GSA rotor in Sorvall's RC5C centrifuge at 4^0C for 15 minutes. Decant the supernatant and drain pellets by inverting the centrifuge bottles at -20^0C for 10 minutes.
3. Re-suspend the cell pellets in 1 mL of suspension buffer (DEPC treated), transfer the re-suspended cells into screw cap microcentrifuge tubes, and pellet the cells by centrifugation at 10,000 rpm for 1 minute at room temperature using Eppendorf's centrifuge 5415C. If the pellets still smell like phenol, repeat the step. Discard the supernatant and store the cell pellets at -80°C freezer.
4. Thaw the cell pellets on ice and add 38 µL 0.5 M Na_2EDTA, pH 8.0 and 320 µL of ice cold cell suspension buffer (both reagents DEPC treated). Vortex gently.
5. Add 340 µL of 111 mM sodium acetate (DEPC treated) to the tubes and mix well.
6. Add 38 µL of 20% SDS (DEPC treated) to the tubes, mix well, and incubate at 65ºC for 10 minutes with intermittent gentle vortexing.

7. Add 700 µL of hot acidic phenol (at 65ºC), mix well, and incubate the tubes at 65ºC for 5 minutes. Cool at -80ºC for 45 seconds and centrifuge at 10,000 rpm for 10 minutes at room temperature using Eppendorf's centrifuge 5415C.
8. Transfer the aqueous phase to new microfuge tubes and repeat the hot acidic phenol step.
9. Transfer the aqueous phase to new microfuge tubes; to which, add equal volume of 25:24:1 phenol/chloroform/isoamyl alcohol and centrifuge at 10,000 rpm for 10 minutes at room temperature using Eppendorf's centrifuge 5415C.
10. Transfer the aqueous phase to new microfuge tubes and repeat the 25:24:1 phenol/chloroform/isoamyl alcohol step.
11. Transfer the aqueous phase to new microfuge tubes, to which add equal volume of 24:1 chloroform/isoamyl alcohol and centrifuge at 10,000 rpm for 10 minutes at room temperature using Eppendorf's centrifuge 5415C.
12. Transfer the aqueous phase to new microfuge tubes and repeat the 24:1 chloroform/isoamyl alcohol step.
13. Transfer the aqueous phase to new microfuge tubes and add $1/4^{th}$ its volume LiCl (DEPC treated) and 3 times its volume absolute ethanol. Let the samples sit at -20°C for 60 minutes.
14. Centrifuge the tubes at 10,000 rpm for 10 minutes at 4^0C using Eppendorf's centrifuge 5415C.

15. Gently wash the pellets by sliding 1 mL of 70% ethanol and centrifuge the tubes at 10,000 rpm for 10 minutes at 4^0C using Eppendorf's centrifuge 5415C. Repeat the step once more.
16. Drain the supernatant without disturbing the pellets. Let the pellets air dry for 1 hour. Re-suspend the pellets gently in 50 µL 10T/0.1E buffer, pH 8.2 (DEPC treated).
17. Take 1 µL of crude RNA into 60 µL dH_2O and measure the O.D. at 260 nm. Calculate concentrations of crude RNA using formula $O.D._{260}$ 1= 44 µg/µL and store the tubes at -80^0C.

II] First DNase treatment

1. Based on the concentration of crude RNA, calculate the amount of 10 µg containing fractions of crude RNA re-suspended in 10T/0.1E buffer for every sample. For example 'x'µL.
2. Thaw crude RNA samples on ice. The reagents required per sample are as follow. Adjust the total volume to 50 µL using nuclease free water.

Ingredient	**Quantity (*µ*L)**
10 µg of crude RNA containing fraction	'x'
10X Turbo™ DNase buffer	5.0
2 units/µL Turbo™ DNase enzyme	1.0
Nuclease free water	50-(x+5+1)

3. Mix by gentle vortexing and incubate the reaction tubes at 37^0C for 45 minutes.
4. Add 5 µL Turbo™ DNase inactivation reagent and incubate the reaction tubes for 2 minute at room temperature.

5. Centrifuge the contents at 10,000 rpm for 2 minutes using Eppendorf 's centrifuge 5415C.
6. Transfer the supernatant to new microfuge tubes without disturbing the pellets.
7. Take 1 µL of DNase treated RNA into 60 µL dH_2O and measure the O.D. at 260 nm. Calculate concentrations of crude RNA using formula $O.D._{260}$ 1= 44 µg/µL and store the tubes at -80^0C.

III] Second DNase treatment

1. Thaw RNA samples that have undergone first DNase treatment. For example, volume of a sample is 'y' µL. The reagents required per sample are as follow.

Ingredient	**Quantity (*µ*L)**
RNA sample after first DNase treatment	'y'
Second DNase digest buffer	y/10
2 units/µL Turbo™ DNase enzyme	1.0

2. Mix the contents by gentle vortexing and incubate the reaction tubes at 37^0C for 45 minutes.
3. Add y/10 µL Turbo™ DNase inactivation reagent and incubate at 2 minute at room temperature.
4. Centrifuge the contents at 10,000 rpm for 2 minutes using Eppendorf 's centrifuge 5415C.
5. Transfer the supernatant to new microfuge tubes without disturbing the pellets.

6. Take 1 µL of DNase treated RNA into 60 µL dH_2O and measure the O.D. at 260 nm. Calculate concentrations of crude RNA using formula $O.D._{260}$ 1= 44 µg/µL and store the tubes at -80^0C.

IV] PCR and RT-PCR

1. Thaw RNA samples. For PCR, the ingredients required per sample are as follow. Adjust the total volume per sample to 50 µL using nuclease free water which is 37 µL in this case.

Ingredient	**Quantity (*µ*L)**
AMV/*Tfl* 5X buffer	10.0
10 mM each dNTPs	1.0
20 pM/µL forward primer	2.5
20 pM/µL reverse primer	2.5
25 mM $MgSO_4$	2.0
5 units/µL *Tfl* polymerase	1.0
RNA sample	4.0
Nuclease free water	50-(10+1+2.5+2.5+2+1+4)

2. Maintain a negative control that contains nuclease free water instead of RNA sample and also a positive control containing similar volume of crude RNA-DNA mixture (from the same organism).
3. While working with a number of samples, prepare a master mix by multiplying volume of each ingredient except RNA sample by number of samples including two controls plus 1 taking into account pipeting error. Use 50 µL thin walled tubes for PCR/RT-PCR.
4. For RT-PCR, the ingredients required per sample are as follow. Adjust the total volume per sample to 50 µL using nuclease free water which is 36µL in this case.

Ingredient	Quantity (μL)
AMV/*Tfl* 5X buffer	10.0
10 mM each dNTPs	1.0
20 pM/µL forward primer	2.5
20 pM/µL reverse primer	2.5
25 mM $MgSO_4$	2.0
5 units/µL *Tfl* polymerase	1.0
5 units/µL AMV reverse transcriptase	1.0
RNA sample	4.0
Nuclease free water	50-(10+1+2.5+2.5+2+1+1+4)

5. Maintain a negative control that contains nuclease free water instead of RNA sample and also a positive control containing similar volume of crude RNA-DNA mixture (from the same organism).
6. While working with a number of samples, prepare a master mix by multiplying volume of each ingredient except RNA sample by number of samples including a negative control plus 1 taking into account pipeting error. Use 50 µL thin walled tubes for PCR/RT-PCR.
7. Load the thin walled PCR/RT-PCR tubes on tube holder and set following cycling program on Eppendorf mastercycler gradient™.

Specification	Number of cycles
Bring lid temperature to 95^0C	-
45^0C for 45 minutes	1
94^0C for 2 minutes	1
94^0C for 30 seconds	40
60^0C for 1 minute	
68^0C for 2 minutes	
Maintain the reaction tubes at 4^0C	-

8. Store the PCR/RT-PCR tubes at -20^0C.

V] Agarose gel electrophoresis

1. Mix 15 mL (1 part) of 5X TBE buffer with 60 mL (4 parts) of dH_2O to obtain 1X TBE buffer.
2. In a 250 mL conical flask, add 75 mL 1X TBE buffer and 1.125 g agarose to have final agarose concentration of 1.5%. 75 mL 1X TBE is sufficient for making a 12 lane gel.
3. Apply Parafilm^{TM} on the mouth of the flask and microwave it several times for 15 seconds until the agarose gets completely dissolved into the 1X TBE buffer. Once the content of the flask gets lukewarm, gently add it on the gel plates and insert combs to create wells for loading of samples.
4. Allow the gel to set for 30 minutes. After 30 minutes, take the combs out and to avoid drying of the gel, place it into Biorad's electrophoresis kit and add 325 mL of 1X TBE buffer (65 mL of 5X TBE buffer added to 260 mL of dH_2O) to the kit to have the gel surface submerged in the buffer.
5. Thaw the PCR and RT-PCR samples. Take 5 µL samples in 50 µL snap capped tubes. Add 1 µL gel loading buffer to each sample. Mix well by pipeting.
6. Along with the samples and control, also maintain a tube with 3 µL standard 1 kb ladder from Bayou.
7. Incubate the samples plus ladder at 65^0C for 10 minutes followed by cooling on ice for 5 minutes.
8. To all the tubes, add 2 µL SYBR green I (1/1000). Mix the contents well by pipeting.

9. Incubate the tubes at room temperature under dark for 20 minutes.
10. Load the samples in the wells of the gel avoiding bubbles.
11. Apply voltage of 75V for 90 minutes. Once the bands reach 3/5th distance, disconnect the current and scan the gel immediately using BioRad's Molecular Imager Fx^{TM}.

VI] Complementary DNA (cDNA) synthesis

1. Based on the concentrations of DNA free RNA, calculate the amount of sample containing 500 ng RNA which varies for every sample. For example 'z'µL.
2. Thaw RNA samples on ice. Ingredients required per sample are as follow. Adjust the total volume to 50 µL using nuclease free water.

Ingredient	**Quantity (*µ*L)**
5X AMV reverse transcriptase buffer	10.0
25 mM $MgCl_2$	10.0
10 mM each dNTPs	5.0
40 units/µL RNasin Plus	1.0
0.3 µg/µL random hexamers	1.0
5 units/µL AMV reverse transcriptase	1.5
RNA sample	Z
Nuclease free water	50-(10+10+5+1+11.5+z)

3. While working with a number of samples, prepare a master mix by multiplying volume of each ingredient except RNA sample by number of samples plus one taking into account pipeting error. Use 50 µL thin walled tubes for the reactions.
4. Maintain the tubes at room temperature for 10 minutes to allow binding of primers to the RNA.

5. Load the thin walled tubes on tube holder and set following cycling program on Eppendorf mastercycler gradient^{TM}.

Specification	Number of cycles
Bring lid temperature to 95^0C	-
42^0C for 45 minutes	1
94^0C for 2 minutes	1
Maintain the reaction tubes at 4^0C	-

6. Store the reaction tubes at -20^0C.

VII] Primer-probe validation and efficiency studies

1. Thaw crude RNA or DNA sample of known concentration. Using 10T/0.1E buffer, pH 7.5, make 10 fold serial dilutions from 100 ng/µL to 10 pg/µL. Also, thaw forward, reverse primers and probe.
2. Ingredients required per sample tube are as follow.

Ingredient	Quantity (*µ*L)
AB's 2X universal mix	10.0
20 pM/µL forward primer	1.0
20 pM/µL reverse primer	1.0
20 pM/µL probe	0.25
Crude RNA/DNA sample	1.0
Nuclease free water	6.75

3. Maintain a negative control that contains nuclease free water instead of RNA sample.
4. While working with a number of samples, prepare a master mix by multiplying volume of each ingredient except RNA sample by number of samples including a negative control plus 1 taking into account the pipeting error. The tubes used are Applied Biosystem's 20 µL fast reaction tubes.

5. Load the fast reaction tubes on tube holder in Applied Biosystem's StepOnePlus^{TM} real time PCR system and choose 'Quantitation relative standard curve' program set following cycling program with following cycles.

Specification	Number of cycles
95^0C for 10 minutes	1
95^0C for 15 seconds	40
60^0C for 1 minute	

6. Adjust the threshold for threshold cycle (hereafter C_T) values to 0.05 for all primer-probe sets after verifying that, threshold lies on the exponential phase of the amplification curve.
7. Work in triplicate. For every primer-probe set, plot a graph of log of concentration in pg on X axis against C_T values on Y axis. Consider the replicate only if the R^2 value of the plot is equal to or above 0.99. Take means of C_T values for every concentration of the template from the three replicates and plot a graph of log of concentration in pg on X axis against C_T values on Y axis.

VIII] RT-qPCR; TaqMan^{TM} gene expression assays (Standard Curve Method)

1. Thaw cDNA samples to be tested. Also, thaw forward, reverse primers and probe.
2. Ingredients required per sample tube are as follow.

Ingredient	Quantity (μL)
AB's 2X universal mix	10.0
20 pM/µL forward primer	1.0
20 pM/µL reverse primer	1.0
20 pM/µL probe	0.25
cDNA sample	2.0
Nuclease free water	5.75

3. Maintain a negative control that contains nuclease free water instead of cDNA sample.
4. While working with a number of samples, prepare a master mix by multiplying volume of each ingredient except RNA sample by number of samples including negative controls plus one taking into account pipeting error. The tubes used are Applied Biosystem's 20 µL fast reaction tubes.
5. Load the fast reaction tubes on tube holder in Applied Biosystem's StepOnePlus™ real time PCR system and choose 'Comparative C_T; $\Delta\Delta C_T$' method' program set following cycling program with following cycles. For details, see materials and methods.

Specification	Number of cycles
95^0C for 10 minutes	1
95^0C for 15 seconds	40
60^0C for 1 minute	

6. Adjust the threshold for threshold cycle (hereafter C_T) values to 0.05 for all primer-probe sets after verifying that, threshold lies on the exponential phase of the amplification curve.
7. Work with three biological replicates.
8. Take means of C_T values from three biological replicates. Using equation of the graph for every primer-probe set plotted during primer efficiency test; normalize the gene expression results for different genes on the scale of $\log_{10}$ of concentration (pg/µL). Plot graphs for the gene expression assays taking into

account the standard deviation while working with the three biological replicates as relative gene expression on $\log_2$ of concentraton (pg/μL) vs. time of harvest.

IX] Metabolic labeling and isolation of membrane proteins

1. Grow the wild type strain (which has been growing in ^{15}N BG-11 containing flask for several generations) in BG-11 medium containing ^{15}N to serve as the reference culture. Grow wild type as well as ΔPetC1 mutant in BG-11 medium containing ^{14}N as 'test' cultures. When the cultures reach $O.D._{750}$ of 0.5, harvest 150 mL cultures from each Roux flask and mix them in a 500 mL Nalgene plastic bottle. Control culture should be diluted to maintain its $O.D._{750}$ at 0.5. Follow the same procedure for samples under 12^{th} hour dark-anaerobic conditions.
2. Centrifuge the mixed cultures (control and test) at 8,500 rpm for 10 minutes using SLA3000 rotor in Sorvall's RC5C plus centrifuge.
3. Re-suspend the cell pellet in 15 mL of 5 mM HEPES-NaOH, pH 7.5 buffer. Transfer the suspension to 50 mL PPCO Oakridge tubes and centrifuge at 14,600 rpm using SS34 rotor in Sorvall's RC5C centrifuge.
4. To the pellets obtained, add 10 mL of 5 mM HEPES-NaOH, pH 7.5 buffer, DNase to the final concentrations of 30 μg/mL and protein inhibitors to the final concentrations; 2 mM DTT, 0.5 mM AEBSF, 1 mM amino caproic acid, 1 mM benzamidine, 1 μM pepstatin A, 10 μM leupeptin, 1 μM E-64 and 1 μM bestatin. Pass the cell suspensions through American Instrument Company's French

pressure cell press at the rate of 1 drop/second at 20,000 psi. Repeat the cell pressing procedure two more times.

5. Centrifuge the pressed cells at 6,000 rpm for 10 minutes using SS34 rotor in Sorvall's RC5C plus centrifuge.
6. Add the supernatant to polycarbonate tubes (16-20 mL per tube) and centrifuge at 50,000 rpm for 1 hour at 4^0C using 70Ti rotor in Beckman's L8-M ultracentrifuge. Re-suspend the pellets containing membrane proteins in 16 mL of 50 mM ammonium bicarbonate and repeat the centrifugation step.
7. Re-suspend the pellets in 500 µL of 50 mM ammonium bicarbonate with the help of a syringe attached to cannula and tissue homogenizer. Estimate the membrane protein contents.

X] Estimation of membrane proteins

1. For estimation of proteins from membrane protein fraction, dilute membrane protein pellet re-suspended in 50 mM ammonium bicarbonate 1 in 50 parts with 5% SDS and gently vortex the mixture for a minute.
2. Mix 'Reagent A' (sodium carbonate, sodium bicarbonate, bicinchoninic acid and sodium tartrate in 100 mM sodium hydroxide) and 'Reagent B' (4% cupric sulfate) supplied by Pierce in ratio 50:2. Also, make dilutions of the bovine serum albumin sample supplied by Pierce as 0.2, 0.4, 0.8, 1.2 and 2.0 mg/mL including using dH_2O.

3. Take 25 µL of the standards and either diluted or undiluted protein samples into microfuge tubes including a blank which contains only dH_2O and 5% SDS. To the tubes, add 500 µL of the working solution. Mix gently.
4. Incubate all of the tubes at 37^0C for 30 minutes.
5. Measure the absorbance at 562 nm against the absorbance of blank sample. For membrane protein samples, subtract absorbance given by 5% SDS from the samples.
6. Plot a graph with concentrations of standards on X axis against absorbance at 562 nm at Y axis along with the line of best fit. Using equation of the graph, calculate protein concentrations from the unknown samples.

XI] Trypsin digestion of bulk membrane protein fractions and C18 column purification of tryptic digests

1. To 100 µL bulk membrane protein containing fractions re-suspended in 50 mM ammonium bicarbonate, add equal volume of methanol plus Promega's porcine trypsin in the ratio 1:40 w/w. Incubate the tubes at 37^0C for 24 hours with gentle shaking.
2. After trypsin digestion step, add formic acid to have 5% (v/v) final concentration.
3. Equilibrate the Varian Spec C18 columns (200-250 µg peptide binding range) by passing 1 mL of 90% acetonitrile, 0.1% formic acid followed by 1 mL of dH_2O, 0.1% formic acid.

4. Pass the peptide containing sample through the column by passing peptide containing samples 20 times followed by 1 mL of dH_2O, 0.1% formic acid.
5. Elute the peptides using 50 µL 90% acetonitrile, 0.1% formic acid. Repeat the elution and mix two elutes together. Vacuum dry the elute using Labconco's centrivap concentrator and re-suspend them in 0.3% formic acid to final protein concentration of 1 µg/µL.
6. Analyze the samples using LC (Agilent 1100 series) -MS/MS (Bruker Daltonics' esquire3000plus™ instruments following the parameters, instructions and references as described in the materials and methods.
7. For every protein identification showing same light and heavy peptides; draw extracted ion chromatograms. Compare the peptide levels on the basis of peak heights of the extracted ion chromatograms.

XII] Kinetic estimation of electron transfer chain components

1. Grow the wild type and ΔPetC1 cultures to until OD_{750} reaches 1.0 under optimal photosynthetic conditions. Take 8 mL of the cultures into 15 mL conical tubes.
2. Centrifuge the tubes at 3,900 rpm for 10 minutes using Beckman's GP centrifuge. Decant all of the supernatant.
3. Re-suspend the cell pellets in 2 mL re-suspension buffer (10% Ficoll, 10 mM sodium chloride, 5 mM HEPES, pH 7.5) to concentrate the cells 4 times to O.D. 4.0.

4. Using a syringe, load 1 mL of the concentrated cultures into cuvettes adaptable with the Biologic's JTS-10 spectrophotometer without forming any bubbles.
5. Using the operating software for the spectrophotometer, either set or select a program that involves 10 seconds dark phase for dark adaptation of cyanobacterial cells followed by 10 seconds continuous illumination phase and followed further by 10 seconds dark phase. Select continuous actinic light intensity of 590 $\mu E\ m^{-2}s^{-1}$. Set the voltage required detection of absorption signal between 3 and 4, but preferably close to 4 Volts.
6. Insert 'BG39' (3 mm wide) cut off filters in the light paths, before the reference as well as sample detectors. Record the redox spectra thrice using 546 nm, 554 nm, 563 nm and 573 nm interference filters in presence as well as in absence of actinic light.
7. Insert 'P700' cut off filters in the light paths, before the reference as well as sample detectors. Record the redox spectra thrice using 705 nm interference filter in presence as well as in absence of actinic light.
8. Using a function of the operating software; for every individual strain, for every individual interference filter, subtract spectra obtained in absence of actinic light from the spectra obtained in presence of actinic light.
9. After these subtractions, using a function of the operating software, deconvolute the spectra obtained with 546, 554, 563 and 573 nm to obtain individual spectra for cytochrome b_6, cytochrome *f* and plastocyanin. There is no need to

deconvolute any spectra to derive PS I spectrum which is obtained with 705 nm interference filter.

10. Using a function of operating software, convert the data into Microsoft Excel format.
11. Use formula | [(maximum value of dI/I) / 10^6] cm^{-1} ÷ [extinction coefficient] $mM^{-1}cm^{-1}$| for cytochrome b_6 and plastocyanin while for cytochrome *f* and PS I, use formula | [(minimum value of dI/I) / 10^6] cm^{-1} ÷ [extinction coefficient] $mM^{-1}cm^{-1}$| to calculate the amounts of electron transfer chain components in pM. Take extinction coefficients of cytochrome b_6, cytochrome *f*, plastocyanin and PS I as 18 $mM^{-1}cm^{-1}$, 21 $mM^{-1}cm^{-1}$, 4.9 $mM^{-1}cm^{-1}$ and 57 $mM^{-1}cm^{-1}$ respectively. Considering both strains, take the wild type strain's cytochrome *f* value as 1.0 and then normalize the values of remaining electron transfer chain components to 1.0.

XIII] Study of catalytic efficiencies of PetC1 and PetC2 Rieske ISPs

1. Grow the wild type and ΔPetC1 cultures till OD_{750} reaches 1.0 under optimal photosynthetic conditions. Take 8 mL of the cultures into 15 mL conical tubes.
2. Centrifuge the tubes at 3,900 rpm for 10 minutes using Beckman's GP centrifuge. Decant all of the supernatant.
3. Re-suspend the cell pellets in 2 mL re-suspension buffer (10% Ficoll, 10 mM sodium chloride, 5 mM HEPES, pH 7.5) to concentrate the cells 4 times to O.D. 4.0.

4. Using a syringe, load 1 mL of the concentrated cultures into cuvettes adaptable with the Biologic's JTS-10 spectrophotometer without forming any bubbles.
5. Using the operating software for the spectrophotometer, either set or select a program that involves 50 miliseconds dark phase for dark adaptation of cyanobacterial cells followed by 9 miliseconds continuous illumination phase and followed further by 180 seconds dark phase. Set the voltage required detection of absorption signal between 3 and 4, but preferably close to 4 Volts. Insert 'BG39' (3 mm wide) cut off filters in the light paths, before the reference as well as sample detectors.
6. For the strains under study; record five redox spectra 30 times for five different light intensities (14, 37, 80, 150 and 300 μE $m^{-2}s^{-1}$) using 546 nm, 554 nm, 563 nm and 573 nm interference filters for every actinic light intensity, in presence as well as in absence of actinic light. Use different culture samples for different light intensities.
7. Using a function of the operating software; for every individual strain, for every individual interference filter, subtract spectra obtained in absence of actinic light from the spectra obtained in presence of actinic light. Ignore the spectra containing high noise.
8. After these subtractions, using a function of the operating software, deconvolute the spectra obtained with 546, 554, 563 and 573 nm to obtain individual spectra for cytochrome *f*. Using a function of operating software, convert the data into Microsoft Excel format.

9. Using a function of operating software, calculate half times of re-reduction for all of the cytochrome *f* spectra obtained with different actinic light intensities, for both strains.

XIV] Estimation of chlorophyll

1. Take 1 mL culture in a 1.5 mL microfuge tube and centrifuge at 14,000 rpm for 15 minutes using Eppendorf's centrifuge 5415C.
2. Remove 950 µL of the clear medium and re-suspend cell pellet in remaining 50 µL medium.
3. Add 950 µL of methanol to the tube and vortex lightly to mix the contents. Keep the tube in dark for 5 minutes with intermittent shaking.
4. Centrifuge the tube at 14,000 rpm for 5 minutes using Eppendorf's centrifuge 5415C and using supernatant, measure absorbance values at 665.2 nm and 750 nm against those for methanol set as 'blank'.
5. Calculate the chlorophyll content using equation: Chlorophyll (µM) = [(Absorption 665.2 nm – Absorption 750 nm) / 71.43] × [1000/50] × 1000.

XV] Impact of the ΔPetC1 mutation and dark anaerobiosis on PQ pool redox state

1. Grow the wild type and ΔPetC1 cultures till the OD_{750} reaches 0.5 under optimal photosynthetic conditions after which impose dark anaerobic conditions as described. Measure the chlorophyll contents as described previously. Harvest 12 mL culture volumes (2 mL × 6, 15 ml conical tubes) at every time point (1 mL for

every actinic light intensity) under optimal photosynthetic conditions and 1st, 2nd, 4th, 6th, 8th and 12th hour under dark anaerobic conditions. Bubble the samples collected for dark anaerobic conditions with argon for 5 seconds. 1st hour dark anaerobic sample onwards, bubble the culture flasks with argon for 15 seconds.

2. Using a syringe, load 1 mL of the concentrated cultures into cuvettes adaptable with the Biologic's JTS-10 spectrophotometer without forming any bubbles.
3. Using the operating software for the spectrophotometer, either set or select a program that involves 115 seconds dark phase for dark adaptation of cyanobacterial cells followed by continuous actinic light illumination phase for 70 seconds which is followed further by dark phase e.g. 230 seconds. The program should include exposure of the sample to 200 ms intense pulses of 7900 μE $m^{-2}s^{-1}$ followed by short detecting pulses of 10 μs.
4. Insert fluorescence specific 'Fluo' cut off filter before the sample detector and 'BG39' (6 mm wide) cut off filter before the reference detector. Insert fluorescence emitting board consisting of 59 LEDs which serves as the source of actinic as well as probing light.
5. Perform six fluorescence measurements for six different light intensities (14, 37, 80, 150, 300 and 590 μE $m^{-2}s^{-1}$) for the time points under study. Use different culture samples for different light intensities.
6. Using a function of operating software, convert the data obtained into Microsoft Excel format.

7. For every specific spectrum obtained; record, *F*m' (maximum fluorescence value elicited by saturating light pulse during continuous illumination by actinic light), *F*s1 (steady state fluorescence value before NPQ) and *F*s2 (steady state fluorescence value after NPQ).
8. Calculate quantum efficiencies before and after NPQ, for every fluorescence spectrum using formula ΦPSII = (*F*m' –*F*s)/ *F*m' with *F*s1 and *F*s2 values. Plot two graphs (before NPQ and after NPQ) for every time point of harvest, for both strains as continuous actinic light intensity on X axis and quantum efficiency on Y axis.

REFERENCES

Allen, J. F. (2004). Cytochrome b_6f: Structure for signaling and vectorial metabolism. *Trends in Plant Science*, *9*(3), 130-137.

Altschul, S. F., Madden, T. L., Schaffer, A. A., Zhang, J., Zhang, Z., Miller, W., & Lipman, D. (1997). Gapped BLAST and PSI BLAST: A new generation of protein database search programs. *Nucleic Acid Research*, *25*(17), 3389-3402.

Antal, T. K., & Lindblad, P. (2004). Production of H_2 by sulphur deprived cells of the unicellular cyanobacteria *Gloeocapsa alpicola* and *Synechocystis* sp. PCC 6803 during dark incubation with methane or at various extracellular pH. *Journal of Applied Microbiology*, *98*(1), 114-120.

Applied Biosystems. (2002). TaqMan™ universal PCR master mix protocol. Part number 4304449 Rev. C.

Applied Biosystems. (2007). Applied Biosystems StepOne™ and StepOnePlus™ real time PCR systems: Relative standard curve and comparative C_T experiments. Part number 4376785 Rev. D.

Applied Biosystems. (2008). Real time PCR: Understanding C_T. Publication number 136AP01-01.

Applied Biosystems. (2009). Turbo DNase treatment and removal reagents. Part number AM1907.

Berry, S., Schneider, D., Vermaas, W. F. J., & Rögner, M. (2002). Electron transport routes in whole cells of *Synechocystis* sp. strain PCC 6803: The role of cytochrome *bd*

type oxidase. *Biochemistry*, *41*(10), 3422-3429.

Blankenship, R. E. (2002). *Molecular Mechanisms of Photosynthesis*. Oxford, UK: Blackwell Science Limited.

Bose, S. (1985). Post-illumination kinetics of cytochrome reduction in plant chloroplast thylakoid in the presence of dibromothymoquinone. *Biochemical and Biophysical Research Communications*, *130*(1), 16-21.

Breyton, C., Nandha, B., Johnson, G. N., Joliot, P., & Finazzi, G. (2006). Redox modulation of cyclic electron flow around photosystem I in C3 plants. *Biochemistry*, *45*(45), 13465-13475.

Burrows, E. H., Chaplen, F. W. R., & Ely, R. L. (2008). Optimization of media nutrient composition for increased photofermentative hydrogen production by *Synechocystis* sp. PCC 6803. *International Journal of Hydrogen Energy*, *33*(21), 6092-6099.

Carr, M., Friedrichs, M. A., Aita, M. N., Antoine, D., Arrigo, K. R., Asunama, I., … Yamanaka, Y. (2006). A comparison of global estimates of marine primary production from ocean color. *Deep-Sea Research II*, *53*(5-7), 741-770.

Cournac, L., Guedeney, G., Peltier, G., & Vignais, P. M. (2004). Sustained photoevolution of molecular hydrogen in a mutant of *Synechocystis* sp. strain PCC 6803 deficient in the type I NADPH-dehydrogenase complex. *Journal of Bacteriology*, *186*(6), 1737-1746.

Cramer, W. A., Yan, J., Zhang, H., Kurisu, G., & Smith, J. L. (2005) Structure of the cytochrome b_6f complex: New prosthetic groups, Q-space, and the 'hors d' oeuvres hypothesis' for assembly of the complex. *Photosynthetic Research*, *85*(1), 133-143.

Cramer, W. A., Zhang, H., Yan, J., Kurisu, G., & Smith, J. L. (2006). Transmembrane traffic in the cytochrome b_6f complex. *Annual Review of Biochemistry*, *75*, 769-790.

Darrouzet, E., Moser, C. C., Dutton, P. L., & Daldal, F. (2001). Large scale domain movement in cytochome *bc*1: a new device for electron transfer in proteins. *Trends in Biochemical Sciences*, *26*(7), 445-451.

Demming-Adams, B., & Adams, W. W. III., (2002). Antioxidants in photosynthesis and human nutrition. *Science*, *298*(5601), 2149-2153.

De Muizon, C., McDonald, H. G., Salas, R., & Urbina, M. (2004). The Youngest species of the aquatic sloth Thalassocnus and a reassessment of the relationships of the Nothrothere sloths (Mammalia: Xenarthra). *Journal of Vertebrate Paleontology*, *24*(2), 387-397.

DeRuyter, Y. S., & Fromme, P. (2008). Molecular structure of the photosynthetic apparatus. In A. Herrero & E. Flores (Eds.), *The cyanobacteria: Molecular biology, Genomics and Evolution*. (pp. 217-269). Nolfolk, UK: Caister Academic Press.

De Vitry, C., Finazzi, G., Baymann, F., & Kallas, T. (1999). Analysis of the nucleus encoded and chloroplast targeted Rieske protein by classic and site directed mutagenesis of *Chlamydomonas*. *Plant Cell*, *11*(10), 2031-2044.

Dickons, D. J., Page, C. J., & Ely, R. L. (2009). Photo biological hydrogen production from *Synechocystis* sp. PCC 6803 encapsulated in silica sol gel. *International Journal of Hydrogen Energy*, *34*(1), 204-215.

Dong, C., Tang, A., Zhao, J., Mullineaux, C. W., Shen, G., & Bryant, D. A. (2009). ApcD is necessary for efficient energy transfer from phycobilisomes to photosystem I

and helps to prevent photoinhibition in the cyanobacterium *Synechococcus* sp. PCC 7002. *Biochimica et Biophysica Acta*, *1787*(9), 1122-1128.

Douzery, E. J., Snell, E. A., Bapteste, E., Delsuc, F., & Philippe, H. (2004). The timing of eukaryotic evolution: Does a relaxed molecular clock reconcile proteins and fossils? *Proceedings of Natural Academy of Sciences*, *101*(43), 15386-15391.

Evans, J. R. (1986). A quantitative analysis of light distribution between the two photosystems, considering variation in both the relative amounts of the chlorophyll-protein complexes and the spectral quality of light. *Photobiochemistry and Photobiophysics*, *10*, 135-147.

Finazzi, G., & Kallas, T. (2000-2005). Study of kinetics of cytochrome *bf* complex in cyanobacterum *Synechocystis* sp. PCC 6803. Unpublished raw data.

Harbinson, J., Genty, B., & Baker, N. R. (1989). Relationship between the quantum efficiencies of photosystems I and II in pea leaves. *Plant Physiology*, *90*(3), 1029-1034.

Hart, S. E., Schlarb-Ridley, B. G., Bendall, D. S., & Howe, C. J. (2005). Terminal oxidases of cyanobacteria. *Biochemical Society Transactions*, *33*(4), 832-835.

Houot, L., Floutier, M., Marteyn, B., Michaut, M., Picciocchi, A., Legrain, P.,... Chauvat, F. (2007). Cadmium triggers an integrated reprogramming of metabolism of *Synechocystis* PCC 6803, under the control of the Slr1738 regulator. *BioMedCentral Genomics*, *8*(350). doi:10.1186/1471-2164-8-350.

Hurt, E., & Hauska, G. (1981). A cytochrome *f*/b_6 complex of five polypeptides with plastoquinol-plastocyanin-oxidoreductase activity from spinach chloroplasts.

European Journal of Biochemistry, *117*(3), 591-599.

Ivanov, B., & Khorobrykh, S. (2003). Participation of photosynthetic electron transport in production and scavenging of reactive oxygen species. *Antooxidants and Redox Signaling*, *5*(1), 43-53.

Iwata, S., Saynovits, M., Link, T. A., & Michel, H. (1996). Structure of a water soluble fragment of the 'Rieske' iron-sulfur protein of the bovine heart mitochondrial cytochrome bc_1 complex determined by MAD phasing at 1.5å resolution. *Structure*, *4*(5), 567-579.

Kallas, T. (1994). The cytochrome b_6f complex. In D. A. Bryant (Ed.), *The Molecular Biology of the Cyanobacteria*. (pp. 259-317). Dordrecht, The Netherlands: Kluwer Academic Publishers.

Kallas, T., Spiller, S., & Malkin, R. (1988a). Characterization of two operons encoding the cytochrome b6-f complex of the cyanobacterium *Nostoc* PCC 7906. Highly conserved sequences but different gene organization than in chloroplasts. *Journal of Biological Chemistry*, *263*(28), 14334-14342.

Kallas, T., Spiller, S., & Malkin, R. (1988b). Primary structure of cotranscribed genes encoding the Rieske Fe-S and cytochrome *f* proteins of the cyanobacterium *Nostoc* PCC 7906. *Proceedings of National Academy of Science*, *85*(16), 5794-5798.

Kallas, T. (1990-2007). Study of cyanobacteria *Synechocystis* sp. PCC 6803 and *Synechococcus* sp. PCC 7002. Unpublished raw data.

Kallas, T., Mana, Z. (Personal communication, 2007).

Karapetyan, N. V. (2007). Non-photochemical quenching of fluorescence in

cyanobacteria. *Biochemistry (Moscow)*, *72*(10), 1127-1135.

Katoh, S., Suga, I., Shiratori, I., & Takamiya, A. (1961). Distribution of plastocyanin in plants, with special reference to its localization in chloroplasts. *Archives of Biochemistry and Biophysics*, *94*(1), 136-141.

Keren, N., & Ohad, I. (1998). State transition and photoinhibition. In J. D. Rochix, M. Goldschmidt-Clermont & S. Merchant (Eds.), *The Molecular biology of Chlamydomonas: chloroplast and mitochondria*. (pp. 569-596). Dordrecht, The Netherlands: Kluwer Academic Publishers.

Kramer, D. M., Nitschke, W., & Cooley, J. W. (2008). The cytochrome *bc*1 and related *bc* complexes: The Rieske/Cytochrome *b* complex as the functional core of a central electron/proton transfer complex. In N. Hunter, F. Daldal & M. Thurnauer (Eds.), *The Purple Phototrophic Bacteria*. (pp. 451-473). Dordrecht, The Netherlands: Springer.

Kurisu, G., Zhang, H., & Cramer, W. A. (2003). Structure of the cytochrome b_6f complex of oxygenic photosynthesis: Tuning the cavity. *Science*, *302*(5647), 1009-1014.

Köhrer, K., & Domdey, H. (1991). Preparation of high molecular weight RNA. *Methods in Enzymology*, *194*, 398-405.

Lindberg, P., Park, S., & Melis, A. (2009). Engineering a platform for photosynthetic isoprene production in cyanobacteria, using *Synechocystis* as the model organism. *Metabolic Engineering*, *12*(1), 70-79.

Mao, H. B., Li, G. F., Ruan, X., Wu, Q. Y., Gong, Y. D., Zhang, X. F., & Zhao, N. M. (2002). The redox state of plastoquinone pool regulates state transitions via cytochrome b_6f complex in *Synechocystis* sp. PCC 6803. *Federation of European*

Biochemical Societies Letters, *519*(1-3), 82-86.

Matsui, M., Yoshimura, T., Wakabayashi, Y., Imamura, S., Tanaka, K., Takahashi, H., … Shirai, M. (2007). Interference expression at levels of the transcript and protein among group 1, 2 and 3 sigma factor genes in a cyanobacterium. *Microbes and Environments*, *22*(1), 32-43.

Mayes, S. R., & Barber, J. (1991). Primary structure of the *psbN-psbH-petC1-petA* gene cluster of the cyanobacterium *Synechocystis* PCC 6803. *Plant Molecular Biology*, *17*(2), 289-293.

McFadden, G. I. (2001). Primary and secondary endosymbiosis and the origin of plastids. *Journal of Phycology*, *37*(6), 951-959.

Mi, H. L., Endo, T., Schreiber, U., Ogawa, T., & Asada, K. (1994). NAD(P)H dehydrogenase- dependant cyclic electron flow around photosystem I in the cyanobacterium *Synechocystis* PCC 6803. *Plant and Cell Physiology*, *35*(2), 163-173.

Muller, F. (2000). The nature and mechanism of superoxide production by the electron transport chain: Its relevance to aging. *Journal of Americal Aging Association*, *23*(4), 227-253.

Müller, P., Li, X. P., & Niyogi, K. K. (2001). Non-photochemical quenching. A response to excess light energy. *Plant Physiology*, *125*(4), 1558-1566.

Mullineaux, C. W., & Allen, J. F. (1986). The state 2 transition in the cyanobacterium *Synechococcus* 6301 can be driven by respiratory electron flow into the plastoquinone pool. *Federation of Eueopean Biochemical Societies Letters*, *205*(1), 155-160.

Mullineaux, C. W., & Allen, J. F. (1990). State 1- state 2 transitions in the

cyanobacterium *Synechococcus* 6301are controlled by the redox state of electron carriers between photosystems I and II. *Photosynthetic Research*, *23*(4), 297-311.

Nakamura, Y., Kaneko, T., Hirosawa, M., Miyajima, N., & Tabata, S. (1998). CyanoBase, a www database containing the complete nucleotide sequence of the genome of *Synechocystis* sp. PCC 6803. *Nucleic Acids Research*, *26*(1), 63-67.

Nakamura, Y., Kaneko, T., Sato, S., Ikeuchi, M., Katoh, H., Sasamoto, S., … Tabata, S. (2002). Complete genome structure of the thermophilic cyanobacterium *Thermosynechococcus elongatus* BP-1 (supplement). *DNA Research*, *9*(4), 135-148.

Nakamura, Y., Kaneko, T., Sato, S., Mimuro, M., Miyashita, H., Tsuchiya, T., … Tabata, S. (2003). Complete genome structure of *Gloeobacter violaceus* PCC 7421, a cyanobacterium that lacks thylakoids (supplement). *DNA Research*, *10*(4), 181-201.

Nelson, C. J., Huttlin, E. L., Hegeman, A. D., Harms, A. C., & Sussman, M. R. (2007). Implications of 15N-metabolic labeling for automated peptide identification in *Arabidopsis thaliana*. *Proteomics*, 7*(8),* 1279-1292.

Nelson, M., & Kallas, T. (2000-2007). Study of cyanobacterum *Synechocystis* sp. PCC 6803. Unpublished raw data.

Olson, J. M. (2006). Photosynthesis in the archean era. *Photosynthesis research*, *88*(2), 109-117.

Pakrasi, H. (n.d.). Donald Danford Plant Science Center. Retrieved from http://www.danforthcenter.org/imf/pakrasi/animation.html

Palmer, J. D. (2003). The symbiotic birth and spread of plastids: How many times and whodunit? *Journal of Phycology*, *39*(1), 4-11.

Pappin, D. J., Hojrup, P., & Bleasby, A. J. (1993). Rapid identification of proteins by peptide-mass fingerprinting. *Current Biology*, *3*(6), 327-332.

Pfannschmidt, T., Nilsson, A., Tullberg, A., Link, G., & Allen, J. F. (1999). Direct transcriptional control of the chloroplast genes *psbA* and *psaAB* adjusts photosynthesis to light energy distribution in plants. *International Union of Biochemistry and Molecular Biology Life*, *48*(3), 271-276.

Pierce. (2008). Instructions: BCA™ protein assay kit. Kit number 23227.

Pischke, M. S., Huttlin, E. L., Hegeman, A. D., & Sussman, M. R. (2006). A transcriptome-based characterization of habituation in plant tissue culture. *Plant Physiology*, *140*(4), 1255-1278.

Porra, R. J., Thompson, W. A., & Kriedemann, P. E. (1989). Determination of accurate extinction coefficients and simultaneous equations for assaying chlorophylls a and b extracted with four different solvents: Verification of the concentration of chlorophyll standards by atomic absorption spectroscopy. *Biochimica et Biophysica Acta*, *975*(3), 384-394.

Pratte, B. S., Eplin, K., & Thiel, T. (2006). Cross-functionality of nitrogenase components NifH1 and VnfH in *Anabaena variabilis*. *Journal of Bacteriology*, *188*(16), 5806-5811.

Rikkinen, J., Oksanen, I., & Lohtander, K. (2002). Lichen guilds share related cyanobacterial symbionts. *Science*, *297*(5580), 357.

Roberts, A. G., Bowman, M. K., & Kramer, D. M. (2002). Certain metal ions are inhibitors of cytochrome b_6f complex 'Rieske' iron-sulfur protein domain movements.

Biochemistry, *41*(12), 4070-4079.

Rozen, S., & Skaletsky, H. J. (2000). Primer3 on the WWW for general users and for biologist programmers. In S. Krawetz and S. Misner (Eds.), *Bioinformatics Methods and Protocols: Methods in Molecular Biology*. (pp. 365-386). Totowa: Humana Press.

Schansker, G., Tóth, S. Z., & Strasser, R. J. (2005). Methylviologen and dibromothymoquinone treatments of pea leaves reveal the role of photosystem I in the Chl a fluorescence rise OJIP. *Biochimica et Biophysica Acta*, *1706*(3), 250-261.

Schneider, D., Altenfeld, U., Thomas, H., Schrader, S., Muhlenhoff, U., & Rögner, M. (2000). Sequence of the two operons encoding the four core subunits of the cytochrome *b(6)f* complex from the thermophilic cyanobacterium *Synechococcus elongates*. *Biochimica et Biophysica Acta*, *1491*(1-3), 364-368.

Schneider, D., Berry, S., Rich, P., Seidler, A., & Rögner, M. (2001). A regulatory role of the PetM subunit in a cyanobacterial cytochrome b_6f complex. *The Journal of Biological Chemistry*, *276*(20), 16780-16785.

Schneider, D., Berry, S., Volkmer, T., Seidler, A., & Rögner, M. (2004a). PetC1 is the major Rieske iron-sulfur protein in the cytochrome b_6f complex of *Synechocystis* sp. PCC 6803. *The Journal of Biological Chemistry*, *279*(38), 39383-39388.

Schneider, D., & Schmidt, C. L. (2005). Multiple Rieske proteins in prokaryotes: Where and why? *Biochimica et Biophysica Acta*, *1710*(1), 1-12.

Schneider, D., Skrzypczak, S., Anemüller, S., Schmidt, C. L., Seidler, A., & Rögner, M. (2002). Heterogeneous Rieske proteins in the cytochrome b_6f complex of

Synechocystis PCC6803. *The Journal of Biological Chemistry*, *277*(13), 10949-10954.

Schneider, D., Volkmer, T., Berry, S., Seidler, A., & Rögner, M. (2004b). Characterization of the *petC* gene family in the cyanobacterium *Synechocystis* PCC 6803. *Cellular and Molecular Biology Letters*, *9* (Supplement), 51-55.

Schultze, M., Forberich, B., Rexroth, S., Dyczmons, N. G., Rögner, M., & Appel, J. (2009). Localization of cytochrome b_6f complexes implies an incomplete respiratory chain in cytoplasmic membranes of the cyanobacterium *Synechocystis* sp. PCC 6803. *Biochimica et Biophysica Acta*, *1787*(12), 1479-1485.

Smillie, R. M. & Levin, R. P. (1963). The photosynthetic electron transfer chain of *Chlamydomonas reinhardi*. *The Journal of Biological Chemistry*, *238*(12), 4058-4061.

Stroebel, D., Choquet, Y., Popot, J. L., & Picot, D. (2003). An atypical haem in the cytochrome *b(6)f* complex. *Nature*, *426*(6965), 413-418.

Stuart, A. L., & Wasserman, A. R. (1973). Purification of cytochrome b_6, a tightly bound protein in chloroplast membranes. *Biochimica et Biophysica Acta*, *314*(3), 284-297.

Summerfield, T., Toepel, J., & Sherman, L. A. (2008). Low oxygen induction of normally cryptic *psbA* genes in cyanobacteria. *Biochemistry*, *47*(49), 12939-12941.

Takahashi, S., Milward, S.E., Fan, D. Y., Chow, W. S., & Badger, M. R. (2009). How does cyclic electron flow alleviate photoinhibition in Arabidopsis? *Plant Physiology*, *149*(3), 1560-1567.

Tran, H. L., Hong, S. J., & Lee, C. G. (2009). Evaluation of extraction methods for recovery of fatty acids from *Botryococcus braunii* LB 572 and *Synechocystis* sp. PCC 6803. *Biotechnology and Bioprocess Engineering*, *14*(2), 187-192.

Trebst, A. (1980). Inhibitors in electron flow: Tools for the functional and structural localization of carriers and energy conservation sites. *Methods in Enzymology*, *69*(C), 675-715.

Tsunoyama, Y., Bernàt, G., Dyczmons, N. G., Schneider, D., & Rögner, M. (2009). Multiple Rieske proteins enable short and long term light adaptation of *Synechocystis* sp. PCC 6803. *The Journal of Biological Chemistry*, *284*(41), 27875-27883.

Vener, A. V., Van Kan, P. J., Rich, P. R., Ohad, I., & Andersson, B. (1997). Plastoquinol at the quinol oxidation site of reduced cytochrome *bf* mediates signal transduction between light and protein phosphorylation: Thylakoid protein kinase deactivation by a single-turnover flash. *Proceedings of the National Academy of Sciences*, *94*(4), 1585-1590.

Volkmer, T., Schneider, D., Bernàt, G., Kirchhoff, H., Wenk, S. O., & Rögner, M. (2007). Ssr2998 of *Synechocystis* sp. PCC 6803 is involved in regulation of cyanobacterial electron transport and associated with the cytochrome b_6f complex. *The Journal of Biological Chemistry*, *282*(6), 3730-3737.

Ward, D. M. (2006). Microbial diversity in natural environments: Focusing on fundamental questions. *Antonie Van Leeuwenhoek*, *90*(4), 309-324.

Weis, E., & Berry, J. (1987). Quantum efficiency of photosystem II in relation to 'energy'-dependant quenching of chlorophyll fluorescence. *Biochimica et Biophysica Acta*, *894*(2), 198-208.

Witt, H., Bordignon, E., Carbonera, D., Dekker, J. P., Karapetyan, N., Teutloff, C., … Schlodder, E. (2003). Species-specific differences of the spectroscopic properties of

P700: Analysis of the influence of non-conserved amino acid residues by site-directed mutagenesis of photosystem I from *Chlamydomonas reinhardtii*. *The Journal of Biological Chemistry*, *278*(47), 46760-46771.

Wollman, F. A. (2001). State transitions reveal the dynamics and flexibility of the photosynthetic apparatus. *European Molecular Biology Organization Journal*, *20*(14), 3623-3630.

Yamashita E, Zhang, H., & Cramer, W. A. (2003). Structure of the cytochrome b_6f complex: Quinone analog inhibitors as ligands of haem c_n. *Journal of Molecular Biology*, *370*(1), 39-52.

Yan, J. S., & Cramer, W. A. (2003). Functional insensitivity of the cytochrome b_6f complex to structure changes in the hinge region of the Rieske iron-sulfur protein. *Journal of Biological Chemistry*, *278*(23), 20925-20933.

Yu, L., Zhao, J., Muhlenoff, U., Bryant, D. A., & Golbeck, J. H. (1993). PsaE is required for in Vivo cyclic electron flow around photosystem I in the cyanobacterium *Synechococcus* sp. PCC 7002. *Plant Physiology*, *103*(1), 171-180.

Zangl, J., & Kallas, T. (2006). Effect of processing time on gene expression levels, a RT-qPCR study on *Synechocystis* sp. PCC 6803 cultures. Unpublished raw data.

Zhang, H., Whitelegge, J. P., & Cramer, W. A. (2001). Ferredoxin: $NADP^+$ oxidoreductase is a subunit of the chloroplast cytochrome b_6f complex. *The Journal of Biological Chemistry*, *276*(41), 38159-38165.

Zhang, L., McSpadden, B., Pakrasi, H. B., & Whitmarsh, J. (1992). Copper mediated regulation of cytochrome c_{553} and plastocyanin in the cyanobacterium *Synechocystis*

6803. *The Journal of Biological Chemistry*, *267*(27), 19054-19059.